# GAS FLUX ESTIMATION FROM SURFACE GAS CONCENTRATIONS

A Thesis
Presented to
The Academic Faculty

By

Sabina Shahnaz

In Partial Fulfillment
Of the Requirements for the Degree
Master of Science in Civil and Environmental Engineering

Georgia Institute of Technology

May 2016

**GAS FLUX ESTIMATION FROM SURFACE GAS CONCENTRATIONS**

Approved by:

Dr. Jingfeng Wang, Advisor
School of Civil and Environmental Engineering
*Georgia Institute of Technology*

Dr. Aris P. Georgakakos
School of Civil and Environmental Engineering
*Georgia Institute of Technology*

Jian Luo, Ph.D.
Associate Professor
School of Civil and Environmental Engineering
*Georgia Institute of Technology*

Date Approved: April 28, 2016

## EPIGRAPH

In physical science a first essential step in the direction of learning any subject is to find principles of numerical reckoning and practicable methods for measuring some quality connected with it.

— Baron William Thomson Kelvin

Lecture to the Institution of Civil Engineers, London (3 May 1883)

**DEDICATION**

To my father, M. Nurul Amin

# PREFACE

A gradient-independent model of gas fluxes was formulated and tested. The model is built on the relationship between gas flux and the time history of surface gas concentration, known as half-order derivative (HOD), when the transport of the gas in the boundary layer is described by a diffusion equation. The eddy-diffusivity of gas is parameterized based on the similarity theory of boundary layer turbulence combined with the MEP model of surface heat fluxes. Test of the new model using in-situ data of $CO_2$ concentration and fluxes at several locations with diverse vegetation cover, geographic and climatic conditions confirms its usefulness and potential for monitoring and modeling greenhouse gases. The proposed model may also be used for estimating other GHGS fluxes such as methane ($CH_4$) and Water vapor flux. This proof-of-concept study justifies the proposed model as a practical solution for monitoring and modeling global GHGS budget over remote areas and oceans where ground observations of GHGS fluxes are limited or non-existent. One focus of the on-going research is to investigate its application to producing regional and global distributions of carbon fluxes for identifying sinks and sources of carbon and re-evaluating the regional and global carbon budget at monthly and annual time scales.

Sabina Shahnaz

April 28, 2016

## ACKNOWLEDGEMENTS

My sincerest appreciation is extended to the following members of the faculties in the School of Civil and Environmental Engineering for their extensive support, guidance and encouragement to complete this research successfully,

Jingfeng Wang, Sc.D., Associate Professor, School of Civil and Environmental Engineering, Georgia Institute of Technology.

Aris P. Georgakakos, Ph.D. Professor and Director, Georgia Water Resources Institute, School of Civil and Environmental Engineering, Georgia Institute of Technology

Jian Luo, Ph.D., Associate Professor, School of Civil and Environmental Engineering, Georgia Institute of Technology.

I am also sincerely grateful to Yao Tang, Ph.D. candidate, Civil and Environmental Engineering, Georgia Institute of Technology for his assistance and encouragement to complete this research.

Most Sincerely,

Sabina Shahnaz

M.S. Student

Civil and Environmental Engineering

Georgia Institute of Technology

Atlanta, GA

## TABLE OF CONTENTS

## LIST OF TABLES

## LIST OF FIGURES

## LIST OF ABBREVIATIONS

| | |
|---|---|
| B | Bowen Ratio |
| C | Gas Concentration |
| CMDL | Climate Monitoring and Diagnostic Laboratory |
| $c_p$ | Specific Heat of Air at Constant Pressure |
| CSIRO | Commonwealth Scientific and Industrial Research Organization |
| D | One Dimensional Diffusion Coefficient |
| E | Latent Heat Flux |
| EMEP | MEP Model Latent Heat Flux |
| $e_0$ | Saturation Vapor Pressure at Reference Temperature |
| EOBS | Observed Latent Heat Flux |
| F | Gas Flux |
| FC | $CO_2$ Flux |
| G | Ground Heat Flux |
| GHGS | Green House Gases |
| H | Sensible Heat Flux |
| HMEP | MEP Model Sensible Heat Flux |
| HOBS | Observed Sensible Heat Flux |
| HOD | Half Order Derivative |
| $I_0$ | Apparent Thermal Inertia of the Air |
| IPCC | Intergovernmental Panel on Climate Change |
| IR | Infrared |
| Is | Thermal Inertia of Soil |
| $\kappa$ | Von Karman Constant |
| $\lambda$ | Latent Heat of Vaporization of Liquid Water |
| MEP | Maximum Entropy Production |
| NOAA | National Oceanic and Atmospheric Administration |
| NRMSE | Normalized Root-Mean-Square Error |
| Pg C | Petagram Carbon |
| $P_s$ | Surface Atmospheric Pressure |
| $q_s$ | Specific Humidity at Ground (or Canopy) Surface |
| $\rho$ | Density of Air |
| RMSE | Root-Mean-Square Error |
| Rn | Net Radiation |
| Rv | Gas Constant of Water Vapor |
| Ta | Air Temperature |
| Ts | Canopy (or Soil Skin) Surface Temperature |
| $T_0$ | Reference Temperature (in Kelvin) |
| $u_*$ | Friction Velocity |
| z | Vertical distance between Canopy Top (Ground) and Point of Measurement |

## SUMMARY

The goal of this study is to develop a gradient-independent method for modeling surface gas flux using surface gas concentration data. The proposed method is built on the relationship between gas flux and the time history of surface gas concentration, known as half-order derivative (HOD), when the transport of gas in the boundary layer is described by a diffusion equation. A new parameterization of the eddy-diffusivity of gas is based on the similarity theory of boundary layer turbulence combined with the MEP model of surface heat fluxes reduces the sensitivity of the modeled fluxes to model parameters. The proposed model is tested using in-situ data of $CO_2$ concentration time series, net radiation and surface temperature at canopy (or ground) surface at half hour (or hour) intervals from Ameriflux Network at several locations with diverse vegetation cover, geographic and climatic conditions to test the applicability of model within reasonable endeavor. The study sites are Santarem KM67 Primary Forest, Brazil; Cedar Bridge, New Jersey, USA; Delta Junction 1920 Control, Alaska, USA and Walnut Gulch Lucky Hills Shrubland, Arizona, USA. The modeled $CO_2$ flux demonstrates close agreement with field observations with high value of correlation coefficient and regression coefficient (using observed flux as regressor) between modeled and observed $CO_2$ fluxes. The modeled $CO_2$ fluxes well capture the diurnal variation and magnitude of the observed fluxes. The magnitudes of modeled fluxes are comparable to the observed fluxes except for a small number of points due to the linear interpolation of the missing $CO_2$ concentration data points. The sensible heat flux used in parameterization of

diffusion coefficient of $CO_2$ is estimated using MEP model with other energy fluxes (such as ground heat flux and latent heat flux) using net radiation and canopy (or ground) surface temperature. The estimated energy fluxes using MEP model compared with observed energy fluxes for the study sites shows high correlation and captures diurnal variation and magnitude of the observed energy fluxes. Agreement between modeled and observed $CO_2$ flux is solid during growing season especially at forested sites.

The study demonstrated the usefulness and potential of the proposed gradient independent model of surface gas fluxes using surface gas concentration for monitoring and modeling of regional and global GHGS budget. The parsimony of model input makes it ideal for estimating fluxes of GHGS including $CO_2$ and methane given limited data availability and space-time coverage and resolution. Further field scale tests of the proposed model at daily and longer time scales are underway.

# CHAPTER 1

## INTRODUCTION

Increase in the atmospheric $CO_2$ concentration since 1750 has the largest contribution in climate change and surface warming (IPCC, 2013). Understanding and predicting the impact of increasing $CO_2$ and other greenhouse gases (GHGS) in the atmosphere on climate change requires accurate global $CO_2$ and other GHGS fluxes data. The uncertainties in the existing $CO_2$ fluxes data are arguably responsible for the unbalanced carbon budget at regional and global scales causing missing carbon sink problem (Schimel, 1995). A recent modeling study of the global carbon cycle suggests that the northern hemisphere terrestrial sinks are overestimated while tropical ecosystem sinks are underestimated (Stephens's et al., 2007). This finding implies that imbalance of global carbon budget causes the missing carbon sink in northern hemisphere. Global carbon budget was obtained using the mass balance equation of carbon emissions from fossil fuel and cement production and their partition among land, ocean and atmosphere (Le Quéré et al., 2013). Such derived global carbon budget has large uncertainties especially for terrestrial land, on the order of $\pm$ 0.8 Pg C $yr^{-1}$ when calculated using residual of mass balance equation and on the order of $\pm$ 1 Pg C $yr^{-1}$ when estimated using Dynamic Global Vegetation Models (Le Quéré et al., 2013).

Uncertainty of the current global carbon budget is closely related to the models of $CO_2$ fluxes. Reliable regional and global estimates of trace gas emissions depend on improved methodologies to reduce the uncertainty in the current estimates, which may be alleviated by developing new flux models for different processes, different gas species and on different space-time scales. Gas fluxes estimates of both terrestrial and aquatic systems have substantial uncertainties. In aquatic systems gas fluxes are generally modeled in terms of gas transfer velocity and concentration gradient in the atmosphere. Gas transfer velocity is parameterized in terms of wind speed with large measurement errors. There are large uncertainties in measurement of $CO_2$ concentration due to Webb effect, e.g. signal is sensitive to water vapor by overlapping $CO_2$ and $H_2O$ IR peaks, pressure broadening effects and air density effects of sensitive and latent heat fluxes on the $CO_2$ gas which causes measured flux an order of magnitude greater than actual flux over ocean. The uncertainty in the global emission rate is illustrated by the difference of more than a factor of 4 between the lowest and highest global emission rate (Boumann et al., 1999).

Current modeling and measurement methods of surface gas flux (such as $CO_2$, Methane) estimation in terrestrial ecosystem include: Chamber methods, Flux gradient methods, Eddy Correlation Methods, Mass Balance methods, Energy Balance methods, Convective Boundary Layer Budget methods, Nocturnal Boundary Layer Budget methods and Inverse Lagrangian model. Uncertainties in flux estimation in terrestrial ecosystem depend on specific measurement or modeling methods. For example, Chamber method is used for process level studies measuring trace gas fluxes and uncertainties

result from chamber effects on perturbation of the original natural environment (Hutchinson and Moiser, 1981; Moiser, 1989; Livingston and Hutchinson, 1995). Gradient method uses air samples from different levels having different foot prints causing potential problems to flux measurement (Denmead and Raupach, 1993). Although eddy correlation methods provide the most direct measurement of fluxes but, using fast response sensors make this method to technically demanding and expensive (Lapitan et al. 1999). Mass balance method works well for homogeneous ecosystems with known geometry of study area. The uncertainties of flux estimates result from surface roughness, horizontal wind velocity, mean background concentration and atmospheric stability conditions (Denmead and Raupach, 1993; Lenschow, 1995). Energy balance method has difficulty in making accurate measurements during nighttime and rainy events (Wagner-Riddle et al, 1996 a, b). Sensitivity to weather conditions limits the applicability of Convective Layer Budgeting methods (Denmead et al., 1996). Nocturnal Layer Budgeting method also has difficulties during nighttimes due to reduced height of nocturnal layer. Uncertainties of Inverse Lagrangian Dispersion modeled fluxes are caused by heterogeneous canopies such as re-growth forests as this model assumes homogeneous canopies with uniform distribution of source and sink horizontally (Raupach, 1989a, b). Although models developed for specific ecosystems may have less uncertainty but when extrapolating for a larger area with spatial and temporal variability, limited data availability may increase uncertainty (Mosier and Parton, 1985).

Except for limited number of ground observation stations where carbon fluxes are measured directly, $CO_2$ fluxes are commonly derived using the bulk transfer model requiring remote sensing or reanalysis data of near-surface $CO_2$ concentration gradient and wind speed are subject to large measurement errors. $CO_2$ fluxes over oceans are routinely derived using the bulk transfer model from the concentration gradient of $CO_2$ across the air-sea interface with the gas transfer coefficient parameterized in terms of wind speed. However, $CO_2$ concentration gradient in sea-water boundary layer cannot be measured directly, usually inferred from in partial pressure of $CO_2$, $\Delta pCO_2$, which is difficult to estimate (McGillis, 2006). Changes in wind speed have pronounced effect on the parameterization of gas transfer coefficient hence estimation of $CO_2$ flux (Wanninkhof, 2007). The overall uncertainty in the global air-sea $CO_2$ flux is on the order of -19% to +22% due to wind speed (Takahashi, 2002) and on the order of 25% due to the measurement errors of $\Delta pCO_2$ (Wanninkhof, 2007).

Reducing the uncertainty of the estimated $CO_2$ fluxes for solving the mystery of the missing carbon sink in the study of regional and global carbon budget needs a more suitable model of carbon fluxes. The goal of this study is to formulate and test a new model of carbon fluxes that does not use $CO_2$ concentration gradient and wind speed data. The basic idea is to express the $CO_2$ flux in terms of near-surface $CO_2$ concentration time-series, analogous to ground heat flux expressed as a functional of ground temperature (Wang and Bras, 1999), to avoid the use of $CO_2$ concentration gradient. The eddy diffusivity in the governing equation describing the transport of $CO_2$ in the boundary layer is parameterized in terms of sensible heat flux according to a similarity model of

atmospheric turbulence (Wang and Bras, 1999) to avoid the use of wind speed. The proposed model was tested using field observations of $CO_2$ concentration, $CO_2$ fluxes and sensible heat flux. Using the MEP model of surface heat fluxes (Wang and Bras, 2011), sensible heat flux may be derived from net radiation and surface temperature without using wind speed data, paving the way for remote sensing application of the proposed model.

# CHAPTER 2

# LITERATURE REVIEW

## 2.1 Gas Flux Measurement in Terrestrial Ecosystems

Current measurement methods of gas flux estimation in terrestrial ecosystem include Chamber methods and Micrometeorological methods (Lapitan et al., 1999). Chamber techniques are of two types: Closed Chamber and Open Chamber. Micrometeorological methods include: Flux Gradient methods, Eddy Correlation, Eddy Accumulation, Bowen Ratio methods, Mass Balance methods, Convective Boundary Layer Budget methods. Tracer method is used to measure diffusion coefficient which is a significant source of uncertainties in Flux Gradient and Energy Balance (Bowen Ratio) methods. The micrometeorological methods can also be applied for aircraft mounted measurements to provide spatially averaged, aerial assessments of gas fluxes. Above methods are described in the following sections.

### 2.1.1 Chamber Methods

Chamber methods are used for measuring small gas fluxes in process-level studies, identifying sources of spatial variations controlling gas fluxes (Hutchinson and Moiser, 1981; Moiser, 1989; Livingston and Hutchinson, 1995). The chamber methods are of two types: Closed Chamber and Open Chamber. The closed chamber restricts exchange of heat and water vapor between inside and outside of chamber.

In open chamber method, a steady state gas concentration gradient is established by maintaining concentration of gas in the enclosed volume of air at ambient level through continuous air flow of external air. The Formulations for closed and open chamber methods are shown in equation (2.1) and (2.2), respectively,

$$F = \frac{V}{A}\frac{dC_g}{dt} \quad , \tag{2.1}$$

$$F = \frac{f}{A}\left(C_{g(o)} - C_{g(i)}\right) \quad , \tag{2.2}$$

where F is the gas flux, V the chamber volume, A the chamber area, $C_g$ the gas concentration in the chamber, t the time, f the air flow rate, $C_{g(o)}$ the concentration in the air going out of the chamber and $C_{g(i)}$ the concentration in the air coming into the chamber.

Changes in gas concentration due to emission magnified in a closed chamber provides better precision relative to open chamber for detecting small fluxes. Errors in flux measurement primarily caused by chamber effects on perturbation of the original natural environment (Denmead, 1979; Hutchinson and Mosier, 1981; Mosier, 1990; Hutchinson and Livingston, 1993; Livingston and Hutchinson, 1995). Gas flux over an area is obtained by taking spatial averages of chamber fluxes aligned at grid points along wind direction.

### 2.1.2 Flux Gradient Method

The flux gradient method measures gas flux from concentration gradient and eddy diffusivity of the gas. Eddy diffusivity of a gas is inferred using tracers (e.g. heat and water vapor). Fluxes and concentration gradients are measured simultaneously with gas concentration gradient (Denmead and Raupach, 1993). Eddy diffusivity of gas corrected for atmospheric stability condition is estimated from temperature and wind profile measurements (Paulson, 1970; Businger et al., 1971). The Formulation of flux gradient method is shown in equation (2.3).

$$F = \frac{\kappa U_* z}{\varphi_h} \frac{dC_g}{dz} \ , \tag{2.3}$$

where, F is the flux, $\kappa$ the Van Karman's constant, $U_*$ the friction velocity, $\frac{dC_g}{dz}$ the concentration gradient between two layers, z the sensor height and $\varphi_h$ the atmospheric correction for heat. The uncertainty in the estimated flux results from the measurement of concentration gradient and wind velocity, which have uncertainty themselves. Another potential problem with this method is that air samples from different level have different foot prints.

### 2.1.3 Eddy Correlation Method

Eddy correlation method relates the covariance of instantaneous vertical wind velocity with the instantaneous fluctuations of gas concentration to estimate vertical flux density from (in case of deposition to) the surface. The formulation of Eddy Correlation methods is shown in equation (2.4).

$$F = \overline{w'C_g'} + \frac{\overline{C_g}}{\overline{\rho_a}}\left(\frac{\eta}{1+\eta\beta}\right)E + \frac{\overline{C_g}}{(\overline{\rho_a}+\overline{\rho_v})}\left(\frac{H}{c_pT}\right) \quad , \tag{2.4}$$

where, F is the gas flux, $\overline{w'C_g'}$ the time averaged instantaneous fluctuations of vertical wind velocity and instantaneous fluctuations of gas concentration, $\overline{C_g}$ the time averaged concentration, $\overline{\rho_a}$ the time averaged density of dry air, $\overline{\rho_v}$ the time averaged density of moist air, $c_p$ the specific heat of air at constant pressure, T the air temperature, H the sensible heat flux, E the latent heat flux, $\eta$ the ratio of molecular weights of dry and moist air and $\beta$ the ratios of the mean densities of dry and moist air. Eddy correlation method is the most direct method of gas flux measurement but it is technically demanding considering the logistics before and during data acquisition (Lapitan et al. 1999). These include check on instrument drifts, transient errors, vertical alignment and sitting geometry relative to mast and other sensors (Businger, 1986). The sensor sampling height and fetch are also important factors affecting measurement of flux. The minimum sensor (wind and temperature) of 2 m requires a fetch of 200 m (Denmead and Raupach, 1993). Decrease in gas concentration with height and thermal stratification affects gas flux density (Lapitan et al. 1999).

Gas flux obtained in this method is averaged over a period 15 min to 1 hour. Fast response analytical instrumentation (TDL and FTIR spectrometers) can increase the cost but sensitively measure a range of gas fluxes within spatial variability among terrestrial ecosystems (Edwards et al. 1994; Simpson et al. 1995).

### 2.1.4 Eddy Accumulation Method

Eddy accumulation method is similar to eddy correlation, but accumulated instead of instantaneous air samples are measured in two reservoirs for concentration of gas species, slow response and high resolution spectrometer can be used. The Formulation of Eddy Accumulation methods is shown in equation (2.5).

$$F = b\left(\overline{C_g^+} - \overline{C_g^-}\right) , \tag{2.5}$$

where, F is the flux, b the proportionality coefficient has a value close to 0.6 (Denmead, 1994), $\overline{C_g^+}$ and $\overline{C_g^-}$ the average gas concentrations in the air reservoir at 'up' position and 'down' position respectively. Advantages for this method includes: it does not require fast response sensors and need not to be in the field so that high resolution laboratory based instruments can be used, measurements do not need density corrections and it provides direct point measurement (Denmead, 1994). Potential sources of error for this method results from offsets in vertical wind velocity, mechanical failures of fast switches and flow rate circuitry and low resolution of gas analyzer (Hicks and Mcmillen, 1984), especially when updraft and downdraft changes in gas concentration is small.

### 2.1.5 Energy Balance Method

This method measures air temperature, water vapor pressure and gas concentration at two heights above surface. The sensible heat flux and latent heat flux components of energy balance is measured separately from the finite difference of temperature gradient and vapor pressure gradient respectively or by residual knowing total net radiation, ground heat flux, and either sensible heat flux or latent heat flux. The eddy diffusivity coefficient can be derived from ratio between sensible heat flux and temperature gradient and by invoking the similarity assumption, diffusivity of desired gas is obtained. Using this assumption alleviates the need for atmospheric stability correction for energy balance approach. Flux is estimated from product of concentration gradient and diffusivity or from the ratio of measured gas concentration and temperature gradient given net radiation and ground heat flux. The Formulation of Energy balance method is shown in equation (2.6),

$$F = \frac{(R_n - G)(C_g^+ - C_g^-)}{c_p(1+\gamma)(T^+ - T^-)} \quad , \tag{2.6}$$

where F is the flux, $R_n$ the net radiation, G the ground heat flux, $C_g^+$ the gas concentration measured by sensor in the air reservoir at 'up' position, $C_g^-$ the gas concentration measured by sensor in the air reservoir at 'down' position, $c_p$ the specific heat of air at constant pressure, γ the ratio of mean densities of water vapor and air, $T^+$the air temperature measured at 'up' position and $T^-$ the air temperature measured at 'down' position.

Energy balance method does not provide good agreement during nighttime and rainy condition due to low available energy (Wagner-Riddle et al, 1996 a,b). Other sources of error include transient error in heat and moisture sensors, sampling errors during low available energy (Fritschen and Gay, 1979), inequalities in exchange coefficients (Dugus et al., 1997; Meyers et. al., 1996), and differences in horizontal length scale of air sampled at different heights.

## 2.2. Gas Flux Modeling Methods in Terrestrial Ecosystems

Current modeling methods of gas fluxes in terrestrial ecosystem include Inverse Lagrangian model (Raupach, 1989b) to identify sources and sinks of scalars in the canopy space from mean concentration, mass balance method, convective boundary layer budget model (Raupach et al., 1992; Denmead et al., 1996) and nocturnal boundary layer budget model. Descriptions of above models are as follows:

### 2.2.1 Inverse Lagrangian Dispersion Model

Inverse Lagrangian Dispersion model of gas flux proposed by Raupach (1989a, b) infers fluxes of trace gases and their source sink distribution over canopies by building relationship between chamber measurements and canopy measurements at field scale. This method requires a mean concentration profile of gas within the canopy and some knowledge of turbulence and lagrangian time scales of that region. Within the canopy, the source or sink strength of the gas at level z S (z) is related to vertical flux density F (z),

$$S(z) = \frac{dF(z)}{dz}, \tag{2.7}$$

Integrating (2.7) gives

$$F(h) = F(0) + \int_0^h S(z)dz \ , \tag{2.8}$$

where F (0) is the flux density at surface, and h the height of canopy above the surface. Lagrangian dispersion theory (Raupach, 1989a) enables a prediction of mean concentration profile C (z) from S (z). Adding Emissions from all source layers, gas concentration at any height is given by

$$C_i - \ C_R = \sum D_{ij} \ \ S_j \ \Delta Z_j \ \ , \tag{2.9}$$

where, $C_R$, is the concentration at a reference height above the canopy and $D_{ij}$ are the coefficients of the dispersion matrix. These coefficients are calculated from profiles of standard deviation of vertical wind speed, $\sigma_w$ , and lagrangian time scale within canopy, $T_L$ (Raupach, 1989a). Using values of $D_{ij}$, in (2.9) yields a system of linear equations from which $C_i - \ C_R$ can be solved for source densities Sj with known values of concentrations, $C_i$. Redundant concentration data should be included so that source densities $S_j$ are sought in m layers with n measured concentration values such that n > m. This method is based on the assumption of homogeneous canopies where the source and sink pattern is uniform horizontally. It may not work as well in heterogeneous canopies such as regrowth forests. The method showed some discrepancies with conventional micrometeorological methods during earlier part of day (Denmead and Raupach, 1993).

### 2.2.2 Mass Balance Model

Mass balance model is suitable for small fetches. This method is used to estimate gas flux density at the height of boundary layer developed over a given fetch from the height integral of the product of mean horizontal wind and upwind gas concentration corrected by the mean background concentration. The Formulation of mass balance method is shown as,

$$F = \frac{1}{X}\int_0^z \overline{u\left(C_{g(u)} - C_{g(b)}\right)}\, dz \ , \qquad (2.10)$$

where, F is the flux, X the length of upwind fetch, u the horizontal wind speed, z is the depth of modified layer (1/10 of fetch), $C_{g(u)}$ and $C_{g(b)}$ are the upwind and background gas concentration respectively. The uncertainties of flux estimation result from surface roughness, horizontal wind velocity, atmospheric stability conditions and mean background concentration (Denmead and Raupach, 1993; Lenschow, 1995). Formulation of mass balance method neglects diffusion transport that is 10% of the contribution due to convective transport (Raupach and Legg, 1984). Another possible sources of error involves subtraction of experimentally determined upwind and downwind concentration profiles, an error prone process due to logistic difficulty of measuring two concentration profiles. A third difficulty arises from lack of knowledge about wind speed dependent fetch length. This method becomes unreliable under the condition of variable wind directions.

### 2.2.3 Convective Boundary Layer Budget Model

Convective Boundary Layer (CBL) is a shallow surface layer (about 100m depth) with large concentration gradients. The vertical gas fluxes is nearly constant with height with in this layer. CBL is topped by a mixed layer containing slowly varying fluxes with height and uniform concentrations. CBL is capped by sharp temperature inversion. The mixed layer grows during day time through the input of heat at the ground, entraining air above the inversion extends up to 1-2 km. CBL budgeting methods are based on the rate of change of gas concentration in the mixed layer which acts like a giant mixing chamber moving with mean wind. CBL model is formulated as (Denmead et al., 1996),

$$F = h\frac{dC_m}{dt}\,(C_+ - C_m)\left(\frac{dh}{dt} - W_+\right)\,, \tag{2.11}$$

where, F is the surface flux density, h the height of CBL, $C_m$ the gas concentration in CBL, $C_+$ the free atmosphere just above CBL, t the time and $W_+$ the subsidence velocity. Integrating (2.11) gives cumulated regional flux, I,

$$\begin{aligned} I(t) &= \int_0^t F(t)dt \\ &= h(t)[C_m(t) - C_+(t)] - h(0)[C_m(0) - C_+(0)] \\ &\quad + \frac{\gamma}{2}(h_t^2 - h_0^2) - \int_0^t W_+(\tau)[\,C_m(\tau) - C_+(\tau)]d\tau\,, \end{aligned} \tag{2.12}$$

In (2.12) $\gamma = \frac{dC_+}{dz}$ is the rate of change of concentration with height just above the mixed layer ($h_+$), $C_m$ is obtained from near surface concentration $C_s$ measured at height $z_s$ with an aerodynamic resistance $r_a$ at unstable conditions according to similarity theory,

$$C_m = C_s - r_a F \ , \tag{2.13}$$

$$r_a = \frac{ln\left[\frac{(z_m-d)}{(z_s-d)}\right] - 2ln\left[\frac{1+\sqrt{[1-\frac{16(z_m-d)}{L}]}}{1+\sqrt{[1-\frac{16(z_s-d)}{L}]}}\right]}{ku_*} \ , \tag{2.14}$$

where k = 0.41 is von Karman's constant, $u_*$ the friction velocity, d zero displacement distance, $z_m$ the height from the ground to the bottom of the mixed layer and L is the Monin−Obukhov length. Assuming $W_+$ is small and $\gamma = 0$ (step change from $C_m$ to $C_+$ at h) gives,

$$I(t) = \frac{h(t)[C_s(t)-C_+(t)]-h(0)[C_s(0)-C_+(0)]}{1+\frac{[h(t)r_a(t)-h(0)r_a(0)]}{t}} \ , \tag{2.15}$$

Use of near surface concentration instead of mixed layer concentration may bias the estimates toward local flux values. Measurement at more than one location in regions of heterogeneous landscape will provide better flux estimates. Changing wind conditions, unsuitable weather and high precision gas concentration measurements are limitations of this method. This method is an effective scheme of gas flux estimation scheme at regional scale.

### 2.2.4 Nocturnal Boundary Layer Budget Model

Nocturnal Boundary Layer (NBL) occurs at night as convective heating stops. It is a shallow weakly turbulent layer bounded with a low level radiative inversion. Inversion inhibits vertical mixing so that emission of gases from surface are contained in shallow aerial layer whose concentration changes appreciably. The formulation of nocturnal boundary layer budget model is shown in equation (2.16),

$$F = \int_0^z \frac{dC}{dt} dz \ , \qquad (2.16)$$

where, F is the surface flux, z the height of NBL and C the concentration at the top of the inversion layer (NBL). The growth and height of NBL are not easily predicted especially when radiative inversion layer is deep or absent so application of this method may not be possible.

## 2.3 Gas Flux Measurement and Modeling in Aquatic Ecosystems

Direct measurement of gas fluxes by eddy correlation, relaxed eddy accumulation and flux gradient methods are difficult over water because of small magnitude of net fluxes and large uncertainties in the measurements of temperature and concentration gradients. The flux across the air water interface F can be expressed as,

$$F = kr(C_w - \alpha' C_a) = krK_0\,(pX_w - pX_a)\,, \tag{2.17}$$

where, k is the gas transfer velocity for a nonreactive gas, r the enhancement factor by chemical reaction of the gas at interface, $\alpha'$ the Ostwald solubility coefficient, $C_w$ the gas concentration near water surface, $C_a$ the gas concentration in the air immediately above the water surface given the concentration gradient across the interface$(C_w - \alpha C_a)$ . The concentration gradient equals $K_0\,(pX_w - pX_a)$ when expressed in terms of partial pressure, where, $K_0$ is the solubility of gas in water, $pX_w$ the partial pressure of gas in water and $pX_a$ the partial pressure of gas in air. The gas transfer velocity k is frequently parameterized in terms of wind speed (Liss and Merlivat, 1986; Wannikhof, 1992) obtained using the following equation,

$$k_1 \;=\; k_2\left(\frac{Sc_1}{Sc_2}\right)^n, \tag{2.18}$$

where, $k_1$ is the transfer velocity of gas in question, $k_2$ the transfer velocity of a reference gas, $Sc_1$ and $Sc_2$ the Schmidt numbers of gas in question and reference gas, respectively and n is the Schmidt number equal to -0.66 for smooth surfaces and -0.5 for rough surfaces.

The relative homogeneity of aqueous systems causes the flux to be less scale dependent in comparison to terrestrial systems. Gas concentration in lakes varies less than 5% from the mean suggests smaller spatial variation of fluxes which will be larger on global oceanic scales due to large differences in production and consumption rates. Generally, subtropical and polar gyres on average will be sinks and tropical regions the sources due to equatorial upwelling and heating of surface water. Temporal variation of fluxes on short time scales controlled by changes of environmental forcing on gas transfer velocity k and change in solubility due to temperature change. Simple parameterization of k suggests that it has a quadratic dependence on wind speed. Diurnal change in surface water temperature can be up to 2°C while annual changes in inland waters can be as large as 25°C and 5°C to10°C over the ocean.

Methods of measurement gas flux F and/or gas transfer velocity k across air water interface include: natural $^{14}C$ method, bomb $^{14}C$ method, natural $^{221}$ Rn method, enclosure methods, opportunistic mass balance methods and deliberate tracer method briefly described in following sections.

### 2.3.1 Natural $^{14}C$ Method

Natural $^{14}C$ method uses radioisotope of Carbon -14 in water and air and mean depth of ocean and decay constant of $^{14}C$ to measure global average gas transfer velocity k which is about 21cm/hour with 25% uncertainty (Broecker and Peng, 1982).

### 2.3.2 Bomb $^{14}C$ Method

Bomb $^{14}C$ method uses radioisotope of Carbon -14 inputs from nuclear bomb tests to measure global average gas transfer velocity, which is about 22 cm/hour with less than 15% uncertainty (Broecker et al., 1985). Current observations of atmospheric $^{14}C$ require large sampling of $^{14}C$ from World Ocean Circulation Experiments (Duffy and Caldeira, 1995).

### 2.3.3 Natural $^{221}$ Radon Method

The limitation of Natural $^{14}C$ method due to from limited information on variability gas transfer velocity at regional scale may be overcome by Natural Radon ($^{221}$ Rn) method even though this method is not applicable to inland waters. Global average gas transfer velocity by $^{221}$ Rn method is 20% lower than $^{14}C$ method (Roether et al., 1984).

### 2.3.4 Enclosure Methods

For inland waters, gas transfer velocity is measured by Enclosure (Chamber) method (MacIntyre et al., 1995). The difficulty with this method is that the surface turbulence controlling gas exchange under the chamber differs from the surrounding water, leading to higher values of gas transfer velocity than other methods.

### 2.3.5 Opportunistic Mass Balance Methods

Opportunistic mass balance methods are used to estimate gas transfer velocities in the subtropical gyres by determining air-water disequilibrium of man-made halo carbons, which can be used to measure daily cycle of reactive trace gases (Yvon et al., 1996).

### 2.3.6 Deliberate tracer method

Deliberate tracer method is used to perturb a mass balance by adding a known amount of gas to the water and subsequently follow the mass decrease through time. This method is used in lakes, rivers and coastal waters by injecting Sulfur Hexafluoride ($SF_6$) as tracer in epilimnion. Once the trace gas is homogeneous, samples are taken to determine decrease in concentration over time to measure gas transfer velocity.

One limitation of the methods for measuring gas transfer velocities (k) using the waterside perturbation is caused by slow response time relation to variability in environmental forcing. By using air side measurements such as eddy correlation, eddy accumulation and flux gradient method with faster response times, this problem can be resolved. An alternate method of direct flux measurements over air-water interface is the controlled flux technique in which heat is used as proxy for a gas (Haussecker et al., 1995). In general gas flux measurement across air water interface is favorable using air-side measurement due to short response time. Performing air side measurement aside with water side measurement will resolve the discrepancies between low k values in water side measurements to higher k values in air-side measurements and to use active and passive radiometry remote sensing data to extrapolate gas transfer velocities.

## 2.4 Gas Flux Modeling in Methods in Global Systems

Global models are developed for assessment of main pathways and distribution of emissions and depositions and interaction between the Northern and Southern hemisphere. During recent decades several global networks of trace gas monitoring stations have been developed: for example; by the Climate Monitoring and Diagnostics Laboratory of U.S. National Oceanic and Atmospheric Administration (NOAA/CMDL), the Scripps Institution of Oceanography, CSIRO of Australia routinely monitoring atmospheric composition with comprehensive efficiency and finer temporal and spatial resolution. Atmospheric transport models are used to derive global fluxes applying two methods: 1) Forward Atmospheric Model, 2) Inverse Atmospheric Model.

### 2.4.1 Forward Atmospheric Model

The concentration and deposition fields simulated with Forward Atmospheric Modeling are validated by comparing the model results with measured concentrations and fluxes. After validation model is used for spatial and temporal interpolation between measurement sites with proper spatial and temporal scale (Sofiev, 1999).

### 2.4.2 Inverse Atmospheric Model

Inverse Atmospheric Model uses observations of atmospheric concentration to estimate gas fluxes. The inverse problem is formulated as:

$$\overleftarrow{\Delta C} = T\,(\overleftarrow{q})\ , \qquad (2.19)$$

Where, $\overleftarrow{\Delta C}$ is the temporal change in vector of observed concentrations; $\tilde{q}$ is the vectors of sources and sinks and T is the atmospheric transport model. Transport model cannot be used to describe backward transport due to not being able model backward diffusion. The unknown sources and sinks are found by minimizing differences between measured and modeled concentrations by varying sink/source strengths. Similar to forward atmospheric model, spatial and temporal interpolation between measurement sites with proper spatial and temporal scale is applied after comparison of modeled and measured fluxes. Inverse method provides error covariance matrix quantifying uncertainty of model fluxes. For trace gases such as $CO_2$, methane transport and chemistry of equation (2.18) can be linearly approximated.

Bayesian approach to inverse problem provides a means to include a priori information on unknown source components in the inversion procedure (Tarantola, 1987). The priori information is based on a formulation of the problem in terms of Gaussian probability distribution in the joint space of sources and concentrations. An optimal posteriori source estimate is derived by inverse model which is as close as possible to the priori sources and resulting concentrations as close as the observed concentrations. Bayesian inversions trace gases such as $CO_2$ and methane are carried out in many experiments (Enting et al., 1995; Bousquet, 1997; Rayner et al., 1998; Kaminski, 1998; Hein and Heimann, 1994).

# CHAPTER 3

# PROPOSED METHOD OF GAS FLUX ESTIMATION

## 3.1 Model Formulation

Turbulent Dispersion of passive contaminants can be described by a diffusion equation (Monin and Yaglom, 1971; Pasquill, 1974),

$$\frac{\partial \chi}{\partial t} + u\frac{\partial \chi}{\partial x} + v\frac{\partial \chi}{\partial y} = K_x\frac{\partial^2 \chi}{\partial x^2} + K_y\frac{\partial^2 \chi}{\partial y^2} + K_z\frac{\partial^2 \chi}{\partial z^2} \quad , \tag{3.1}$$

where, t is time, x, y and z the space co-ordinates, $K_x$, $K_y$ and $K_z$ diffusion coefficients in x, y and z directions, $\chi$ the concentration of a passive contaminant and u and v the component of the horizontal mean wind, while vertical mean wind is assumed to be zero. When horizontally homogeneous concentration distribution is assumed, turbulent diffusion coefficients $K_x$ and $K_y$ become zero (Nieuwstadt, 1980). (3.1) reduces to,

$$\frac{\partial \chi}{\partial t} = K_z\frac{\partial}{\partial z}\left(\frac{\partial \chi}{\partial z}\right) \quad , \tag{3.2}$$

(3.2) has been frequently used to model turbulent transport including turbulent transfer of heat in the lower atmosphere over a homogeneous land surfaces (Wang and Bras, 1998). The transport of $CO_2$ over a homogeneous surface in the atmospheric

boundary layer is predominantly vertical hence may be described by one dimensional diffusion equation,

$$\frac{\delta C}{\delta t} = \frac{\delta}{\delta z}\left(D_C \frac{dC}{dz}\right) , \tag{3.3}$$

where, $C$ (kg $m^{-3}$) is the mean atmospheric $CO_2$ concentration, $Dc$ ($z$, $t$) ($m^2$ $s^{-1}$) the turbulent diffusion coefficient or eddy diffusivity of $CO_2$ and $z$ (m) the distance above the (ground or canopy) surface. The Proposed study assumes that the turbulent flow in the boundary layer responsible for transport of heat is also responsible for the transport of other passive tracers such as water vapor and $CO_2$ (Yakir and Wang, 1996). Following initial profile and boundary condition is applicable in deriving the solution of (3.3)

Initial Condition, $C = C_0 \ , \ z > 0 \ , \ t = 0$ (3.4)

Boundary Condition, $C = C_0 \ , \ z \to \infty \ , \ t > 0$ (3.5)

The full solution of C as a function of z and t requires an additional boundary condition at surface. Use of a mathematical tool called fractional calculus (presented in **Appendix A**) will facilitate the derivation of a solution of (3.3)

## 3.2 Parameterization of Diffusion Coefficient

Eddy diffusivity of $CO_2$ $D_c$ in (3.3) may be parameterized (Wang and Bras, 2010) as

$$D_c = C_k \kappa z u_* \ , \tag{3.6}$$

where, $z$ is the distance between height of measurement and that of canopy top or ground surface, $\kappa$ ($\approx 0.4$) the Von Karman constant, $u_*$ the friction velocity, $C_k$ the empirical coefficient characterizing representing the stability of the surface layers. Friction velocity, $u_*$ is parameterized using extremum solution of Monin-Obukhov similarity equations (Wang and Bras, 2010) expressed as

$$u_* = -\left(\frac{2\beta g \kappa H z}{\rho c_p T_o}\right)^{\frac{1}{3}} \ , \ H < 0 \tag{3.7}$$

$$u_* = \left(\frac{\gamma_2 g \kappa H z}{2\rho c_p T_o}\right)^{\frac{1}{3}} \ , \ H > 0 \tag{3.8}$$

where, H is the sensible heat flux parameterized using Maximum Entropy Production (MEP) Model (Wang and Bras, 2009, 2011) in terms of surface net radiation and surface temperature (details of MEP model is presented in **Appendix B)**. H is positive when heat transfer in upward direction from ground surface to atmospheric boundary layer characterizing unstable condition of atmosphere. H is negative when heat transfer in downward direction from atmospheric boundary layer to ground surface

characterizing stable condition of atmosphere. $T_o$ (≈ 300 K) is the representative environmental temperature, $\rho$ (≈ 1.2 kg m$^{-3}$) the representative density of air, $c_p$ the specific heat at constant pressure, g (9.8 m s$^{-2}$) the gravitational acceleration and the universal empirical coefficients $\alpha \approx 0.75$, $\beta \approx 4.7$, $\gamma_2 \approx 9$ (Businger et al. 1971). Empirical coefficients $C_k$ characterizing the boundary stability in the Monin-Obukhov similarity equations representing the stability of the surface layers (Businger et. al.1971) given as follows

$$C_k = \frac{2}{1+\alpha} \ , \ H < 0 \tag{3.9}$$

$$C_k = \frac{\sqrt{3}}{\alpha} \ , \ H > 0 \tag{3.10}$$

Substituting (3.7) - (3.10) into (3.6) $D_c$ can be expressed as:

$$D_c = \left(\frac{2}{1+\alpha}\right)\left\{-\left(\frac{2\beta g \kappa H z}{\rho c_p T_o}\right)^{\frac{1}{3}}\right\}\kappa z \ , \quad H < 0 \tag{3.11}$$

$$D_c = \left(\frac{\sqrt{3}}{\alpha}\right)\left\{\left(\frac{\gamma_2 g \kappa H z}{2\rho c_p T_o}\right)^{\frac{1}{3}}\right\}\kappa z \ , \quad H > 0 \tag{3.12}$$

Combining terms independent of t and z in (3.11) and (3.12), the expression of turbulent diffusion equation is parameterized as

$$D_C\,(z,t) = D_o\, z^{\frac{4}{3}}\,|H|^{\frac{1}{3}}\ , \tag{3.13}$$

where, $D_o$ is the empirical constant,

$$D_o = \frac{2(2\beta)^{\frac{1}{3}}}{1+\alpha}\left(\frac{g\kappa^4}{\rho c_p T_o}\right)^{\frac{1}{3}}\ ,\ H\ < 0 \tag{3.14}$$

$$D_o = \frac{\sqrt{3}}{\alpha}\left(\frac{\gamma_2}{2}\right)^{\frac{1}{3}}\left(\frac{g\kappa^4}{\rho c_p T_o}\right)^{\frac{1}{3}}\ ,\ H\ > 0 \tag{3.15}$$

## 3.3 Derivation of Surface Flux

The surface $CO_2$ Flux, $F_C$ (defined positive for upward transport of $CO_2$) at a distance z from ground (or canopy) surface can be expressed as,

$$F_C(z,t) = D_C\,(z,t)\,\frac{\partial C(z,t)}{\partial z}\ , \tag{3.16}$$

where, $D_C\,(z,t)$ is the eddy diffusivity of $CO_2$ parameterized in (3.13). Derivation of $F_C$ involves solution of (3.3) with boundary conditions described in (3.4) and (3.5). In order to incorporate $D_C\,(z,t)$ in (3.13) three new variables $\acute{t}$ (functions of time t), $\xi$ (functions of height z) and $A$ (function of $D_0$) are introduced assuming $H$ invariant within height (z) of within surface layer then (3.3) is rewritten as,

$$\frac{\delta C}{\delta \acute{t}} = A\left(\frac{2}{\xi}\frac{\delta C}{\delta \xi} + \frac{\delta^2 C}{\delta \xi^2}\right)\ , \tag{3.17}$$

where,

$$\acute{t} = \int_0^t |H(\tau)|^{\frac{1}{3}}\,d\tau\ , \tag{3.18}$$

$$\xi = z^{\frac{1}{3}}\ , \tag{3.19}$$

$$A = \frac{D_0}{9}\ , \tag{3.20}$$

Analytic solution of (3.17) follows Oldham and Spanier (2002, page 204) given by,

$$\frac{\delta C(\xi,\acute{t}\,)}{\delta\xi} = -\frac{1}{\sqrt{A}}\frac{\delta^{\frac{1}{2}}}{\delta \acute{t}^{\frac{1}{2}}}(\mathrm{C}(\xi,\acute{t}\,) - C_0) - \frac{\mathrm{C}(\xi,\acute{t}\,)-C_0}{\xi+R}\ , \tag{3.21}$$

Initial and boundary condition given in terms of new variables

Initial condition, $C = C_0$ as $\acute{t}\ = 0$ at $\xi > 0$ (3.22)

Boundary condition, $C = C_0$ as $\acute{t}\ > 0$ at $\xi \to \infty$ (3.23)

For horizontal surface $\xi = 0\ and\ R \to \infty$, (3.21) becomes,

$$\frac{\delta C(\xi,\acute{t}\,)}{\delta\xi} = -\frac{1}{\sqrt{A}}\frac{\delta^{\frac{1}{2}}}{\delta \acute{t}^{\frac{1}{2}}}(\mathrm{C}(\xi,\acute{t}\,) - C_0)\ , \tag{3.24}$$

where, the half order derivative (see appendix A for details) of a function f (t) is defined as,

$$\frac{d^{\frac{1}{2}} f(t)}{\delta t^{\frac{1}{2}}} = \frac{1}{\sqrt{\pi}}\ \frac{d}{dt}\ \int_0^t \frac{f(\tau)d\tau}{\sqrt{t-\tau}}\ , \tag{3.25}$$

Replacing the variables $\xi$ and $\acute{t}$ and $A$ by the original variables in (3.24) leads to,

$$\frac{\delta C(z,t)}{\delta z} = \frac{1}{\sqrt{\pi}}\int_0^t \frac{\delta C(z,\tau)}{\delta\tau}\left[\int_\tau^t D_C\,(z,\eta)d\eta\right]d\tau\ , \tag{3.26}$$

The $CO_2$ Flux, $F_C$ is given as,

$$F_C(z,t) = \frac{D_C(z,t)}{\sqrt{\pi}} \int_0^t \frac{\delta C(z,\tau)}{\delta \tau} \left[ \int_\tau^t D_C(z,\eta) d\eta \right]^{-\frac{1}{2}} d\tau \quad , \qquad (3.27)$$

where, $\tau$ and $\xi$ are integration (dummy) variables. Theoretically the starting time (t = 0) is the time when $CO_2$ concentration is constant in z in order to obtain the analytic solution of (3.27). Case studies indicate that $F_C$ is not sensitive to this initial condition as long as ***t*** is on the order of hours. According to (3.27) surface $CO_2$ flux ($F_C$) at a given time (and a certain height above surface) is expressed as the weighted average of the time history of $CO_2$. The weighting function is expressed as an integrated time history of diffusion coefficient of $CO_2$ ($D_C$). In fact, Fc over the entire period can be obtained according to (3.27) from the time history data of surface (or canopy) $CO_2$ concentration and the time history data of $D_C$. Calculation of $F_C$ using (3.27) involves numerical computation of a singular integral as the weighting function is divergent at $\tau = t$. The input variables for computation of $F_C$ include time series of $CO_2$ concentration data and time series of diffusion coefficient using net radiation and surface (or near surface air) temperature data to compute sensible heat flux H**.**

### 3.4 Numerical Algorithm for Computing Surface Flux

Given the time-series data of $CO_2$ concentration at height z from canopy surface C ($t_i$, z), net radiation $R_n(t_i)$ and surface temperature at canopy $T_s(t_i)$ measured at discrete times $t_i$ ( $i = 1, \ldots, N$ , $t_1 = 0$) surface $CO_2$ flux $F_C$ (z, $t_i$ ) may be calculated using the following numerical algorithm. To remove singularity of the integrand, the double integral in (3.27) can be rewritten as

$$\int_0^t \frac{\delta C(z,\tau)}{\delta \tau}\left[\int_\tau^t D_C(z,\eta)d\eta\right]^{-\frac{1}{2}} d\tau = -2\int_0^t \frac{\delta C(z,\tau)}{\delta \tau}\frac{1}{D(z,\tau)} d\left[\int_\tau^t D_C(z,\eta)d\eta\right]^{\frac{1}{2}} , \quad (3.28)$$

The integral on right hand side of (3.28) is the Riemann-Stieltjes integral

$$\int_0^t f(\tau)d[g(\tau)] , \quad (3.29)$$

where,

$$f(\tau) = \int_0^t \frac{\delta C(z,\tau)}{\delta \tau}\frac{1}{D(z,\tau)} , \quad (3.30)$$

$$g(\tau) = \left[\int_\tau^t D_C(z,\eta)d\eta\right]^{\frac{1}{2}} , \quad (3.31)$$

The Riemann-Stieltjes integral may be numerically computed as

$$\int_0^t f(\tau)d[g(\tau)] = \sum_{i=1}^{N} f(t_i)[g(t_i) - g(t_{i-1})] \ , \tag{3.32}$$

where,

$$f(t_i) = \frac{C(z,t_i)-C(z,t_{i-1})}{t_i - t_{i-1}} \frac{1}{D(z,t_i)} \ , \tag{3.33}$$

$$g(t_i) = \left[\sum_{j=i+1}^{N} D_C\left(z,t_j\right)(t_j - t_{j-1})\right]^{\frac{1}{2}} \ , \tag{3.34}$$

$$g(t_{i-1}) = \left[\sum_{j=i}^{N} D_C\left(z,t_j\right)(t_j - t_{j-1})\right]^{\frac{1}{2}} \ , \tag{3.35}$$

## 3.5 Computing Turbulent Diffusion Coefficient

Computation of turbulent diffusion coefficient of $CO_2$, $D_C\,(z,t_i)$ at height z from canopy surface at discrete times $t_i$ ( $i = 1, \ldots, N$ , $t_1 = 0$) requires surface sensible heat flux $H(t_i)$ which is calculated using surface temperature at canopy $T_s(t_i)$ and net radiation $R_n(t_i)$ MEP Model described in Appendix B. According to (B9) sensible heat flux over canopy is expressed as,

$$H(t_i) = \frac{R_n(t_i)}{1+B(\sigma)} \ , \tag{3.36}$$

$$B(\sigma) = 6\left(\sqrt{1+\frac{11}{36}\sigma} - 1\right) , \tag{3.37}$$

$$\sigma = \frac{\lambda^2 q_s[\,T_s(t_i)]}{c_p R_v[\,T_s(t_i)]^2} \quad , \tag{3.38}$$

where, $T_s(t_i)$ is the temperature at canopy surface (K), $\lambda$ the latent heat of vaporization of liquid water (2.5 $\times 10^6$ J kg$^{-1}$ K$^{-1}$), $c_p$ the specific heat of air at constant pressure ($10^3$ J kg$^{-1}$K$^{-1}$) and $R_v$ is the gas constant of water vapor (461 J kg$^{-1}$K$^{-1}$). $q_s$ is the specific humidity at ground (or canopy) surface (kg kg$^{-1}$). $q_s$ is expressed in terms $T_s$ according to Clausius-Clapeyron equation

$$q_s[\,T_s(t_i)] = 0.62\ \left(\frac{e_0}{P_s}\right) \exp\left[\frac{\lambda}{R_v}\left(\frac{1}{T_0} - \frac{1}{T_s}\right)\right] \ , \tag{3.39}$$

where, $e_0$ is the saturation vapor pressure at (an arbitrary reference temperature $T_0$, $P_s$ is the surface atmospheric pressure (~$10^5$ Pa). At $T_0 = 273K, e_0 = 611\ Pa$.

## 3.6 Advantages of Proposed Model

The proposed model has several advantages. The model uses a single level $CO_2$ concentration data (at surface or canopy level) instead of $CO_2$ concentration gradient data that are subjected to greater measurement errors and modeling complexity. Second, the modeled $CO_2$ fluxes (3.27) is not sensitive to uncertainties of $CO_2$ diffusion coefficient (3.17). As parameterization of the $CO_2$ diffusion coefficient is has one-sixth power dependence of sensible heat flux. Third, the model is parsimonious not using near surface wind speed, surface roughness and vegetation specific data. Fourth, the model formulation facilitates its generalization from field scale to regional and global scale as all model input parameters namely, $CO_2$ concentration time series, net radiation time series and surface (or near surface air) temperature may be obtained from remote sensing observations.

These advantageous features results mainly from the parameterization of eddy diffusivity of $CO_2$ (3.13). The MEP model allows sensible heat flux to be derived from surface net radiation, surface temperature (and / or humidity) data. When field observations of these variables are not available a recently developed method (Moghim et al., 2014) may be used to obtain the field to regional scales from visible images of satellite data. Due to reduced sensitivity of the diffusion coefficient to sensible heat flux especially for the case of dense canopy, it would be sufficient to assume wet condition to calculate sensible heat flux only from net radiation and surface (or near surface air) temperature time series using MEP the model.

# CHAPTER 4

# MODEL TESTING

## 4.1 Test Sites

Field data of $CO_2$ concentration, net radiation and surface temperature over canopy measured at four sites (Clark et al., 2010; Liu et al., 2005; Saleska et al., 2003; and Scott et al., 2006) from AmeriFlux network provide the input of the proposed $CO_2$ flux model. The modeled $CO_2$ flux is compared with eddy-covariance $CO_2$ flux data. AmeriFlux sites are managed by the AmeriFlux Management Project (AMP) at Lawrence Berkeley National Laboratory (LBNL) supported by U.S. Department of Energy (DOE).

The test sites are selected with contrasting climatic, geographic, vegetation condition to assess the applicability of the model in diverse environments. The four sites are: Santarem KM67 Primary Forest, Brazil; Cedar Bridge, New Jersey, USA; Delta Junction 1920 Control, Alaska, USA and Walnut Gulch Lucky Hills Shrubland, Arizona, USA. Description of the sites are presented in Table 4.1.

**Table 4.1** Description of the study sites.

| Sites | Latitude, Longitude | Climate Condition | Vegetation Type |
|---|---|---|---|
| 1. Santarem KM67 Primary Forest, Brazil | -2.86°, -54.96° | Tropical monsoon, with mean annual temperature 26.13 °C and mean annual precipitation 2075 mm. | Evergreen Broad Leaf Forest |
| 2. Cedar Bridge, New Jersey, USA | 39.84°, -74.38° | Cool temperate, mean annual temperature 11.04 °C (with mean monthly temperatures of 0.3 °C in January and 23.8 8°C in June) and mean annual precipitation is 1123 mm (S.D. 82 mm). | Mixed Forest |
| 3. Delta Junction 1920 Control, Alaska, USA | 63.89°, -145.74° | Dry continental, mean annual temperature -2.3 °C, mean annual Rainfall : 304 mm, mean annual Snowfall: 940 mm | Evergreen Needle Leaf Forest |
| 4. Walnut Gulch Lucky Hills Shrubland, Arizona, USA | 31.74°, -110.052° | Temperate semi- arid with mean annual temperature 17.6 °C and mean annual precipitation 320 mm. | Open Shrub lands |

## 4.2 Results and Discussion

### 4.2.1 Site 1

Santarem KM67 Primary forest site (2.86˚S, 54.96˚W) is located in the Tapajos National Forest. This is a 450,000 ha closed-canopy upland forest in Brazilian Amazon with evergreen board leaf vegetation class and 45 m mean canopy height. The tropical climate is strongly influenced by the monsoon with annual mean temperature of 26.13˚C and mean precipitation of 2075 mm. A 5-month dry season (months with <100 mm of rainfall) that extends from July to December. The 64-m eddy covariance tower is located on a flat plateau (or planalto) that extends up to 150 km to the north, south, and east. Within the National Forest, anthropogenic disturbances are limited to a few small hunting trails. The surrounding stand is classified as primary or "old-growth"" predominantly by its uneven age distribution, emergent trees, numerous epiphytes and abundant large logs.

The model uses hourly time-series data of $CO_2$ concentration ($\mu mol\ mol^{-1}$), canopy surface temperature $T_s$ (˚C) and net radiation $R_n$ ($W\ m^{-2}$). Downward $CO_2$ flux (FC) as well as latent (E) and sensible (H) heat flux from the atmosphere to canopy surface are defined as negative. Ground heat flux (G) is defined negative from the surface into the soil layer. Due to dense canopy cover at this site the observed ground heat flux is very small. The MEP model as in (B8) – (B10) of appendix B is used to estimate H, which is used in parameterization of diffusion coefficient of $CO_2$, $D_c$. The distance above the canopy surface z is measured by the difference of mean canopy height

(45 m) and height of $CO_2$ measurement (64 m) is 19 m. Scattered missing data are filled using linear interpolation when the time interval between missing data are not very large (< 3 hours). The dataset is re-grouped into multiple no-gap time series to avoid larger gaps (> 3hrs) of the time-series records.

The comparison of modeled $CO_2$ flux using equation (3.27) with the observed eddy-covariance flux is characterized by the root-mean-square error (RMSE), the normalized root-mean-square error (NRMSE defined as the RMSE divided by the magnitude of the observed fluxes), correlation coefficient (covariance of the observed and modeled $CO_2$ fluxes divided by the product of their standard deviations) and regression coefficient (covariance of the observed and modeled $CO_2$ fluxes divided by the variance of observed $CO_2$ fluxes). The maximum and minimum observed fluxes over the test period and maximum and minimum modeled fluxes over test period are reported. As the MEP modeled sensible heat flux is used in the parameterization of eddy diffusivity of $CO_2$, the MEP modeled energy fluxes are compared with observed energy fluxes from eddy covariance measurements. This includes: root-mean-square error (RMSE), normalized root-mean-square error (NRMSE), correlation coefficient, maximum and minimum flux of the observed and MEP modeled heat fluxes over the test period. The results are shown in figures and tables followed by summary tables.

## Test Period 1: Day 1-8, 2003, Santarem KM67 Primary Forest, Brazil

**Table 4.2.1** Result summary for MEP modeled vs. observed sensible and latent heat fluxes at Santarem Primary Forest, Brazil. Day 1-8, 2003.

| Sensible Heat Flux (H) Statistics | | Latent Heat Flux (E) Statistics | |
|---|---|---|---|
| Correlation Coefficient | 0.935 | Correlation Coefficient | 0.937 |
| RMSE (W $m^{-2}$) | 27.62 | RMSE (W $m^{-2}$) | 65.64 |
| NRMSE | 0.1209 | NRMSE | 0.1585 |
| Max HOBS (W $m^{-2}$) | 189.28 | Max EOBS (W $m^{-2}$) | 404.83 |
| Min HOBS (W $m^{-2}$) | -39.07 | Min EOBS (W $m^{-2}$) | -9.195 |
| Max HMEP (W $m^{-2}$) | 201.35 | Max EMEP (W $m^{-2}$) | 552.50 |
| Min HMEP (W $m^{-2}$) | -13.12 | Min EMEP (W $m^{-2}$) | -33.74 |

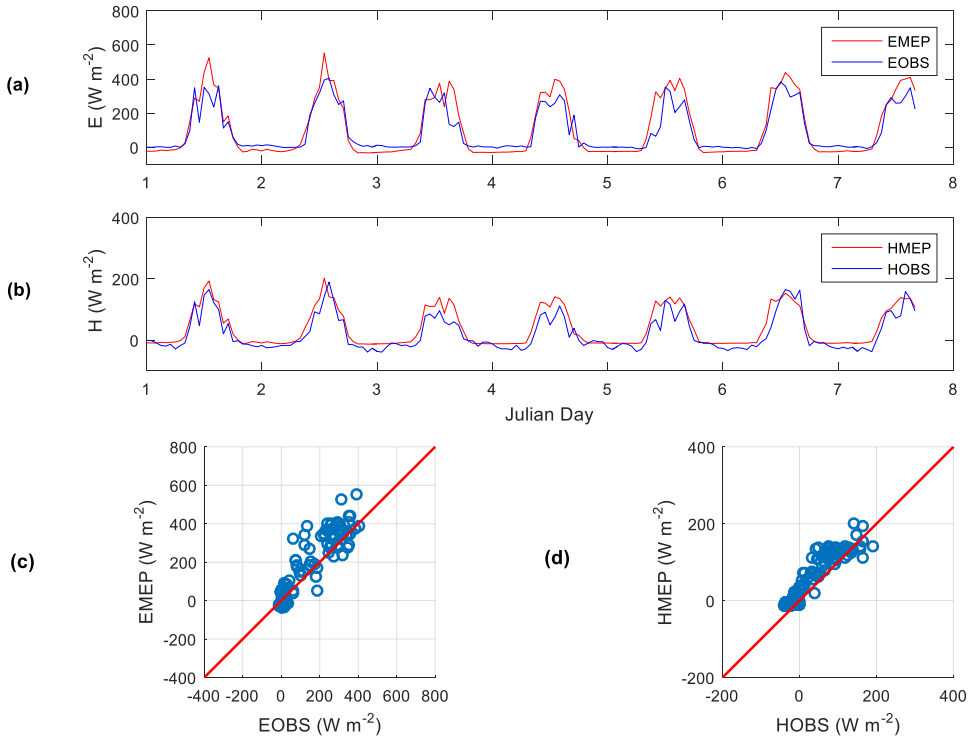


**Figure 4.2.1** (a) MEP model latent heat fluxes (EMEP) vs. observed latent heat fluxes (EOBS) (b) MEP model sensible heat fluxes (HMEP) vs. observed sensible heat fluxes (HOBS) (c) Scatter plot of EMEP vs. EOBS, (d) Scatter plot of HMEP vs. HOBS at Santarem Primary Forest, Brazil. Day 1-8, 2003.

**Table 4.2.2** Result summary for modeled vs. observed $CO_2$ fluxes at Santarem Primary Forest, Brazil. Day 1-8, 2003.

| $CO_2$ Flux (FC) Statistics | |
|---|---|
| RMSE ($\mu molm^{-2}s^{-1}$) | 6.36 |
| NRMSE | 0.1285 |
| Correlation Coefficient | 0.73 |
| Regression Coefficient | 0.66 |
| Max Modeled FC ($\mu molm^{-2}s^{-1}$) | 44.30 |
| Min Modeled FC ($\mu molm^{-2}s^{-1}$) | -35.49 |
| Max Observed FC ($\mu molm^{-2}s^{-1}$) | 23.76 |
| Min Observed FC ($\mu molm^{-2}s^{-1}$) | -25.77 |
| Number of Data Points | 168 |
| SD Observed FC ($\mu molm^{-2}s^{-1}$) | |
| MAE ($\mu molm^{-2}s^{-1}$) | |
| Max Observed $CO_2$($\mu$mol/mol) | |
| Min Observed $CO_2$($\mu$mol/mol) | |
| SD Observed $CO_2$($\mu$mol/mol) | |
| Mean Observed $CO_2$($\mu$mol/mol) | |

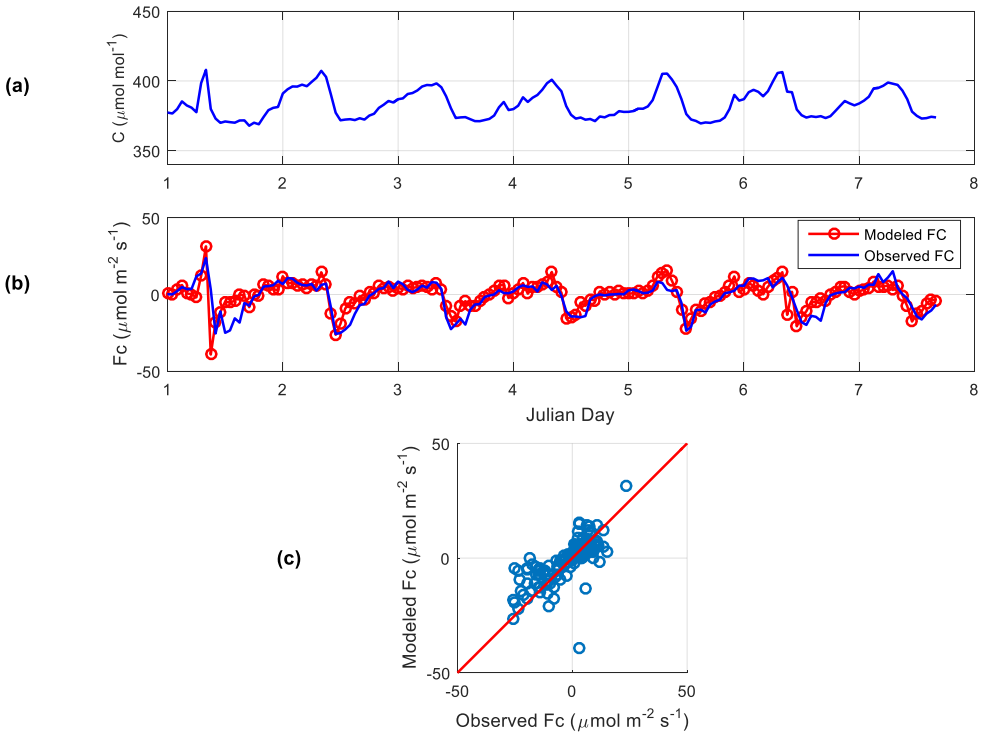


**Figure 4.2.2** (a) $CO_2$ profile, (b) Observed vs. modeled $CO_2$ fluxes, (c) Scatterplot of observed vs. modeled $CO_2$ fluxes at Santarem Primary Forest, Brazil. Day 1-8, 2003.

The modeled $CO_2$ fluxes using equation (3.27) well capture the diurnal variation and magnitude of the observed fluxes (Figure 4.2.2 (b)) during test period 1 (day 1 to 8, 2003). The RMSE and the NRMSE of the modeled $CO_2$ fluxes are 6.36 $\mu molm^{-2}s^{-1}$ and 12.85% respectively, with the $CO_2$ fluxes on the order of 49.53 $\mu mol\ m^{-2}\ s^{-1}$. The scatterplot of modeled vs. observed fluxes show good agreement (Figure 4.2.2 (c)) with correlation coefficient, 0.73 and regression coefficient, 0.66. The magnitudes of modeled fluxes are comparable to the observed fluxes except for a small number of points due to the linear interpolation of the missing $CO_2$ concentration data points (such as 398.54 μmol/mol to 407 μmol/mol) causing relatively large numerical errors of the calculated derivative term in (3.27) associated with large value maximum modeled flux (44.3 $\mu mol\ m^{-2}\ s^{-1}$). The MEP energy fluxes have correlation coefficients 0.935 and 0.937 for sensible heat (H) and latent heat (E) fluxes, respectively. The RMSE and NRMSE for this test period are 27.62 W $m^{-2}$ and 12% with the sensible heat fluxes on the order of 228.35 W $m^{-2}$. The RMSE and NRMSE for this test period are 65.64 W $m^{-2}$ and 15.85% with the latent heat fluxes on the order of 414 W $m^{-2}$.

## Test Period 2: Day 13-21, 2003, Santarem KM 67 Primary Forest, Brazil

**Table 4.2.3** Result summary for MEP modeled vs. observed sensible and latent heat fluxes at Santarem Primary Forest, Brazil. Day 13-21, 2003.

| Sensible Heat Flux (H) Statistics | | Latent Heat Flux (E) Statistics | |
|---|---|---|---|
| Correlation Coefficient | 0.919 | Correlation Coefficient | 0.945 |
| RMSE (W $m^{-2}$) | 27.94 | RMSE (W $m^{-2}$) | 62.85 |
| NRMSE | 0.0819 | NRMSE | 0.1341 |
| Max HOBS (W $m^{-2}$) | 298.95 | Max EOBS (W $m^{-2}$) | 459.99 |
| Min HOBS (W $m^{-2}$) | -42.33 | Min EOBS (W $m^{-2}$) | -8.744 |
| Max HMEP (W $m^{-2}$) | 188.98 | Max EMEP (W $m^{-2}$) | 533.57 |
| Min HMEP (W $m^{-2}$) | -11.01 | Min EMEP (W $m^{-2}$) | -29.17 |

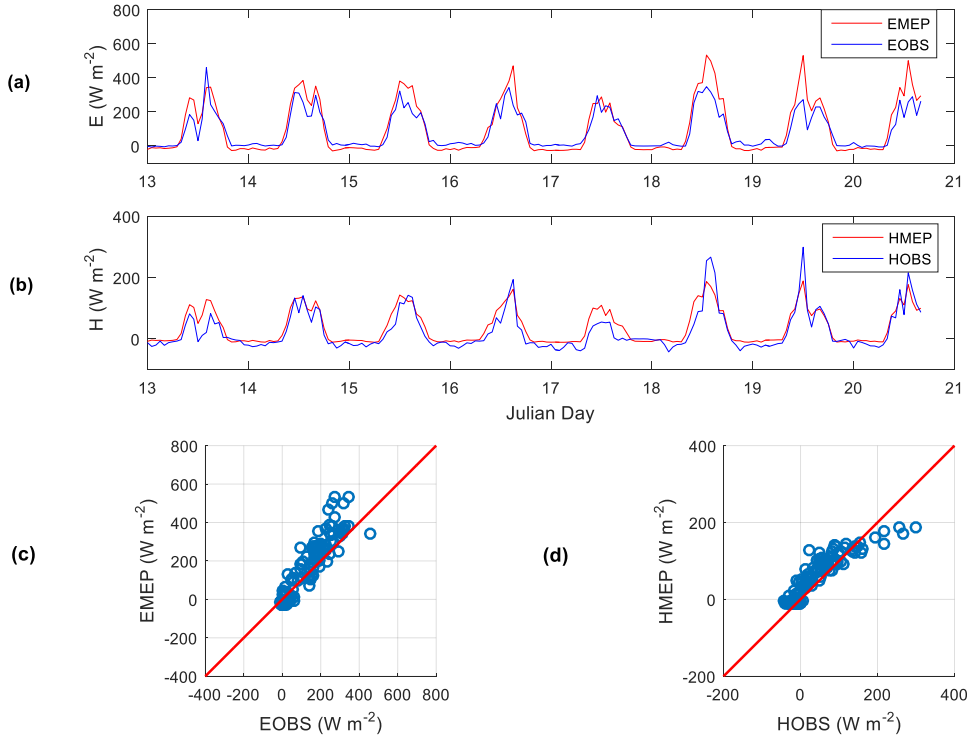


**Figure 4.2.3** (a) MEP model latent heat fluxes (EMEP) vs. observed latent heat fluxes (EOBS) (b) MEP model sensible heat fluxes (HMEP) vs. observed sensible heat fluxes (HOBS) (c) Scatter plot of EMEP vs. EOBS, (d) Scatter plot of HMEP vs. HOBS at Santarem KM67 Primary Forest, Brazil. Day 13-21, 2003.

**Table 4.2.3** Result summary for MEP modeled vs. observed sensible and latent heat fluxes at Santarem Primary Forest, Brazil. Day 13-21, 2003.

| $CO_2$ Flux (FC) Statistics | |
|---|---|
| RMSE ($\mu molm^{-2}s^{-1}$) | 8.386 |
| NRMSE | 0.1981 |
| Correlation Coefficient | 0.422 |
| Regression Coefficient | 0.396 |
| Max Modeled FC ($\mu molm^{-2}s^{-1}$) | 59.71 |
| Min Modeled FC ($\mu molm^{-2}s^{-1}$) | -27.97 |
| Max Observed FC ($\mu molm^{-2}s^{-1}$) | 17.01 |
| Min Observed FC ($\mu molm^{-2}s^{-1}$) | -25.33 |
| Number of Data Points | 189 |

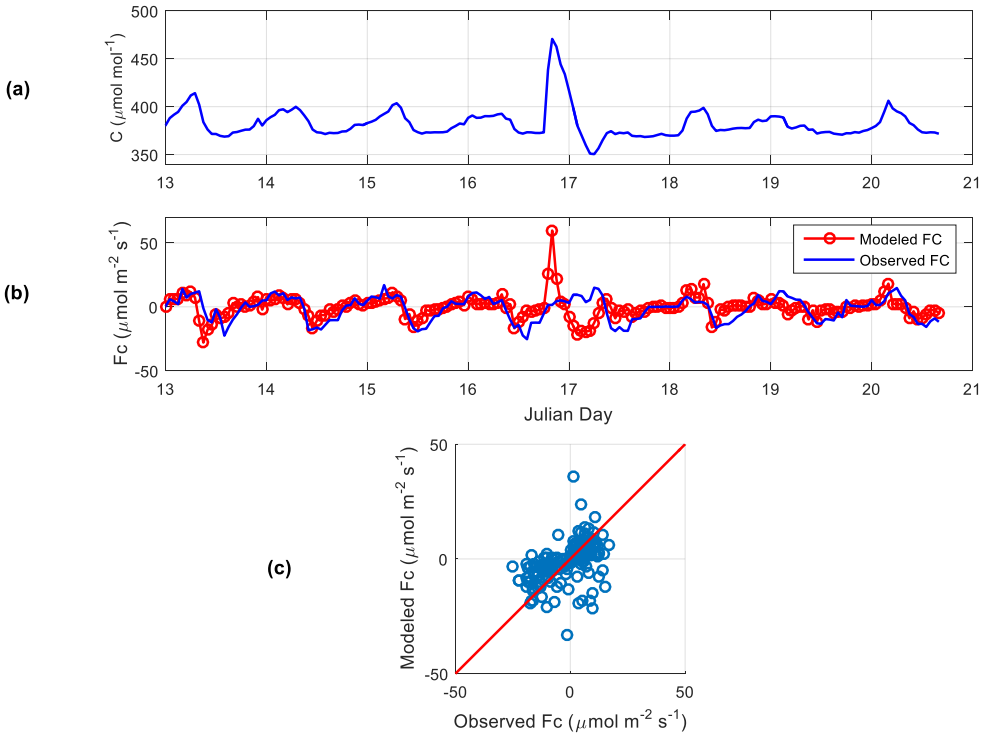


**Figure 4.2.4** (a) $CO_2$ profile, (b) Observed vs. modeled $CO_2$ fluxes, (c) Scatterplot of observed vs. modeled $CO_2$ fluxes at Santarem Primary Forest, Brazil. Day 13-21, 2003.

Test period 2 (day 13 to 21, 2003) contains a large $CO_2$ concentration spike (470.65 μmol/mol) during day 16-17 (Figure 4.2.4 (a)) which causes large value maximum modeled flux (59.71μmol $m^{-2}$ $s^{-1}$) (Figure 4.2.4 (b)). The scatterplot shows outliers (Figure 4.2.4 (c)) causing reduced correlation coefficient, 0.422 and regression coefficient, 0.396. The RMSE and the NRMSE of the modeled $CO_2$ fluxes are 8.386 μmol$m^{-2}s^{-1}$ and 19.81% with the $CO_2$ fluxes on the order of 42 μmol $m^{-2}$ $s^{-1}$ for this period. The MEP energy fluxes have correlation coefficients 0.919 and 0.945 for sensible heat (H) and latent heat (E) fluxes respectively. The RMSE and NRMSE for this test period are 27.94 W $m^{-2}$ and 8.19% with the sensible heat fluxes on the order of 341 W $m^{-2}$. The RMSE and NRMSE for this test period are 62.85 W $m^{-2}$ and 13.41% with the latent heat fluxes on the order of 468 W $m^{-2}$.

## Test Period 3: Day 33-43, 2003, Santarem KM 67 Primary Forest, Brazil

**Table 4.2.5** Result summary for MEP modeled vs. observed sensible and latent heat fluxes at Santarem Primary Forest, Brazil. Day 33-43, 2003.

| Sensible Heat Flux (H) Statistics | | Latent Heat Flux (E) Statistics | |
|---|---|---|---|
| Correlation Coefficient | 0.9351 | Correlation Coefficient | 0.9421 |
| RMSE (W $m^{-2}$) | 26.21 | RMSE (W $m^{-2}$) | 55.30 |
| NRMSE | 0.0869 | NRMSE | 0.1381 |
| Max HOBS (W $m^{-2}$) | 239.50 | Max EOBS (W $m^{-2}$) | 382.645 |
| Min HOBS (W $m^{-2}$) | -62.09 | Min EOBS (W $m^{-2}$) | -17.81 |
| Max HMEP (W $m^{-2}$) | 187.96 | Max EMEP (W $m^{-2}$) | 499.746 |
| Min HMEP (W $m^{-2}$) | -10.57 | Min EMEP (W $m^{-2}$) | -27.72 |

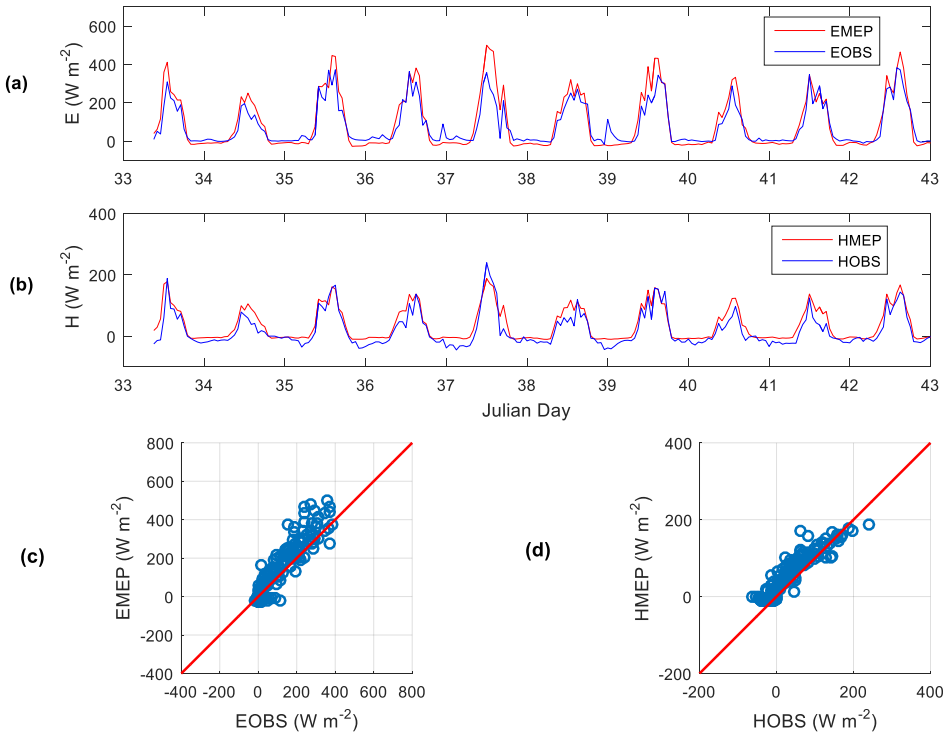


**Figure 4.2.5** (a) MEP model latent heat fluxes (EMEP) vs. observed latent heat fluxes (EOBS) (b) MEP model sensible heat fluxes (HMEP) vs. observed sensible heat fluxes (HOBS) (c) Scatter plot of EMEP vs. EOBS, (d) Scatter plot of HMEP vs. HOBS at Santarem Primary Forest, Brazil. Day 33-43, 2003.

**Table 4.2.6** Result summary for modeled vs. observed $CO_2$ fluxes at Santarem Primary Forest, Brazil. Day 33-43, 2003.

| $CO_2$ Flux (FC) Statistics | |
|---|---|
| RMSE ($\mu molm^{-2}s^{-1}$) | 7.52 |
| NRMSE | 0.1263 |
| Correlation Coefficient | 0.71 |
| Regression Coefficient | 0.56 |
| Max Modeled FC ($\mu molm^{-2}s^{-1}$) | 23.26 |
| Min Modeled FC ($\mu molm^{-2}s^{-1}$) | -39.429 |
| Max Observed FC ($\mu molm^{-2}s^{-1}$) | 32.347 |
| Min Observed FC ($\mu molm^{-2}s^{-1}$) | -27.133 |
| Number of Data Points | 248 |

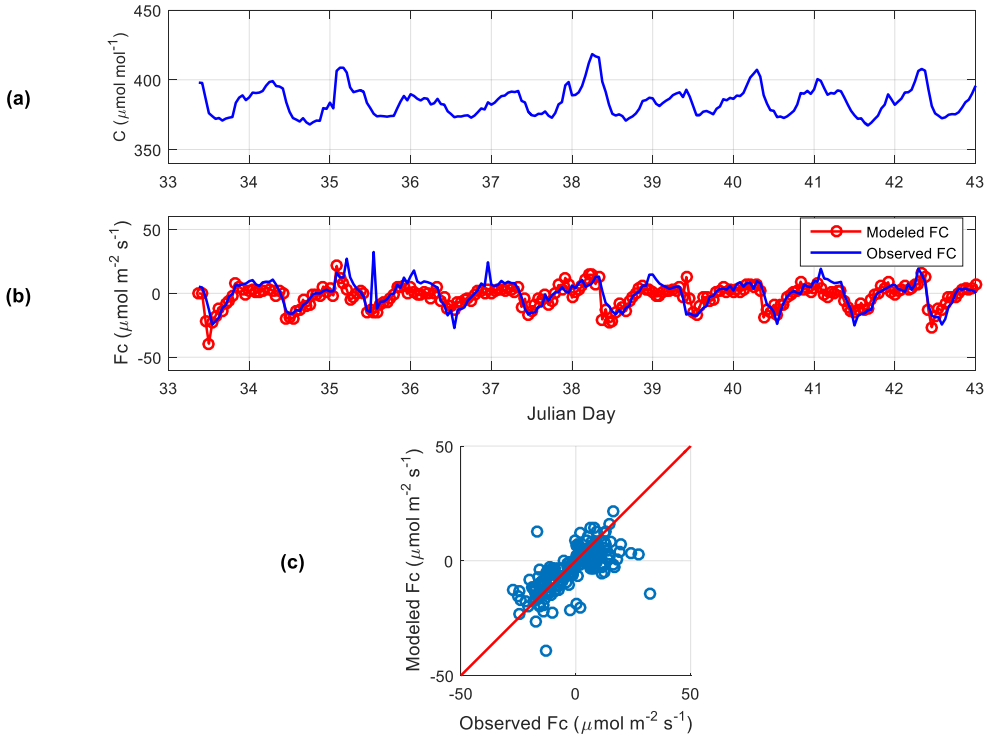


**Figure 4.2.6** (a) $CO_2$ profile, (b) Observed vs. modeled $CO_2$ fluxes, (c) Scatterplot of observed vs. modeled $CO_2$ fluxes at Santarem Primary Forest, Brazil. Day 33-43, 2003.

Test period 3 starts from day 33 to 43, 2003. During this period modeled fluxes show good agreement with observation with the correlation coefficient, 0.71 and s regression coefficient, 0.56. Except for day 35 the observed maximum $CO_2$ flux during this period, 32.347 $\mu molm^{-2}s^{-1}$ (Figure 4.2.6 (b)) is erroneous as it was measured at 1 PM during daytime (when the photosynthesis occurs) which is inconsistent with observed flux at 12 PM, -14.663 $\mu molm^{-2}s^{-1}$ and 2 PM, -11.921 $\mu molm^{-2}s^{-1}$. The modeled $CO_2$ flux at 1 PM (-13.761 $\mu molm^{-2}s^{-1}$) shows consistency with observed fluxes at 12 PM and 2 PM. The RMSE and the NRMSE of the modeled $CO_2$ fluxes during this period is 7.52 $\mu molm^{-2}s^{-1}$ and 12.63% respectively, with the $CO_2$ fluxes on the order of 59.48 $\mu mol\ m^{-2}\ s^{-1}$. The MEP energy fluxes have correlation coefficients 0.9351 and 0.9421 for sensible heat (H) and latent heat (E) fluxes respectively. The RMSE and NRMSE for this test period are 26.21 W $m^{-2}$ and 8.69% with the sensible heat fluxes on the order of 301.59 W $m^{-2}$. The RMSE and NRMSE for this test period are 55.30 W $m^{-2}$ and 13.81% with the latent heat fluxes on the order of 400 W $m^{-2}$.

## Test Period 4: Day 40-50, 2003, Santarem KM 67 Primary Forest, Brazil

**Table 4.2.7** Result summary for MEP modeled vs. observed sensible and latent heat fluxes at Santarem Primary Forest, Brazil. Day 40-50, 2003.

| Sensible Heat Flux (H) Statistics | | Latent Heat Flux (E) Statistics | |
|---|---|---|---|
| Correlation Coefficient | 0.866 | Correlation Coefficient | 0.941 |
| RMSE (W $m^{-2}$) | 30.16 | RMSE (W $m^{-2}$) | 44.74 |
| NRMSE | 0.1225 | NRMSE | 0.1099 |
| Max HOBS (W $m^{-2}$) | 165.77 | Max EOBS (W $m^{-2}$) | 382.65 |
| Min HOBS (W $m^{-2}$) | -80.38 | Min EOBS (W $m^{-2}$) | -24.47 |
| Max HMEP (W $m^{-2}$) | 173.99 | Max EMEP (W $m^{-2}$) | 464.48 |
| Min HMEP (W $m^{-2}$) | -9.33 | Min EMEP (W $m^{-2}$) | -24.95 |

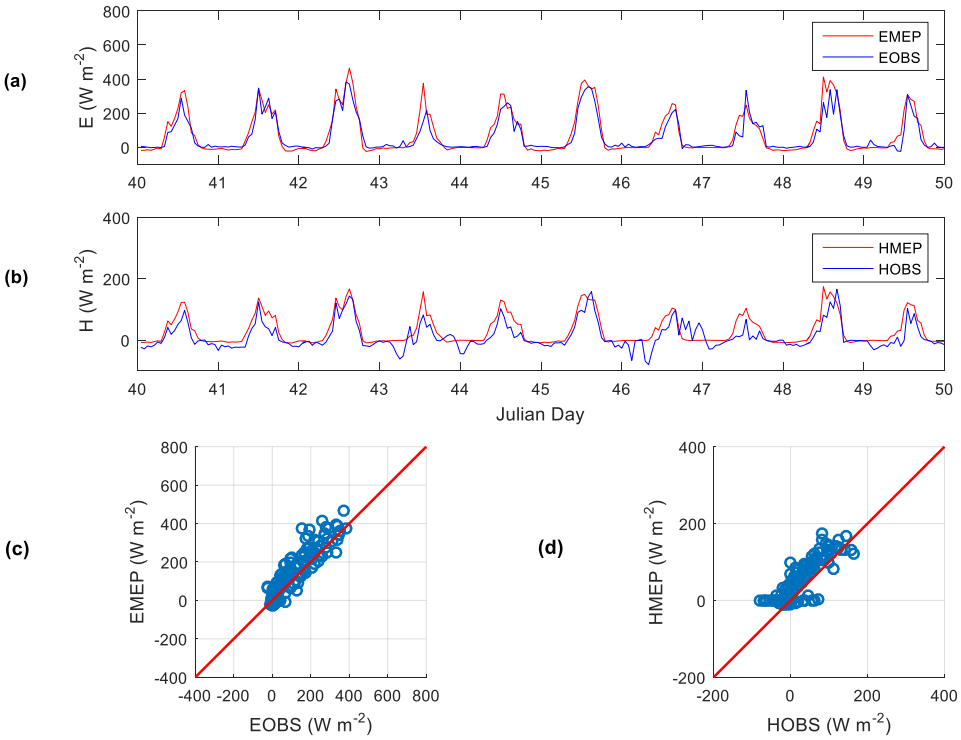


**Figure 4.2.7** (a) MEP model latent heat fluxes (EMEP) vs. observed latent heat fluxes (EOBS) (b) MEP model sensible heat fluxes (HMEP) vs. observed sensible heat fluxes (HOBS) (c) Scatter plot of EMEP vs. EOBS, (d) Scatter plot of HMEP vs. HOBS at Santarem Primary Forest, Brazil. Day 40-50, 2003.

**Table 4.2.8** Result summary for modeled vs. observed $CO_2$ fluxes at Santarem Primary Forest, Brazil. Day 40-50, 2003.

| $CO_2$ Flux (FC) Statistics | |
|---|---|
| RMSE ($\mu molm^{-2}s^{-1}$) | 7.90 |
| NRMSE | 0.1646 |
| Correlation Coefficient | 0.55 |
| Regression Coefficient | 0.70 |
| Max Modeled FC ($\mu molm^{-2}s^{-1}$) | 71.91 |
| Min Modeled FC ($\mu molm^{-2}s^{-1}$) | -73.71 |
| Max Observed FC ($\mu molm^{-2}s^{-1}$) | 22.86 |
| Min Observed FC ($\mu molm^{-2}s^{-1}$) | -25.13 |
| Number of Data Points | 226 |

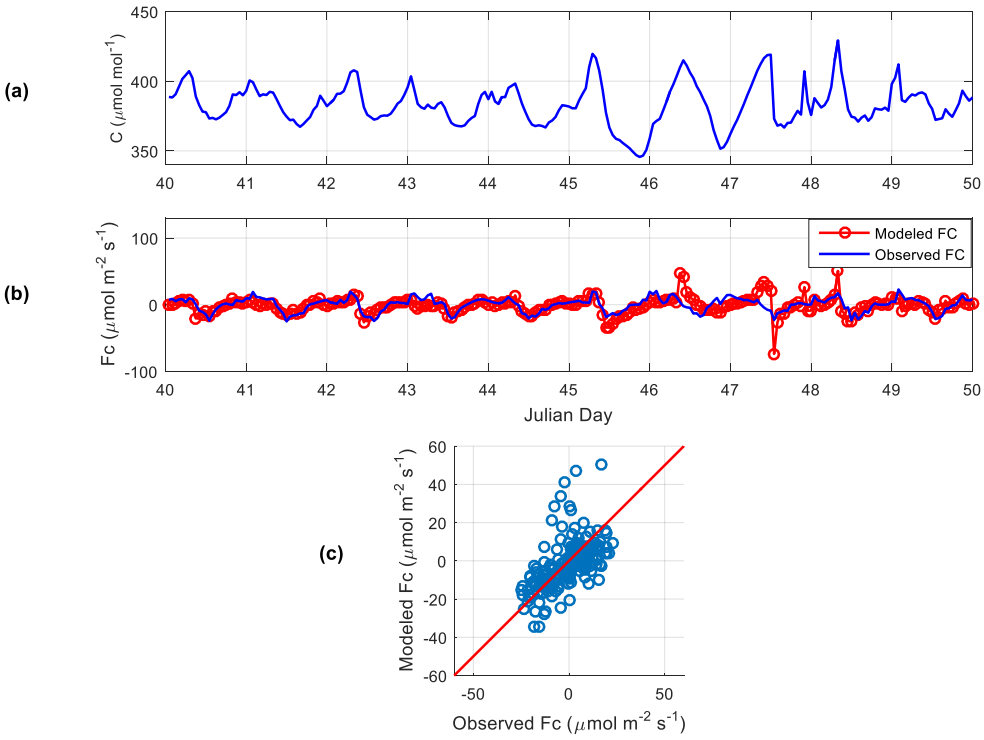


**Figure 4.2.8** (a) $CO_2$ profile, (b) Observed vs. modeled $CO_2$ fluxes, (c) Scatterplot of observed vs. modeled $CO_2$ fluxes at Santarem Primary Forest, Brazil. Day 40-50, 2003.

Test period 4 (day 40 to 50, 2003) shows good agreement between modeled and observed fluxes till day 46 (Figure 4.2.8 a, b). The spurious spikes in $CO_2$ concentration data (> 400 to 429 μmol/mol) during 8 AM to 12 PM occur consistently during day 46, 47 and 48 leading to relatively large numerical errors of the calculated derivative term in (3.27) which causes large value maximum modeled flux (71.91 μmol $m^{-2}$ $s^{-1}$) in day 48. Such spikes followed by large drop (419.007 μmol/mol to 373.01 μmol/mol) causes small value in minimum modeled flux (-73.71 μmol $m^{-2}$ $s^{-1}$) on day 47. The scatterplot of modeled vs. observed $CO_2$ flux shows some spread (Figure 4.2.8 (c)) with correlation coefficient, 0.55 and regression coefficient, 0.7 for this period. The RMSE and the NRMSE of the modeled $CO_2$ fluxes are 7.90 μmol$m^{-2}s^{-1}$ and 16.46 % with the $CO_2$ fluxes on the order of 47.99 μmol $m^{-2}$ $s^{-1}$. The MEP energy fluxes have correlation coefficients 0.866 and 0.941 for sensible heat (H) and latent heat (E) fluxes respectively. The RMSE and NRMSE for this test period are 30.16 W $m^{-2}$ and 12.25 % with the sensible heat fluxes on the order of 246 W $m^{-2}$. The RMSE and NRMSE for this test period are 44.74 W $m^{-2}$ and 10.99 % with the latent heat fluxes on the order of 407.12 W $m^{-2}$.

## Test Period 5: Day 56-70, 2003, Santarem KM 67 Primary Forest, Brazil

**Table 4.2.9** Result summary for MEP modeled vs. observed sensible and latent heat fluxes at Santarem Primary Forest, Brazil. Day 55-70, 2003.

| Sensible Heat Flux (H) Statistics | | Latent Heat Flux (E) Statistics | |
|---|---|---|---|
| Correlation Coefficient | 0.932 | Correlation Coefficient | 0.951 |
| RMSE (W $m^{-2}$) | 28.77 | RMSE (W $m^{-2}$) | 51.43 |
| NRMSE | 0.1093 | NRMSE | 0.1133 |
| Max HOBS (W $m^{-2}$) | 212.02 | Max EOBS (W $m^{-2}$) | 439.32 |
| Min HOBS (W $m^{-2}$) | -51.26 | Min EOBS (W $m^{-2}$) | -14.74 |
| Max HMEP (W $m^{-2}$) | 189.2 | Max EMEP (W $m^{-2}$) | 487.91 |
| Min HMEP (W $m^{-2}$) | -10.64 | Min EMEP (W $m^{-2}$) | -26.26 |

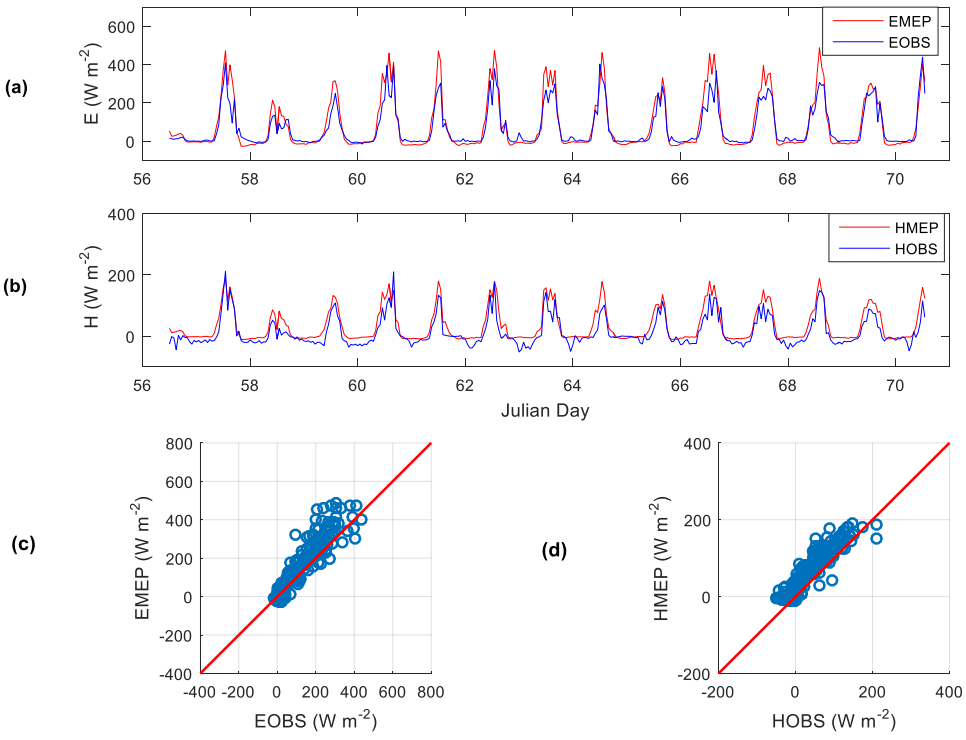


**Figure 4.2.9** (a) MEP model latent heat fluxes (EMEP) vs. observed latent heat fluxes (EOBS) (b) MEP model sensible heat fluxes (HMEP) vs. observed sensible heat fluxes (HOBS) (c) Scatter plot of EMEP vs. EOBS, (d) Scatter plot of HMEP vs. HOBS at Santarem Primary Forest, Brazil. Day 56-70, 2003.

**Table 4.2.10** Result summary for modeled vs. observed $CO_2$ fluxes at Santarem Primary Forest, Brazil. Day 55-70, 2003.

| $CO_2$ Flux (FC) Statistics | |
|---|---|
| RMSE (μmolm$^{-2}$s$^{-1}$) | 7.57 |
| NRMSE | 0.1267 |
| Correlation Coefficient | 0.72 |
| Regression Coefficient | 0.54 |
| Max Modeled FC (μmolm$^{-2}$s$^{-1}$) | 33.84 |
| Min Modeled FC (μmolm$^{-2}$s$^{-1}$) | -32.69 |
| Max Observed FC (μmolm$^{-2}$s$^{-1}$) | 29.19 |
| Min Observed FC (μmolm$^{-2}$s$^{-1}$) | -30.52 |
| Number of Data Points | 338 |

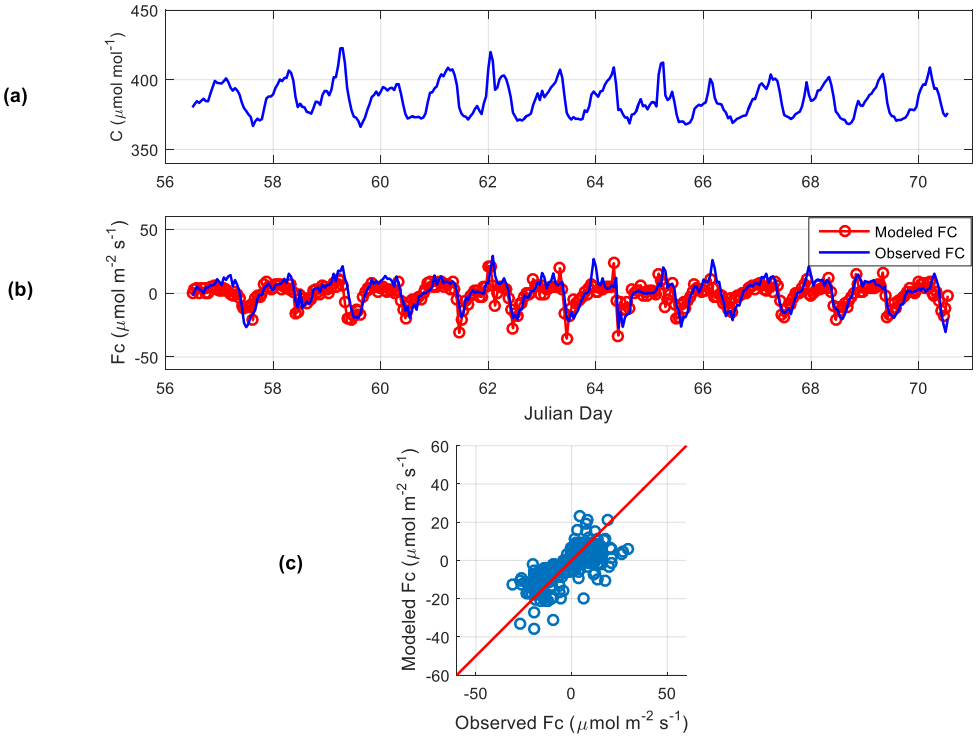


**Figure 4.2.10** (a) $CO_2$ profile, (b) Observed vs. modeled $CO_2$ fluxes, (c) Scatterplot of observed vs. modeled $CO_2$ fluxes at Santarem Primary Forest, Brazil. Day 55-70, 2003.

The modeled $CO_2$ flux during test period 5 (day 55 to 70) well captures the diurnal variation and magnitude of the observed fluxes (Figure 4.2.10 (b)). During this period, the maximum and minimum modeled fluxes (33.84 μmol $m^{-2}$ $s^{-1}$ and -32.69 μmol $m^{-2}$ $s^{-1}$) are comparable to maximum and minimum observed fluxes (29.19 μmol $m^{-2}$ $s^{-1}$ and -30.52 μmol $m^{-2}$ $s^{-1}$) respectively. The scatterplot shows good agreement between the modeled and observed fluxes (Figure 4.2.10 (c)) with correlation coefficient, 0.72 and regression coefficient, 0.54. The RMSE and the NRMSE of the modeled $CO_2$ fluxes are 7.57 μmol$m^{-2}s^{-1}$ and 12.67 % with the $CO_2$ fluxes on the order of 59.71 μmol $m^{-2}$ $s^{-1}$. The MEP energy fluxes have correlation coefficients 0.932 and 0.951 for sensible heat (H) and latent heat (E) fluxes respectively. The RMSE and NRMSE for this test period are 28.77 W $m^{-2}$ and 10.93 % with the sensible heat fluxes on the order of 263.28 W $m^{-2}$. The RMSE and NRMSE for this test period are 51.43 W $m^{-2}$ and 11.33 % with the latent heat fluxes on the order of 454.06 W $m^{-2}$.

## Test Period 6: Day 73-87, 2003, Santarem KM 67 Primary Forest, Brazil

**Table 4.2.11** Result summary for MEP modeled vs. observed sensible and latent heat fluxes at Santarem Primary Forest, Brazil. Day 73-87, 2003.

| Sensible Heat Flux (H) Statistics | | Latent Heat Flux (E) Statistics | |
|---|---|---|---|
| Correlation Coefficient | 0.923 | Correlation Coefficient | 0.925 |
| RMSE (W $m^{-2}$) | 27.32 | RMSE (W $m^{-2}$) | 57.56 |
| NRMSE | 0.0829 | NRMSE | 0.1002 |
| Max HOBS (W $m^{-2}$) | 273.78 | Max EOBS (W $m^{-2}$) | 561.86 |
| Min HOBS (W $m^{-2}$) | -55.61 | Min EOBS (W $m^{-2}$) | -12.91 |
| Max HMEP (W $m^{-2}$) | 211.91 | Max EMEP (W $m^{-2}$) | 580.99 |
| Min HMEP (W $m^{-2}$) | -10.41 | Min EMEP (W $m^{-2}$) | -24.39 |

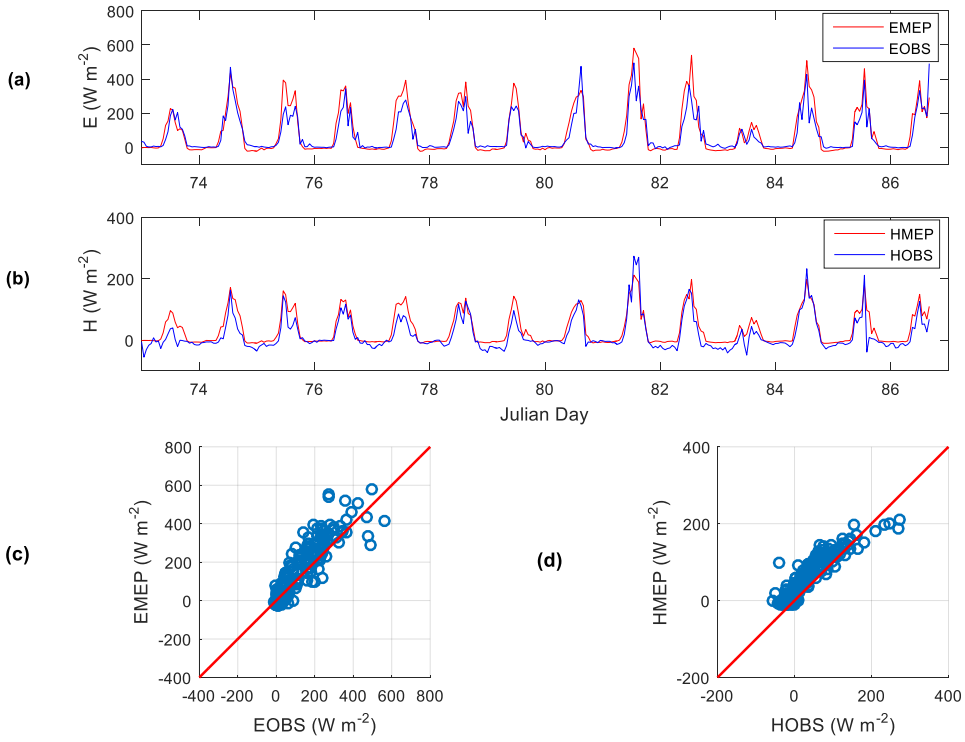


**Figure 4.2.11** (a) MEP model latent heat fluxes (EMEP) vs. observed latent heat fluxes (EOBS) (b) MEP model sensible heat fluxes (HMEP) vs. observed sensible heat fluxes (HOBS) (c) Scatter plot of EMEP vs. EOBS, (d) Scatter plot of HMEP vs. HOBS at Santarem Primary Forest, Brazil. Day 73-87, 2003.

**Table 4.2.12** Result summary for modeled vs. observed $CO_2$ fluxes at Santarem Primary Forest, Brazil. Day 73-87, 2003.

| $CO_2$ Flux (FC) Statistics | |
|---|---|
| RMSE (μmolm$^{-2}$s$^{-1}$) | 6.98 |
| NRMSE | 0.1475 |
| Correlation Coefficient | 0.63 |
| Regression Coefficient | 0.714 |
| Max Modeled FC (μmolm$^{-2}$s$^{-1}$) | 63.67 |
| Min Modeled FC (μmolm$^{-2}$s$^{-1}$) | -37.83 |
| Max Observed FC (μmolm$^{-2}$s$^{-1}$) | 19.93 |
| Min Observed FC (μmolm$^{-2}$s$^{-1}$) | -27.38 |
| Number of Data Points | 325 |

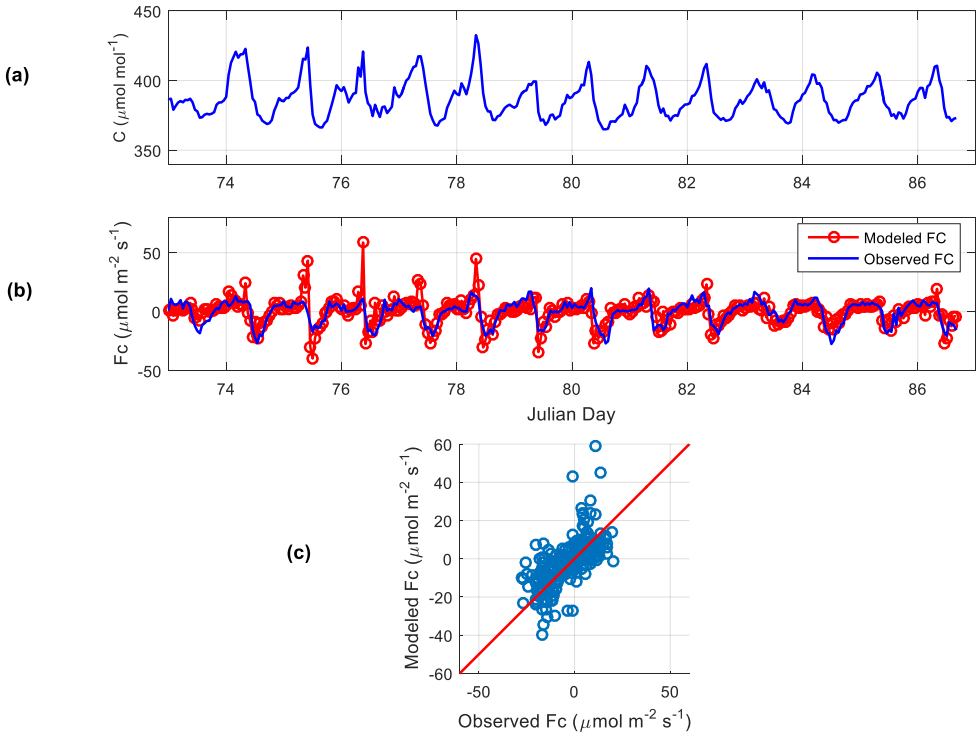


**Figure 4.2.12** (a) $CO_2$ profile, (b) Observed vs. modeled $CO_2$ fluxes, (c) Scatterplot of observed vs. modeled $CO_2$ fluxes at Santarem Primary Forest, Brazil. Day 73-87, 2003.

The modeled $CO_2$ fluxed shows good agreement during test period 6 (day 73 to 87, 2003) except day 73 to 78 during hours 3 AM to 10 AM when the spikes in CO2 concentration occurred (> 410 μmol/mol to 429 μmol/mol) causing spikes in modeled fluxes (Figure 4.2.12 (a), (b)). The spikes in $CO_2$ concentration (416.057 μmol/mol to 432.594 μmol/mol) leading to relatively large numerical errors of the calculative derivative term in (3.27) which causes large value maximum modeled flux (63.67 μmol $m^{-2}$ $s^{-1}$) during day 76 (Figure 4.2.12 (a), (b)). The correlation coefficient, 0.63 and regression coefficient, 0.714 during this period. The RMSE and the NRMSE of the modeled $CO_2$ fluxes are 6.98 $\mu molm^{-2}s^{-1}$ and 14.75 % with the $CO_2$ fluxes on the order of 47.31 μmol $m^{-2}$ $s^{-1}$ for test period 6 (day 73 to 87, 2003). The MEP energy fluxes have correlation coefficients 0.931 and 0.937 for sensible heat (H) and latent heat (E) fluxes respectively. The RMSE and NRMSE for this test period are 27.87 W $m^{-2}$ and 8.76 % with the observed sensible heat fluxes on the order of 329.39 W $m^{-2}$. The RMSE and NRMSE for this test period are 60.22 W $m^{-2}$ and 9.61 % with the observed latent heat fluxes on the order of 574.77 W $m^{-2}$.

## Test Period 7: Day 88-140, 2003, Santarem KM 67 Primary Forest, Brazil

**Table 4.2.13** Result summary for MEP modeled vs. observed sensible and latent heat fluxes at Santarem Primary Forest, Brazil. Day 88-140, 2003

| Sensible Heat Flux (H) Statistics | | Latent Heat Flux (E) Statistics | |
|---|---|---|---|
| Correlation Coefficient | 0.931 | Correlation Coefficient | 0.937 |
| RMSE (W $m^{-2}$) | 27.87 | RMSE (W $m^{-2}$) | 60.22 |
| NRMSE | 0.0876 | NRMSE | 0.0961 |
| Max HOBS (W $m^{-2}$) | 246.29 | Max EOBS (W $m^{-2}$) | 594.02 |
| Min HOBS (W $m^{-2}$) | -71.90 | Min EOBS (W $m^{-2}$) | -32.59 |
| Max HMEP (W $m^{-2}$) | 219.58 | Max EMEP (W $m^{-2}$) | 594.72 |
| Min HMEP (W $m^{-2}$) | -11.12 | Min EMEP (W $m^{-2}$) | -28.23 |

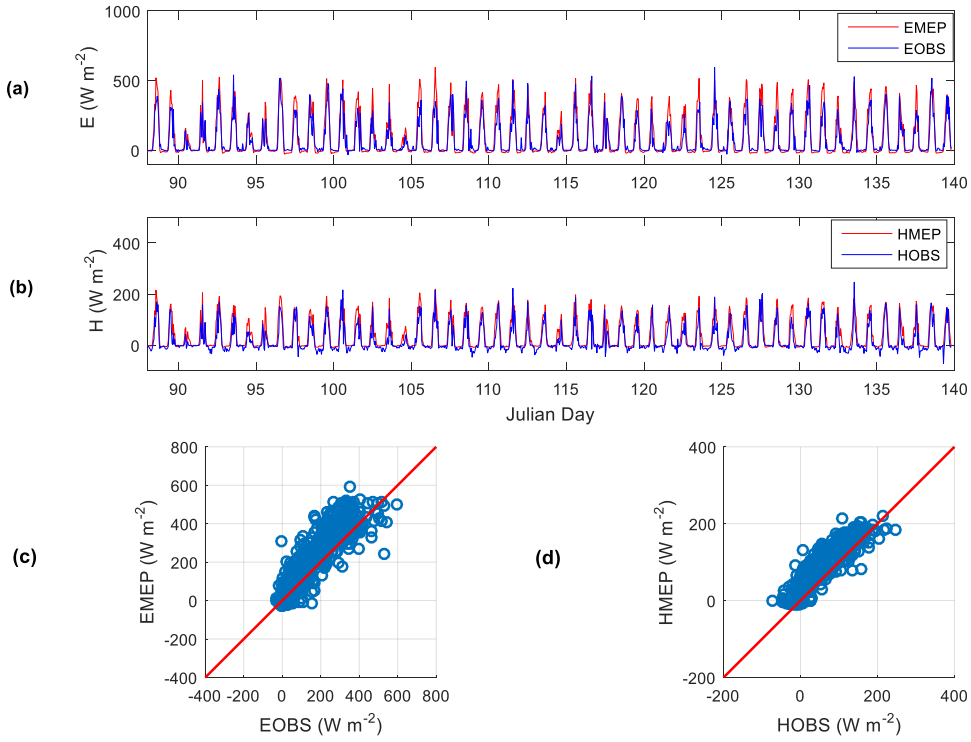


**Figure 4.2.13** (a) MEP model latent heat fluxes (EMEP) vs. observed latent heat fluxes (EOBS) (b) MEP model sensible heat fluxes (HMEP) vs. observed sensible heat fluxes (HOBS) (c) Scatter plot of EMEP vs. EOBS, (d) Scatter plot of HMEP vs. HOBS at Santarem Primary Forest, Brazil. Day 88-140, 2003.

**Table 4.2.14** Result summary for modeled vs. observed $CO_2$ fluxes at Santarem Primary Forest, Brazil. Day 88-140, 2003

.

| $CO_2$ Flux (FC) Statistics | |
|---|---|
| RMSE ($\mu molm^{-2}s^{-1}$) | 6.66 |
| NRMSE | 0.1023 |
| Correlation Coefficient | 0.63 |
| Regression Coefficient | 0.752 |
| Max Modeled FC ($\mu molm^{-2}s^{-1}$) | 107.2 |
| Min Modeled FC ($\mu molm^{-2}s^{-1}$) | -59.53 |
| Max Observed FC ($\mu molm^{-2}s^{-1}$) | 29.52 |
| Min Observed FC ($\mu molm^{-2}s^{-1}$) | -35.6 |
| Number of Data Points | 1227 |

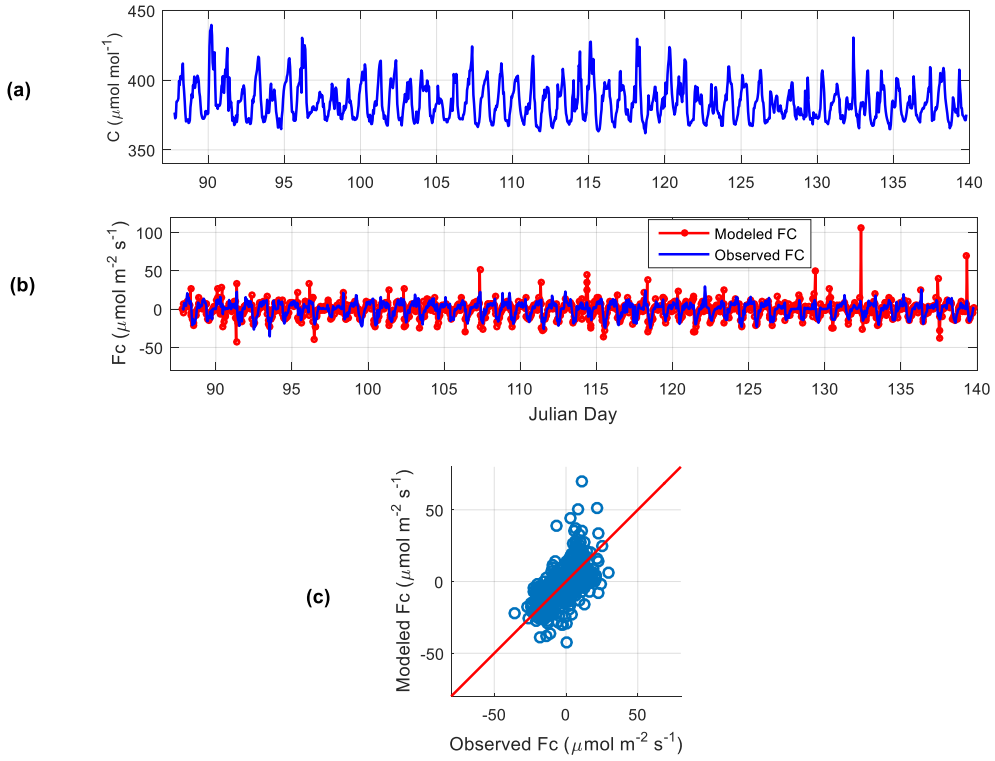


**Figure 4.2.14** (a) $CO_2$ profile, (b) Observed vs. modeled $CO_2$ fluxes, (c) Scatterplot of observed vs. modeled $CO_2$ fluxes at Santarem Primary Forest, Brazil. Day 88 -140, 2003.

Test period 7 starts from day 88 to 140, 2003 and contains 1249 data points. Similar to test period 6, this period contains $CO_2$ concentration spikes (> 410 μmol/mol) during 2 AM to 6 AM in day 88, 90, 91, 93, 95, 96, 100, 101, 102, 107, 109, 111, 114, 115, 118, 120, 121 and 132 (Figure 4.2.14 (a)) causing spikes in modeled fluxes (Figure 4.2.14 (b)). The spikes in $CO_2$ concentration (388.814 μmol/mol to 430.5 μmol/mol) leading to relatively large numerical errors of the calculative derivative term in (3.27) which causes large value maximum modeled flux (107.2 μmol $m^{-2}$ $s^{-1}$) in day 132. Such spikes followed by large drop (392.987 μmol/mol to 378.02 μmol/mol) causes small value in minimum modeled flux (-59.5333 μmol $m^{-2}$ $s^{-1}$) in day 91. The correlation coefficient, 0.63 and regression coefficient, 0.752 during this period. The RMSE and the NRMSE of the modeled $CO_2$ flux are 6.66 μmol$m^{-2}s^{-1}$ and 10.23 % with the $CO_2$ fluxes on the order of 65.12 μmol $m^{-2}$ $s^{-1}$. The MEP energy fluxes have correlation coefficients 0.931and 0.937 for sensible heat (H) and latent heat (E) fluxes respectively. The RMSE and NRMSE for this test period are 27.87 W $m^{-2}$ and 8.76 % with the sensible heat fluxes on the order of 318.19 W $m^{-2}$. The RMSE and NRMSE for this test period are 60.22 W $m^{-2}$ and 9.61 % with the latent heat fluxes on the order of 626.61 W $m^{-2}$.

## Test Period 8: Day 153-170, 2003, Santarem KM 67 Primary Forest, Brazil

**Table 4.2.15** Result summary for MEP modeled vs. observed sensible and latent heat fluxes at Santarem Primary Forest, Brazil. Day 153-170, 2003.

| Sensible Heat Flux (H) Statistics | | Latent Heat Flux (E) Statistics | |
|---|---|---|---|
| Correlation Coefficient | 0.939 | Correlation Coefficient | 0.936 |
| RMSE (W $m^{-2}$) | 23.08 | RMSE (W $m^{-2}$) | 49.28 |
| NRMSE | 0.0935 | NRMSE | 0.0943 |
| Max HOBS (W $m^{-2}$) | 206.28 | Max EOBS (W $m^{-2}$) | 515.28 |
| Min HOBS (W $m^{-2}$) | -40.52 | Min EOBS (W $m^{-2}$) | -7.35 |
| Max HMEP (W $m^{-2}$) | 184.24 | Max EMEP (W $m^{-2}$) | 519.24 |
| Min HMEP (W $m^{-2}$) | -8.47 | Min EMEP (W $m^{-2}$) | -20.32 |

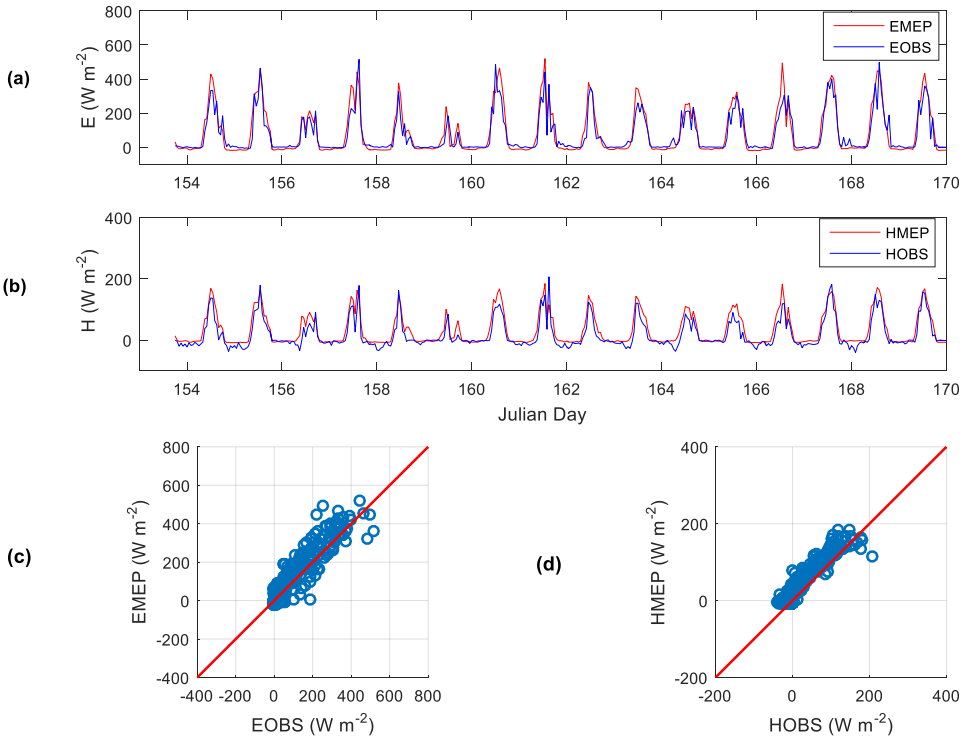


**Figure 4.2.15** (a) MEP model latent heat fluxes (EMEP) vs. observed latent heat fluxes (EOBS) (b) MEP model sensible heat fluxes (HMEP) vs. observed sensible heat fluxes (HOBS) (c) Scatter plot of EMEP vs. EOBS, (d) Scatter plot of HMEP vs. HOBS at Santarem Primary Forest, Brazil. Day 153-170, 2003.

**Table 4.2.16** Result summary for modeled vs. observed $CO_2$ fluxes at Santarem Primary Forest, Day Brazil. 153-170, 2003.

| $CO_2$ Flux (FC) Statistics | |
|---|---|
| RMSE (μmol $m^{-2}s^{-1}$) | 6.50 |
| NRMSE | 0.1353 |
| Correlation Coefficient | 0.633 |
| Regression Coefficient | 0.7192 |
| Max Modeled FC (μmol $m^{-2}s^{-1}$) | 59.59 |
| Min Modeled FC (μmol $m^{-2}s^{-1}$) | -40.33 |
| Max Observed FC (μmol $m^{-2}s^{-1}$) | 27.31 |
| Min Observed FC (μmol $m^{-2}s^{-1}$) | -20.734 |
| Number of Data Points | 392 |

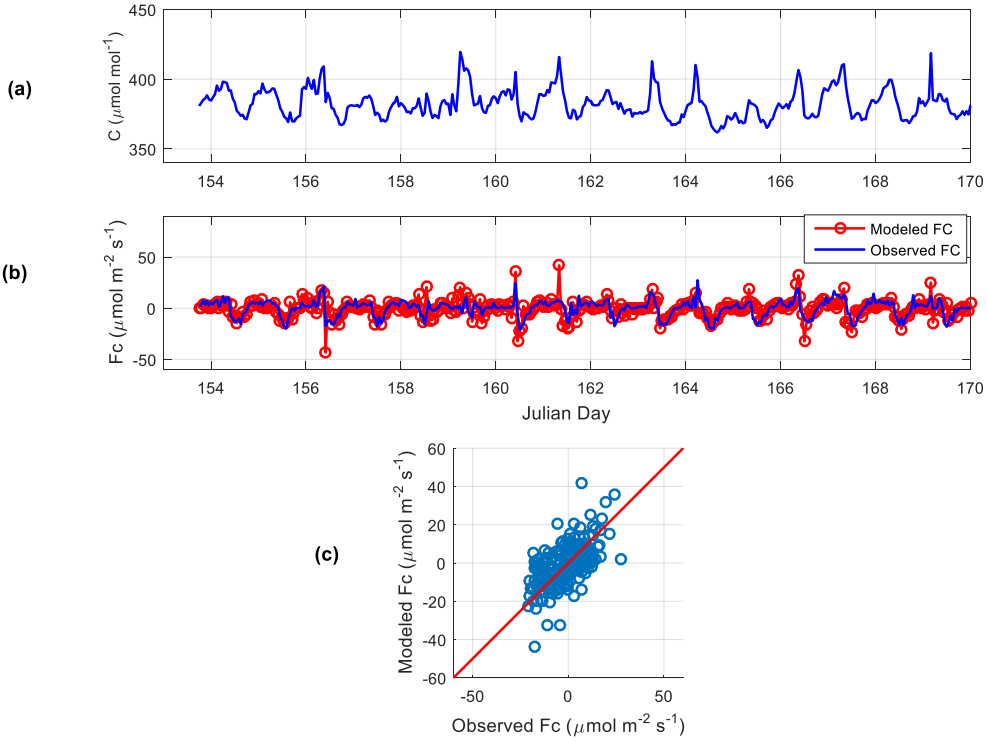


**Figure 4.2.16** (a) $CO_2$ profile, (b) Observed vs. modeled $CO_2$ fluxes, (c) Scatterplot of observed vs. modeled $CO_2$ fluxes at Santarem Primary Forest, Brazil. Day 153 -170, 2003.

The 2 AM to 8 AM concentration spikes (> 410 μmol/mol) continues in test period 8 (day 155 to 170) especially, in day 159, 161 and 169 (Figure 4.2.16 (a) causing relatively large numerical errors of the calculative derivative term in (3.27) which causes large value maximum modeled flux (59.58 μmol $m^{-2}$ $s^{-1}$) in day 161 (Figure 4.2.16 b). The modeled fluxed followed observed fluxed reasonably well as shown by scatterplot (Figure 4.2.16 (c)). The correlation coefficient is 0.633 and regression coefficient is 0.7192 for this period. The RMSE and the NRMSE of the modeled $CO_2$ flux are 6.50 μmol$m^{-2}s^{-1}$ and 13.25 % with the $CO_2$ fluxes on the order of 48.044 μmol $m^{-2}$ $s^{-1}$. The MEP energy fluxes have correlation coefficients 0.9387 and 0.9373 for sensible heat (H) and latent heat (E) fluxes respectively. The RMSE and NRMSE for this test period are 29.43 W $m^{-2}$ and 11.59 % with the observed sensible heat fluxes on the order of 246.8 W $m^{-2}$. The RMSE and NRMSE for this test period are 55.46 W $m^{-2}$ and 8.92 % with the observed latent heat fluxes on the order of 522.63 W $m^{-2}$.

## Test Period 9: Day 310-348, 2003, Santarem KM 67 Primary Forest, Brazil

**Table 4.2.17** Result summary for MEP modeled vs. observed sensible and latent heat fluxes at Santarem Primary Forest, Brazil. Day 310-348, 2003.

| Sensible Heat Flux (H) Statistics | | Latent Heat Flux (E) Statistics | |
|---|---|---|---|
| Correlation Coefficient | 0.9387 | Correlation Coefficient | 0.9373 |
| RMSE (W $m^{-2}$) | 29.43 | RMSE (W $m^{-2}$) | 55.46 |
| NRMSE | 0.1159 | NRMSE | 0.0892 |
| Max HOBS (W $m^{-2}$) | 193.17 | Max EOBS (W $m^{-2}$) | 581.38 |
| Min HOBS (W $m^{-2}$) | -60.66 | Min EOBS (W $m^{-2}$) | -28.94 |
| Max HMEP (W $m^{-2}$) | 189.56 | Max EMEP (W $m^{-2}$) | 537.09 |
| Min HMEP (W $m^{-2}$) | -10.76 | Min EMEP (W $m^{-2}$) | -40.58 |

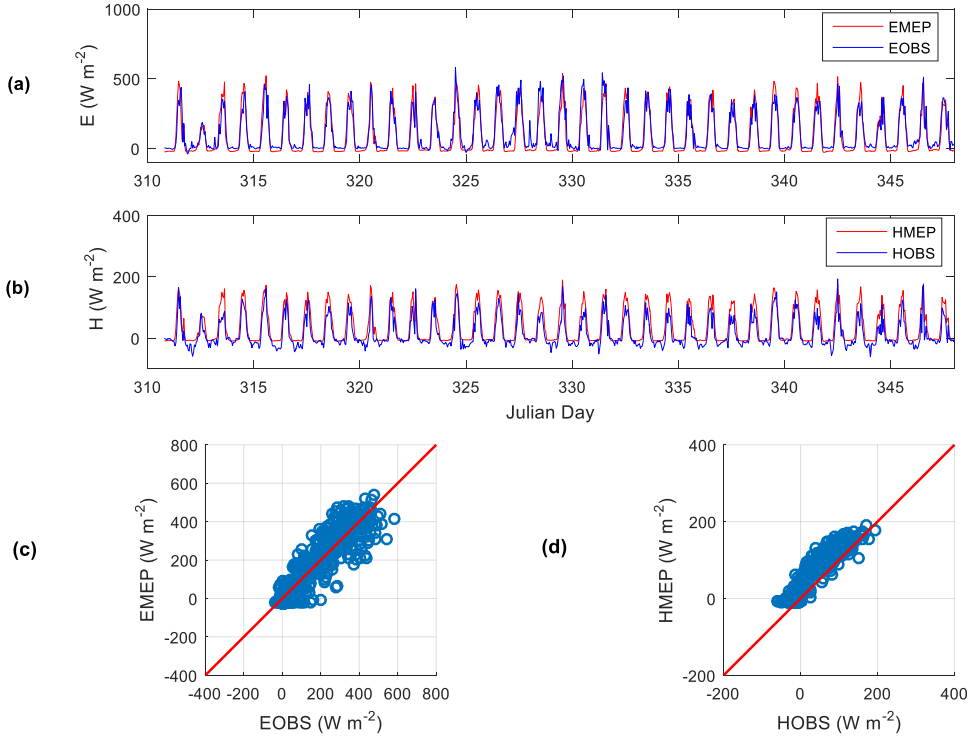


**Figure 4.2.17** (a) MEP model latent heat fluxes (EMEP) vs. observed latent heat fluxes (EOBS) (b) MEP model sensible heat fluxes (HMEP) vs. observed sensible heat fluxes (HOBS) (c) Scatter plot of EMEP vs. EOBS, (d) Scatter plot of HMEP vs. HOBS at Santarem Primary Forest, Brazil. Day 310-348, 2003.

**Table 4.2.18** Result summary for modeled vs. observed $CO_2$ fluxes at Santarem Primary Forest, Brazil. Day 310-348, 2003.

| $CO_2$ Flux (FC) Statistics | |
|---|---|
| RMSE (μmol $m^{-2}s^{-1}$) | 8.75 |
| NRMSE | 0.1525 |
| Correlation Coefficient | 0.5121 |
| Regression Coefficient | 0.4536 |
| Max Modeled FC (μmol $m^{-2}s^{-1}$) | 60.01 |
| Min Modeled FC (μmol $m^{-2}s^{-1}$) | -62.438 |
| Max Observed FC (μmol $m^{-2}s^{-1}$) | 23.446 |
| Min Observed FC (μmol $m^{-2}s^{-1}$) | -33.889 |
| Number of Data Points | 891 |

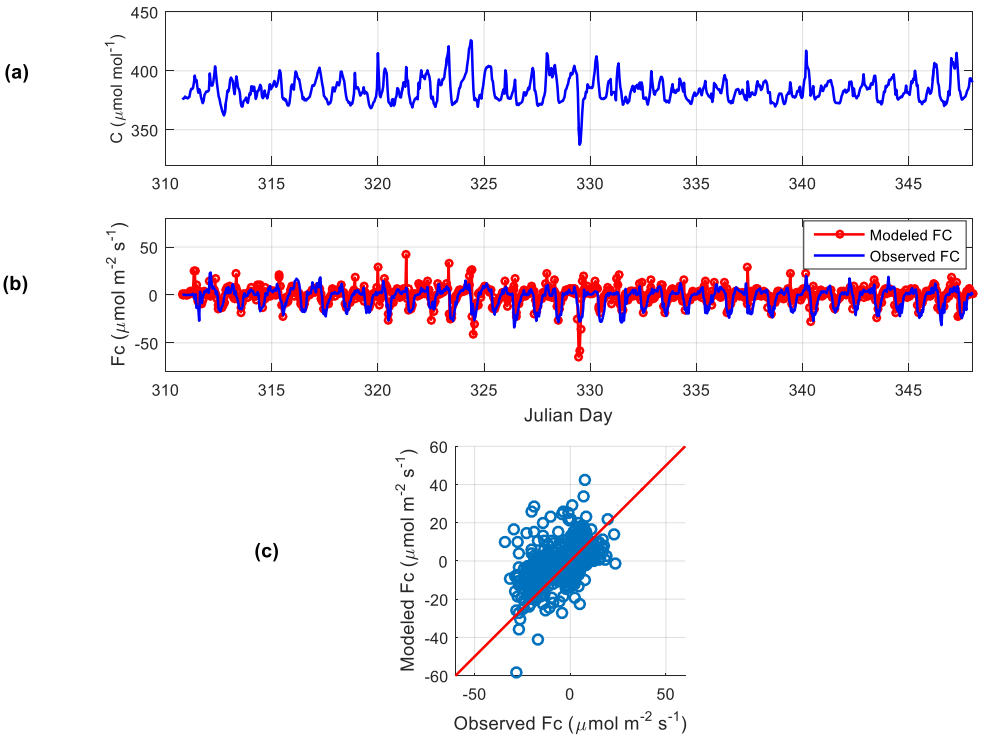


**Figure 4.2.18** (a) $CO_2$ profile, (b) Observed vs. modeled $CO_2$ fluxes, (c) Scatterplot of observed vs. modeled $CO_2$ fluxes at Santarem Primary Forest, Brazil. Day 310 -348, 2003.

Test period 9 is during dry season (July to December) in Amazon basin from day 348 to 365, 2003. This period contains 910 data points. This period has a sharp drop of $CO_2$ concentration in day 329 (Figure 4.2.18 (a)) causes smaller value in modeled flux (-62.438 μmol $m^{-2}$ $s^{-1}$) (Figure 4.2.18 (b)). The correlation coefficient is 0.5121 and regression coefficient is 0.4536 during this period. The RMSE and the NRMSE of the modeled $CO_2$ flux are 8.75 μmol$m^{-2}s^{-1}$ and 15.25 % respectively, with the $CO_2$ fluxes on the order of 57.335 μmol $m^{-2}$ $s^{-1}$. The MEP energy fluxes have correlation coefficients 0.9387 and 0.9373 for sensible heat (H) and latent heat (E) fluxes respectively. The RMSE and NRMSE for this test period are 29.43 W $m^{-2}$ and 11.59 % with the observed sensible heat fluxes on the order of 253.83 W $m^{-2}$. The RMSE and NRMSE for this test period are 55.46 W $m^{-2}$ and 8.92 % with the observed latent heat fluxes on the order of 610.32 W $m^{-2}$.

## Test Period 10: Day 348-365, 2003, Santarem KM 67 Primary Forest, Brazil

**Table 4.2.19** Result summary for MEP modeled vs. observed sensible and latent heat fluxes at Santarem Primary Forest, Brazil. Day 348-365, 2003.

| Sensible Heat Flux (H) Statistics | | Latent Heat Flux (E) Statistics | |
|---|---|---|---|
| Correlation Coefficient | 0.9297 | Correlation Coefficient | 0.942 |
| RMSE (W $m^{-2}$) | 32.792 | RMSE (W $m^{-2}$) | 52.492 |
| NRMSE | 0.1193 | NRMSE | 0.0981 |
| Max HOBS (W $m^{-2}$) | 199.56 | Max EOBS (W $m^{-2}$) | 524.403 |
| Min HOBS (W $m^{-2}$) | -75.41 | Min EOBS (W $m^{-2}$) | -10.422 |
| Max HMEP (W $m^{-2}$) | 184.76 | Max EMEP (W $m^{-2}$) | 535.843 |
| Min HMEP (W $m^{-2}$) | -9.338 | Min EMEP (W $m^{-2}$) | -23.633 |

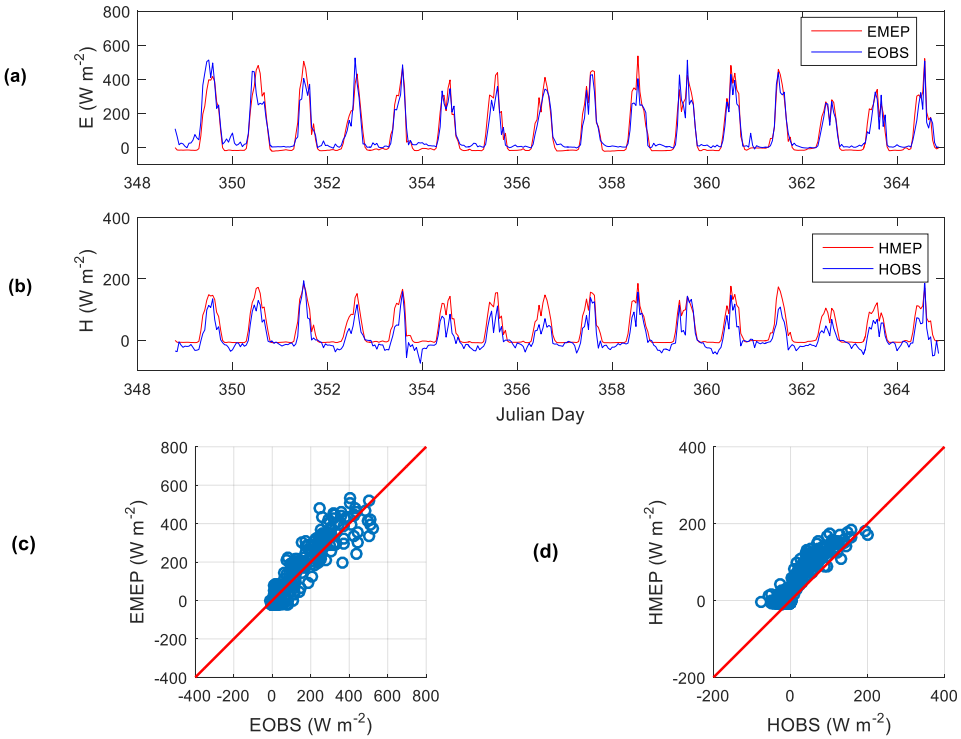


**Figure 4.2.19** (a) MEP model latent heat fluxes (EMEP) vs. observed latent heat fluxes (EOBS) (b) MEP model sensible heat fluxes (HMEP) vs. observed sensible heat fluxes (HOBS) (c) Scatter plot of EMEP vs. EOBS, (d) Scatter plot of HMEP vs. HOBS at Santarem Primary Forest, Brazil. Day 310-348, 2003.

**Table 4.2.20** Result summary for modeled vs. observed $CO_2$ fluxes at Santarem Primary Forest, Brazil. Day 348-365, 2003.

| $CO_2$ Flux (FC) Statistics | |
|---|---|
| RMSE (μmol $m^{-2}s^{-1}$) | 7.97 |
| NRMSE | 0.1521 |
| Correlation Coefficient | 0.5847 |
| Regression Coefficient | 0.4277 |
| Max Modeled FC (μmol $m^{-2}s^{-1}$) | 28.715 |
| Min Modeled FC (μmol $m^{-2}s^{-1}$) | -25.899 |
| Max Observed FC (μmol $m^{-2}s^{-1}$) | 23.938 |
| Min Observed FC (μmol $m^{-2}s^{-1}$) | -28.448 |
| Number of Data Points | 384 |

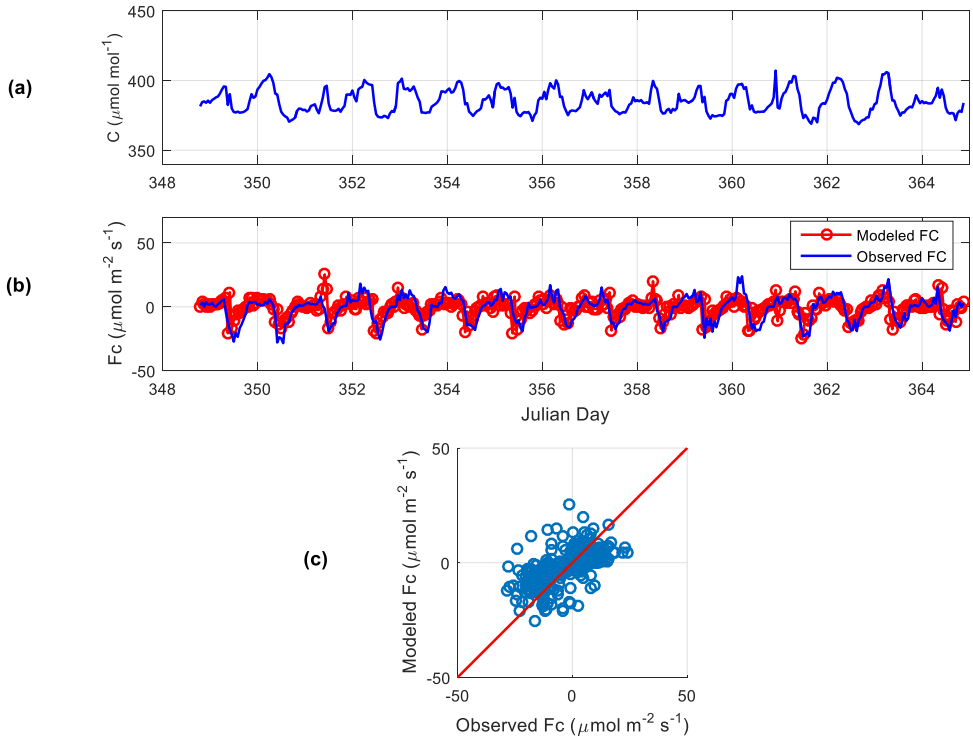


**Figure 4.2.20** (a) $CO_2$ profile, (b) Observed vs. modeled $CO_2$ fluxes, (c) Scatterplot of observed vs. modeled $CO_2$ fluxes at Santarem Primary Forest, Brazil. Day 348-365, 2003.

Test period 10 is the final period of this case study; it contains during dry season (July to December) in Amazon basin from day 348 to 365, 2003. The modeled fluxes show good agreement with observation (Figure 4.2.20 (b)). Due to less spikes in $CO_2$ concentration data during this period the magnitude of maximum and minimum modeled flux (28.715 μmol $m^{-2}$ $s^{-1}$ and -25.89 μmol $m^{-2}$ $s^{-1}$) are comparable to maximum and minimum observed flux (23.938 μmol $m^{-2}$ $s^{-1}$ and -28.448 μmol $m^{-2}$ $s^{-1}$) respectively. The correlation coefficient is 0.5847 and regression coefficient is 0.4277 for this period. The RMSE and the NRMSE of the modeled $CO_2$ flux is 7.97 μmol$m^{-2}s^{-1}$ and 15.21 % with the $CO_2$ fluxes on the order of 57.335 μmol $m^{-2}$ $s^{-1}$. The MEP energy fluxes have correlation coefficients 0.9297 and 0.942 for sensible heat (H) and latent heat (E) fluxes respectively. The RMSE and NRMSE for this test period are 32.792 W $m^{-2}$ and 11.93 % with the observed sensible heat fluxes on the order of 274.966 W $m^{-2}$. The RMSE and NRMSE for this test period are 52.492 W $m^{-2}$ and 9.81 % with the observed latent heat fluxes on the order of 534.825 W $m^{-2}$.

### 4.2.2 Site 2

The Cedar Bridge site (39.84°N, 74.38°W) is located in the upland forests of the New Jersey Pine Barrens, the largest continuous forested landscape on the Northeastern coastal plain. Upland forests occupy 650,000 ha Pine Barrens and can be divided into three dominant stand types, Oak/Pine (19.1%), Pine/Oak (13.1%), and Pitch Pine/Scrub oak (14.3%). This is a mixed forest with canopy height 5.7 m (pine) and 0.4 m (oak) respectively in the year 2005. The height of eddy covariance tower is 16 m. The cool temperate climate has mean annual temperature 11.04 °C (with mean monthly temperatures of 0.3 °C in January and 23.8 8°C in June) and mean annual precipitation is 1123 mm (S.D. 82 mm).

The model uses half-hourly time-series data of $CO_2$ concentration (μmol $mol^{-1}$), canopy surface temperature $T_s$ (˚C) and net radiation $R_n$ (W $m^{-2}$) Downward $CO_2$ flux (FC) as well as latent (E) and sensible (H) heat flux from the atmosphere to canopy surface are defined as negative. Ground heat flux (G) is defined negative from the surface into the soil layer. Due to dense canopy cover at this site the observed ground heat flux is very small. The MEP model as in (B8) – (B10) of appendix B is used to estimate H, which is used in parameterization of diffusion coefficient of $CO_2$, $D_c$. The distance above the canopy surface z is measured by the difference of mean canopy height (4 m) and height of $CO_2$ measurement (16 m) is 12 m. Scattered missing data are filled using linear interpolation when the time interval between missing data are not very large

(< 3 hours). The dataset is re-grouped into multiple no-gap time series to avoid larger gaps (> 3hrs) of the time-series records.

The comparison of modeled $CO_2$ flux using equation (3.27) with the observed eddy-covariance flux is characterized by the root-mean-square error (RMSE), the normalized root-mean-square error (NRMSE defined as the RMSE divided by the magnitude of the observed fluxes), correlation coefficient (covariance of the observed and modeled $CO_2$ fluxes divided by the product of their standard deviations) and regression coefficient (covariance of the observed and modeled $CO_2$ fluxes divided by the variance of observed $CO_2$ fluxes). The maximum and minimum observed flux over the test period and maximum and minimum model flux over test period are reported. As the MEP modeled sensible heat flux is used in the parameterization of eddy diffusivity of $CO_2$, the MEP modeled energy fluxes are compared with observed energy fluxes from eddy covariance measurements. This includes: root-mean-square error (RMSE), normalized root-mean-square error (NRMSE), correlation coefficient, maximum and minimum flux of the observed and MEP modeled heat fluxes over the test period. The results are shown in figures and tables followed by summary tables.

## Test Period 1: Day 160-170, 2006, Cedar Bridge, New Jersey

**Table 4.2.21** Result summary for MEP modeled vs. observed sensible and latent heat fluxes at Cedar Bridge, New Jersey. Day 160-170, 2006

| Sensible Heat Flux (H) Statistics | | Latent Heat Flux (E) Statistics | |
|---|---|---|---|
| Correlation Coefficient | 0.9704 | Correlation Coefficient | 0.9378 |
| RMSE (W $m^{-2}$) | 48.2402 | RMSE (W $m^{-2}$) | 61.887 |
| NRMSE | 0.08907 | NRMSE | 0.1017 |
| Max HOBS (W $m^{-2}$) | 457.36 | Max EOBS (W $m^{-2}$) | 533.305 |
| Min HOBS (W $m^{-2}$) | -84.275 | Min EOBS (W $m^{-2}$) | -75.384 |
| Max HMEP (W $m^{-2}$) | 269.42 | Max EMEP (W $m^{-2}$) | 550.609 |
| Min HMEP (W $m^{-2}$) | -40.127 | Min EMEP (W $m^{-2}$) | -52.673 |

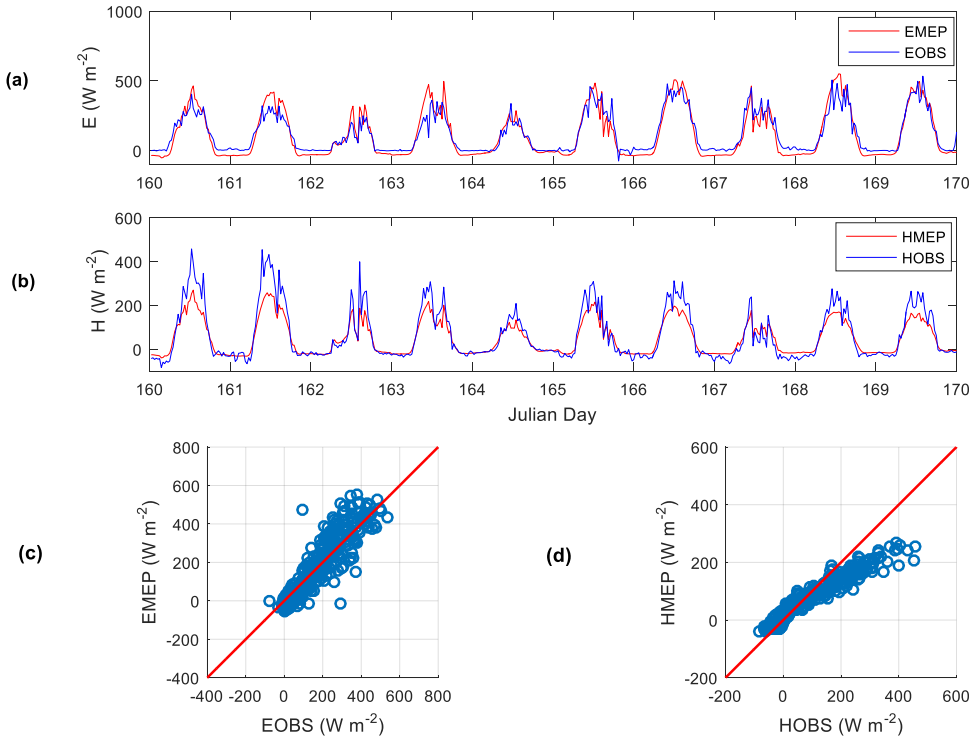


**Figure 4.2.21** (a) MEP model latent heat fluxes (EMEP) vs. observed latent heat fluxes (EOBS) (b) MEP model sensible heat fluxes (HMEP) vs. observed sensible heat fluxes (HOBS) (c) Scatter plot of EMEP vs. EOBS, (d) Scatter plot of HMEP vs. HOBS at Cedar Bridge, New Jersey. Day 160-170, 2006.

**Table 4.2.22** Result summary for modeled vs. observed $CO_2$ fluxes at Cedar Bridge, New Jersey. Day 160-170, 2006.

| $CO_2$ Flux (FC) Statistics | |
|---|---|
| RMSE ($\mu molm^{-2}s^{-1}$) | 5.293 |
| NRMSE | 0.1494 |
| Correlation Coefficient | 0.801 |
| Regression Coefficient | 0.8247 |
| Max Modeled FC ($\mu molm^{-2}s^{-1}$) | 27.502 |
| Min Modeled FC ($\mu molm^{-2}s^{-1}$) | -23.191 |
| Max Observed FC ($\mu molm^{-2}s^{-1}$) | 11.754 |
| Min Observed FC ($\mu molm^{-2}s^{-1}$) | -23.67 |
| Number of Data Points | 480 |

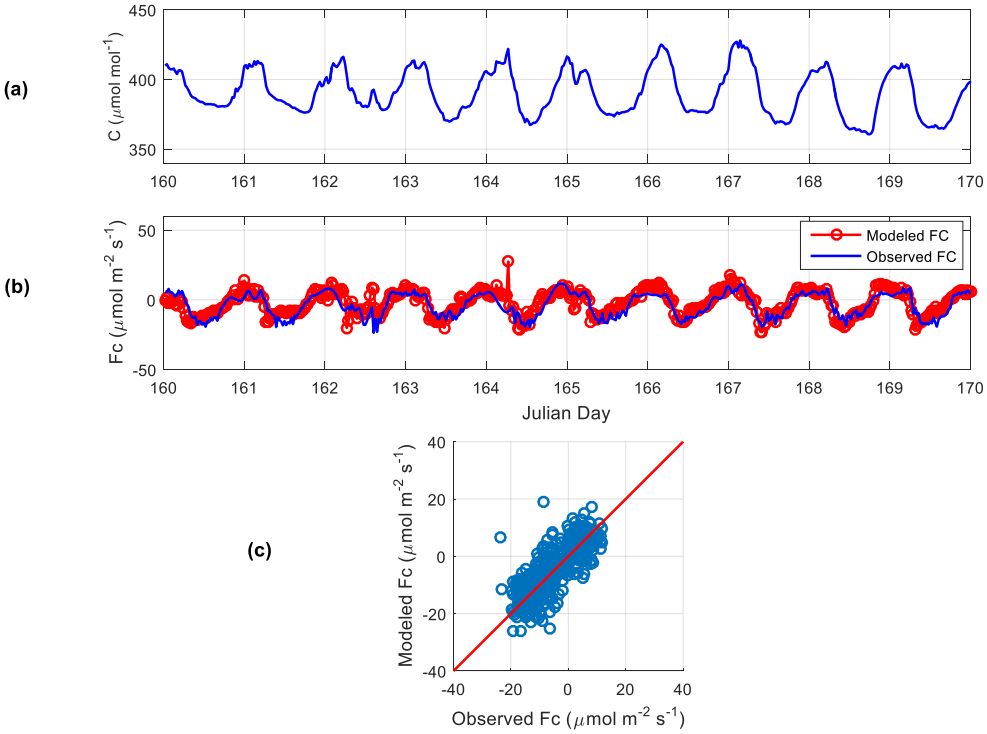


**Figure 4.2.22** (a) $CO_2$ profile, (b) Observed vs. modeled $CO_2$ fluxes, (c) Scatterplot of observed vs. modeled $CO_2$ fluxes at Cedar Bridge, New Jersey. Day 160-170, 2006.

The modeled $CO_2$ fluxes using equation (3.27) well capture the diurnal variation and magnitude of the observed fluxes (Figure 4.2.22 (b)) during test period 1 (day 160 to 170, 2006). The RMSE and the NRMSE of the modeled $CO_2$ fluxes are 5.293 $\mu molm^{-2}s^{-1}$ and 14.94 % respectively, with the $CO_2$ fluxes on the order of 35.424 $\mu mol\ m^{-2}\ s^{-1}$. The scatterplot of modeled vs. observed fluxes show great consistency along the 1:1 line (Figure 4.2.22 (c)) with correlation coefficient, 0.801 and regression coefficient, 0.8247. The magnitudes of modeled fluxes are comparable to the observed fluxes except for day 162 and 164 (Figure 4.2.22 (b)) when the observed nighttime (3 AM to 6:30 AM) $CO_2$ fluxes (-2.29 $\mu mol\ m^{-2}\ s^{-1}$ to - 8.65$\mu mol\ m^{-2}\ s^{-1}$) were erroneous (negative $CO_2$ fluxes indicate photosynthesis). Corresponding modeled $CO_2$ fluxes (5.3 $\mu mol\ m^{-2}\ s^{-1}$to 27.5 $\mu mol\ m^{-2}\ s^{-1}$) is consistent with observed $CO_2$ concentrations (412.11 μmol/mol to 421.897 μmol/mol) which higher than average daytime $CO_2$ concentration (≈ 380 μmol/mol) for that period. The MEP energy fluxes have correlation coefficients 0.9704 and 0.9378 for sensible heat (H) and latent heat (E) fluxes, respectively. The RMSE and NRMSE for this test period are 48.24 $W\ m^{-2}$ and 8.9 % with the sensible heat fluxes on the order of 541.635 $W\ m^{-2}$. The RMSE and NRMSE for this test period are 61.89 $W\ m^{-2}$ and 10.17 % with the latent heat fluxes on the order of 608.69 $W\ m^{-2}$.

## Test Period 2: Day 187-192, 2006, Cedar Bridge, New Jersey

**Table 4.2.23** Result summary for MEP modeled vs. observed sensible and latent heat fluxes at Cedar Bridge, New Jersey. Day 187-192, 2006.

| Sensible Heat Flux (H) Statistics | | Latent Heat Flux (E) Statistics | |
|---|---|---|---|
| Correlation Coefficient | 0.9548 | Correlation Coefficient | 0.9077 |
| RMSE (W $m^{-2}$) | 24.086 | RMSE (W $m^{-2}$) | 73.811 |
| NRMSE | 0.07159 | NRMSE | 0.0959 |
| Max HOBS (W $m^{-2}$) | 289.94 | Max EOBS (W $m^{-2}$) | 681.91 |
| Min HOBS (W $m^{-2}$) | -46.51 | Min EOBS (W $m^{-2}$) | -87.757 |
| Max HMEP (W $m^{-2}$) | 197.31 | Max EMEP (W $m^{-2}$) | 490.624 |
| Min HMEP (W $m^{-2}$) | -22.61 | Min EMEP (W $m^{-2}$) | -37.831 |

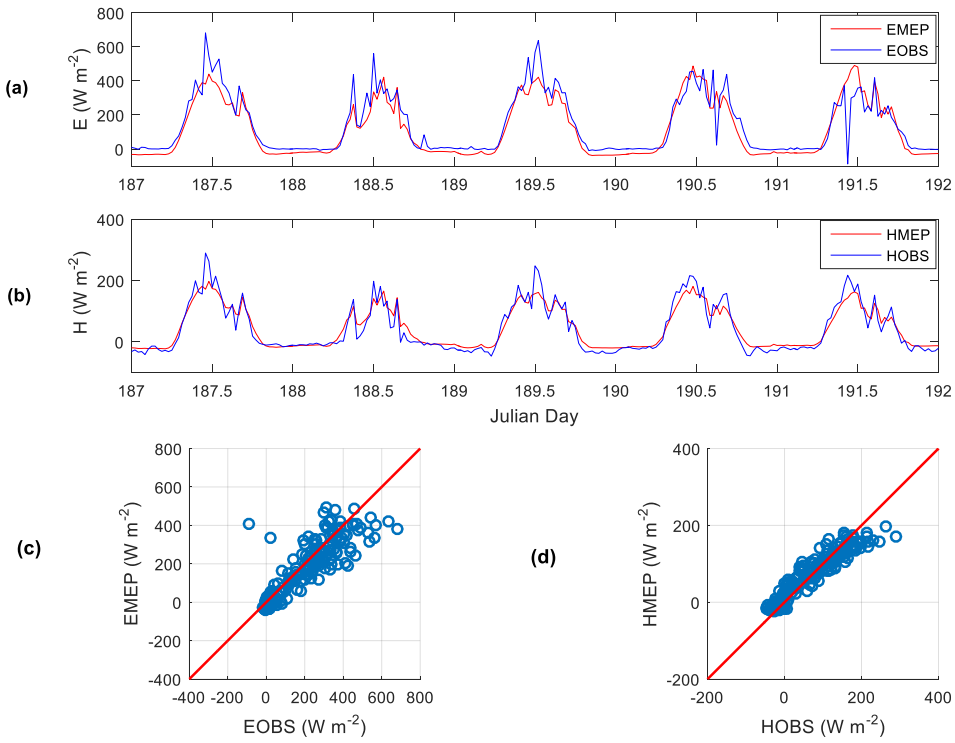


**Figure 4.2.23** (a) MEP model latent heat fluxes (EMEP) vs. observed latent heat fluxes (EOBS) (b) MEP model sensible heat fluxes (HMEP) vs. observed sensible heat fluxes (HOBS) (c) Scatter plot of EMEP vs. EOBS, (d) Scatter plot of HMEP vs. HOBS at Cedar Bridge, New Jersey. Day 187-192, 2006.

**Table 4.2.24** Result summary for modeled vs. observed $CO_2$ fluxes at Cedar Bridge, New Jersey. Day 187-192, 2006.

| $CO_2$ Flux (FC) Statistics | |
|---|---|
| RMSE ($\mu molm^{-2}s^{-1}$) | 6.331 |
| NRMSE | 0.1759 |
| Correlation Coefficient | 0.7299 |
| Regression Coefficient | 0.7305 |
| Max Modeled FC ($\mu molm^{-2}s^{-1}$) | 22.968 |
| Min Modeled FC ($\mu molm^{-2}s^{-1}$) | -24.21 |
| Max Observed FC ($\mu molm^{-2}s^{-1}$) | 10.057 |
| Min Observed FC ($\mu molm^{-2}s^{-1}$) | -25.939 |
| Number of Data Points | 287 |

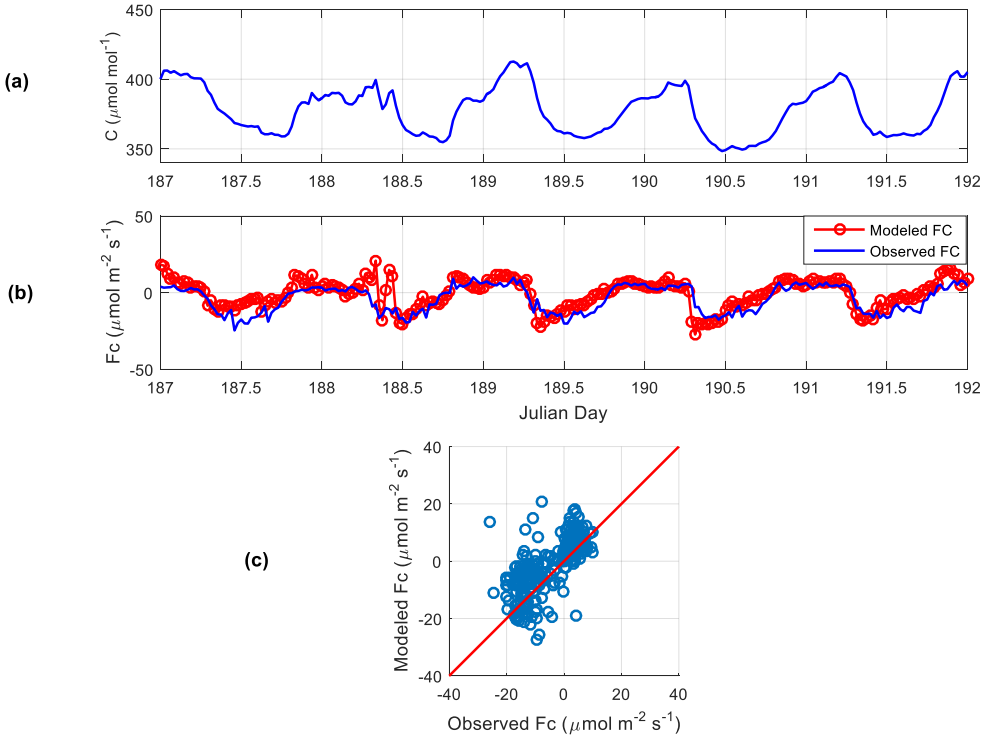


**Figure 4.2.24** (a) $CO_2$ profile, (b) Observed vs. modeled $CO_2$ fluxes, (c) Scatterplot of observed vs. modeled $CO_2$ fluxes at Cedar Bridge, New Jersey. Day 187-192, 2006.

During Test period 2 (day 187 to 192, 2006) modeled fluxes show good agreement with observation except day 188 (10AM to 10:30 AM) (Figure 4.2.24 (b)) due to sudden spike in concentration (381.921 to 392.006 μmol/mol) (Figure 4.2.24 (a)). The correlation coefficient, 0.7299 and regression coefficient, 0.7305 during this period. The scatterplot shows good agreement except few outliers (Figure 4.2.24 (c)). The RMSE and the NRMSE of the modeled $CO_2$ fluxes are 6.331μmol$m^{-2}s^{-1}$ and 17.59% with the $CO_2$ fluxes on the order of 35.996 μmol $m^{-2}$ $s^{-1}$ for this period. The MEP energy fluxes have correlation coefficients 0.9548 and 0.9077 for sensible heat (H) and latent heat (E) fluxes respectively. The RMSE and NRMSE for this test period are 24.086W $m^{-2}$ and 7.159 % with the sensible heat fluxes on the order of 336.45 W $m^{-2}$. The RMSE and NRMSE for this test period are 73.811 W $m^{-2}$ and 9.59 % with the latent heat fluxes on the order of 769.667 W $m^{-2}$.

## Test Period 3: Day 194-202, 2006, Cedar Bridge, New Jersey

**Table 4.2.25** Result summary for MEP modeled vs. observed sensible and latent heat fluxes at Cedar Bridge, New Jersey. Day 194-202, 2006.

| Sensible Heat Flux (H) Statistics | | Latent Heat Flux (E) Statistics | |
|---|---|---|---|
| Correlation Coefficient | 0.9514 | Correlation Coefficient | 0.929 |
| RMSE (W $m^{-2}$) | 50.01 | RMSE (W $m^{-2}$) | 82.65 |
| NRMSE | 0.10801 | NRMSE | 0.1167 |
| Max HOBS (W $m^{-2}$) | 410.898 | Max EOBS (W $m^{-2}$) | 665.72 |
| Min HOBS (W $m^{-2}$) | -52.087 | Min EOBS (W $m^{-2}$) | -42.69 |
| Max HMEP (W $m^{-2}$) | 204.11 | Max EMEP (W $m^{-2}$) | 569.402 |
| Min HMEP (W $m^{-2}$) | -22.76 | Min EMEP (W $m^{-2}$) | -44.67 |

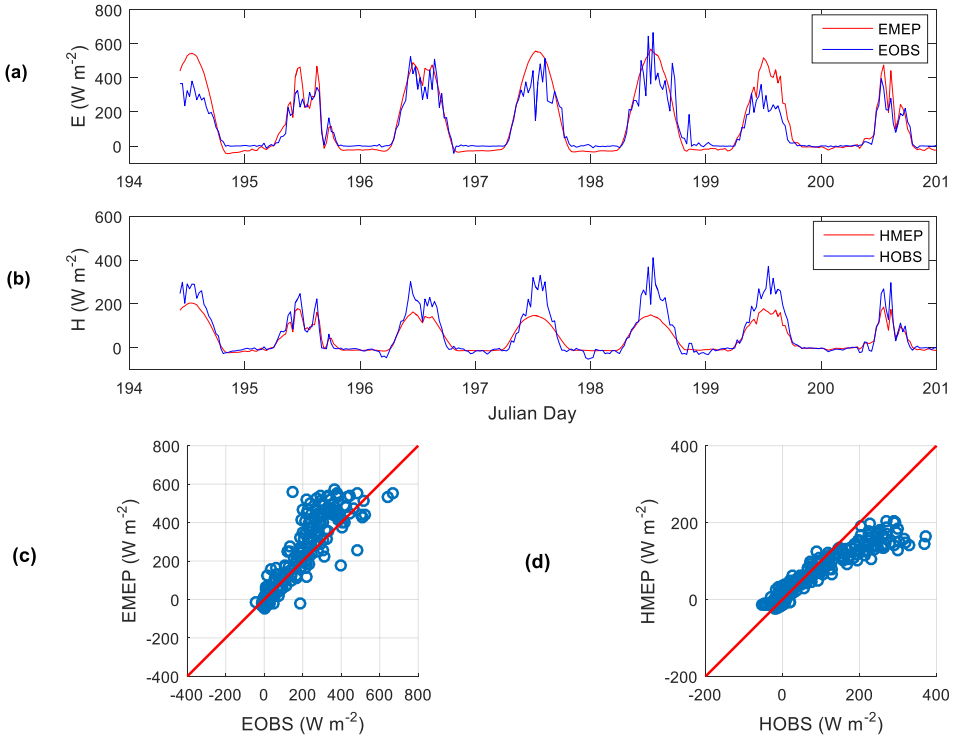


**Figure 4.2.25** (a) MEP model latent heat fluxes (EMEP) vs. observed latent heat fluxes (EOBS) (b) MEP model sensible heat fluxes (HMEP) vs. observed sensible heat fluxes (HOBS) (c) Scatter plot of EMEP vs. EOBS, (d) Scatter plot of HMEP vs. HOBS at Cedar Bridge, New Jersey. Day 194-202, 2006.

**Table 4.2.26** Result summary for modeled vs. observed $CO_2$ fluxes at Cedar Bridge, New Jersey. Day 194-202, 2006.

| $CO_2$ Flux (FC) Statistics | |
|---|---|
| RMSE ($\mu molm^{-2}s^{-1}$) | 7.572 |
| NRMSE | 0.1895 |
| Correlation Coefficient | 0.661 |
| Regression Coefficient | 0.816 |
| Max Modeled FC ($\mu molm^{-2}s^{-1}$) | 39.81 |
| Min Modeled FC ($\mu molm^{-2}s^{-1}$) | -30.616 |
| Max Observed FC ($\mu molm^{-2}s^{-1}$) | 16.944 |
| Min Observed FC ($\mu molm^{-2}s^{-1}$) | -23.01 |
| Number of Data Points | 343 |

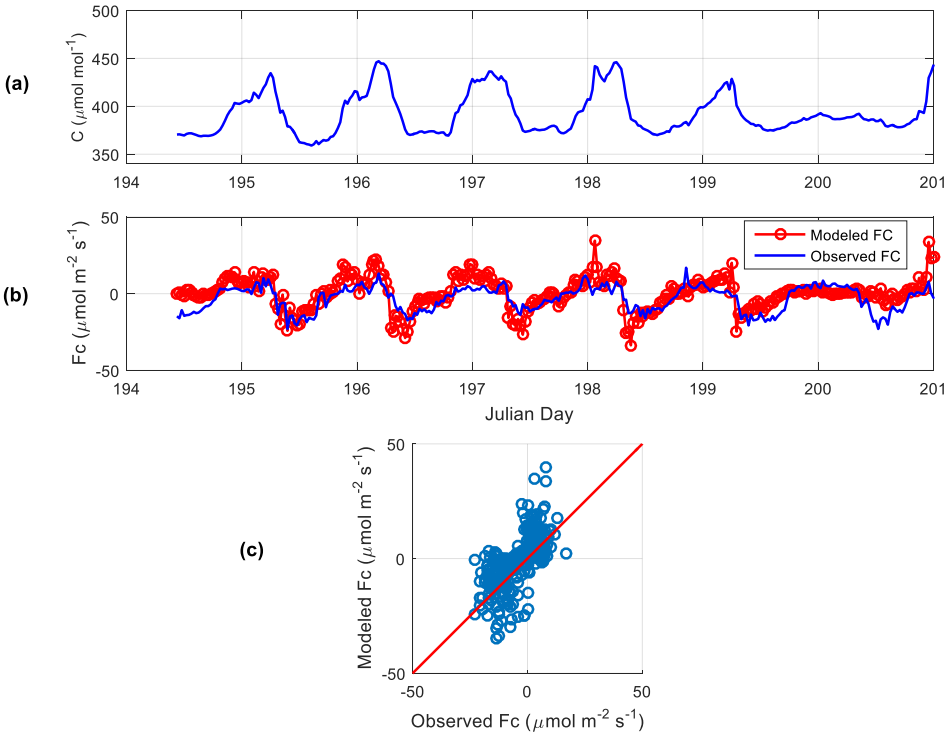


**Figure 4.2.26** (a) $CO_2$ profile, (b) Observed vs. modeled $CO_2$ fluxes, (c) Scatterplot of observed vs. modeled $CO_2$ fluxes at Cedar Bridge, New Jersey. Day 194-202, 2006.

Test period 3 starts from day 194 to 202, 2006. During this period modeled fluxes well capture the diurnal variation and magnitude of the observed fluxes (Figure 4.2.26 (b)) with the correlation coefficient, 0.661 and regression coefficient, 0.816. The spurious spikes in $CO_2$ concentration data (> 400 to 465.156 μmol/mol during 1:30 AM to 3:30 AM occur consistently during this period especially during day 201 leading to relatively large numerical errors of the calculated derivative term in (3.27) which causes large value maximum modeled flux (39.80983 μmol $m^{-2}$ $s^{-1}$). The RMSE and the NRMSE of the modeled $CO_2$ fluxes during this period is 7.572 μmol$m^{-2}s^{-1}$ and 18.95 % respectively, with the $CO_2$ fluxes on the order of 39.954 μmol $m^{-2}$ $s^{-1}$. The MEP energy fluxes have correlation coefficients 0.9514 and 0.929 for sensible heat (H) and latent heat (E) fluxes respectively. The RMSE and NRMSE for this test period are 50.01 W $m^{-2}$ and 10.801 % with the sensible heat fluxes on the order of 462.985 W $m^{-2}$. The RMSE and NRMSE for this test period are 82.65 W $m^{-2}$ and 11.67 % with the latent heat fluxes on the order of 708.41 W $m^{-2}$

## Test Period 4: Day 223-228, 2006, Cedar Bridge, New Jersey

**Table 4.2.27** Result summary for MEP modeled vs. observed sensible and latent heat fluxes at Cedar Bridge, New Jersey. Day 223-228, 2006.

| Sensible Heat Flux (H) Statistics | | Latent Heat Flux (E) Statistics | |
|---|---|---|---|
| Correlation Coefficient | 0.9694 | Correlation Coefficient | 0.9248 |
| RMSE (W $m^{-2}$) | 57.467 | RMSE (W $m^{-2}$) | 75.851 |
| NRMSE | 0.1199 | NRMSE | 0.1308 |
| Max HOBS (W $m^{-2}$) | 429.48 | Max EOBS (W $m^{-2}$) | 567.41 |
| Min HOBS (W $m^{-2}$) | -49.77 | Min EOBS (W $m^{-2}$) | -12.415 |
| Max HMEP (W $m^{-2}$) | 222.262 | Max EMEP (W $m^{-2}$) | 506.15 |
| Min HMEP (W $m^{-2}$) | -26.302 | Min EMEP (W $m^{-2}$) | -46.935 |

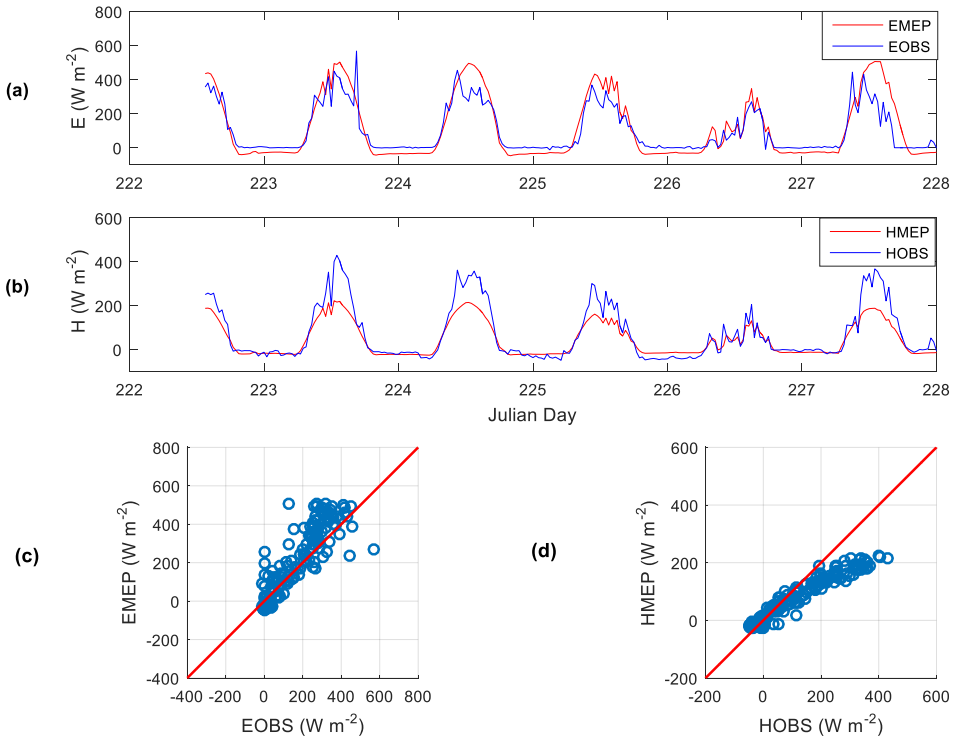


**Figure 4.2.27** (a) MEP model latent heat fluxes (EMEP) vs. observed latent heat fluxes (EOBS) (b) MEP model sensible heat fluxes (HMEP) vs. observed sensible heat fluxes (HOBS) (c) Scatter plot of EMEP vs. EOBS, (d) Scatter plot of HMEP vs. HOBS at Cedar Bridge, New Jersey. Day 223-228, 2006.

**Table 4.2.28** Result summary for modeled vs. observed $CO_2$ fluxes at Cedar Bridge, New Jersey. Day 223-228, 2006.

| $CO_2$ Flux (FC) Statistics | |
|---|---|
| RMSE ($\mu molm^{-2}s^{-1}$) | 5.293 |
| NRMSE | 0.2027 |
| Correlation Coefficient | 0.571 |
| Regression Coefficient | 0.7703 |
| Max Modeled FC ($\mu molm^{-2}s^{-1}$) | 33.74 |
| Min Modeled FC ($\mu molm^{-2}s^{-1}$) | -38.81 |
| Max Observed FC ($\mu molm^{-2}s^{-1}$) | 8.244 |
| Min Observed FC ($\mu molm^{-2}s^{-1}$) | -17.868 |
| Number of Data Points | 345 |

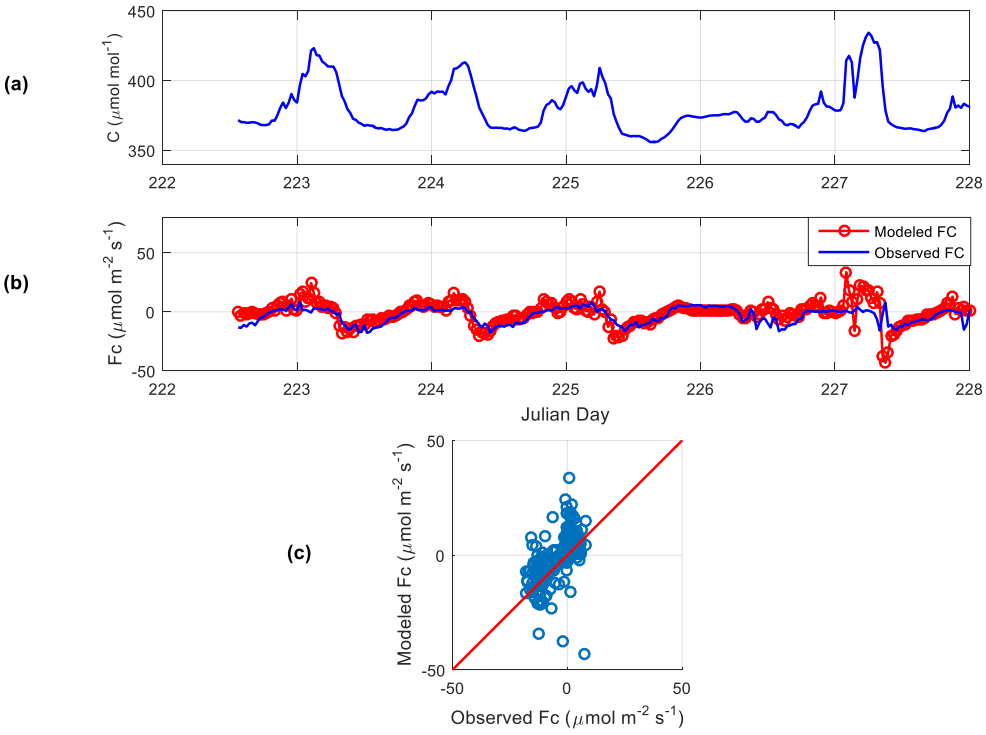


**Figure 4.2.28** (a) $CO_2$ profile, (b) Observed vs. modeled $CO_2$ fluxes, (c) Scatterplot of observed vs. modeled $CO_2$ fluxes at Cedar Bridge, New Jersey. Day 223-228, 2006.

Test period 4 (day 223 to 228, 2006) shows reasonable agreement between modeled and observed fluxes (Figure 4.2.28 (a), (b)) except the spikes in $CO_2$ concentration data (> 400 to 435 μmol/mol) during 2 AM to 8 AM day 227 leading to relatively large numerical errors of the calculated derivative term in (3.27) which causes large value maximum modeled flux (33.74 μmol $m^{-2}$ $s^{-1}$). The scatterplot of modeled vs. observed $CO_2$ flux shows some spread (Figure 4.2.28 (c)) with correlation coefficient, 0.571 and regression coefficient, 0.7703 for this period. The RMSE and the NRMSE of the modeled $CO_2$ fluxes are 5.293 μmol$m^{-2}s^{-1}$ and 20.27 % with the $CO_2$ fluxes on the order of 26.112 μmol $m^{-2}$ $s^{-1}$. The MEP energy fluxes have correlation coefficients 0.9694 and 0.9248 for sensible heat (H) and latent heat (E) fluxes respectively. The RMSE and NRMSE for this test period are 57.467 W $m^{-2}$ and 11.99 % with the sensible heat fluxes on the order of 479.25 W $m^{-2}$. RMSE and NRMSE for this test period are 75.851 W $m^{-2}$ and 13.08 % with the latent heat fluxes on the order of 579.825 W $m^{-2}$.

## Test Period 5: Day 232-236, 2006, Cedar Bridge, New Jersey

**Table 4.2.29** Result summary for MEP modeled vs. observed sensible and latent heat fluxes at Cedar Bridge, New Jersey. Day 232-236, 2006.

| Sensible Heat Flux (H) Statistics | | Latent Heat Flux (E) Statistics | |
|---|---|---|---|
| Correlation Coefficient | 0.948 | Correlation Coefficient | 0.92554 |
| RMSE (W $m^{-2}$) | 67.963 | RMSE (W $m^{-2}$) | 80.65 |
| NRMSE | 0.1235 | NRMSE | 0.1906 |
| Max HOBS (W $m^{-2}$) | 498.01 | Max EOBS (W $m^{-2}$) | 382.78 |
| Min HOBS (W $m^{-2}$) | -52.36 | Min EOBS (W $m^{-2}$) | -40.415 |
| Max HMEP (W $m^{-2}$) | 197.51 | Max EMEP (W $m^{-2}$) | 573.49 |
| Min HMEP (W $m^{-2}$) | -20.44 | Min EMEP (W $m^{-2}$) | -45.257 |

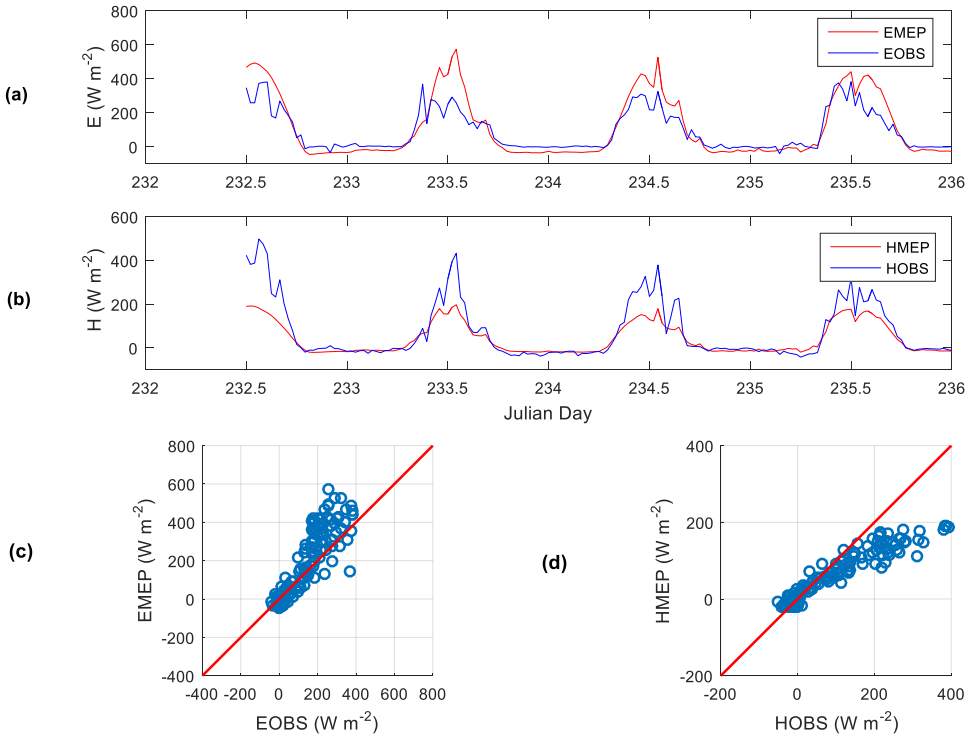


**Figure 4.2.29** (a) MEP model latent heat fluxes (EMEP) vs. observed latent heat fluxes (EOBS) (b) MEP model sensible heat fluxes (HMEP) vs. observed sensible heat fluxes (HOBS) (c) Scatter plot of EMEP vs. EOBS, (d) Scatter plot of HMEP vs. HOBS at Cedar Bridge, New Jersey. Day 232-236, 2006.

**Table 4.2.30** Result summary for modeled vs. observed $CO_2$ fluxes at Cedar Bridge, New Jersey. Day 232-236, 2006.

| $CO_2$ Flux (FC) Statistics | |
|---|---|
| RMSE ($\mu molm^{-2}s^{-1}$) | 5.75 |
| NRMSE | 0.19501 |
| Correlation Coefficient | 0.6594 |
| Regression Coefficient | 0.9473 |
| Max Modeled FC ($\mu molm^{-2}s^{-1}$) | 25.579 |
| Min Modeled FC ($\mu molm^{-2}s^{-1}$) | -30.041 |
| Max Observed FC ($\mu molm^{-2}s^{-1}$) | 9.471 |
| Min Observed FC ($\mu molm^{-2}s^{-1}$) | -20.015 |
| Number of Data Points | 220 |

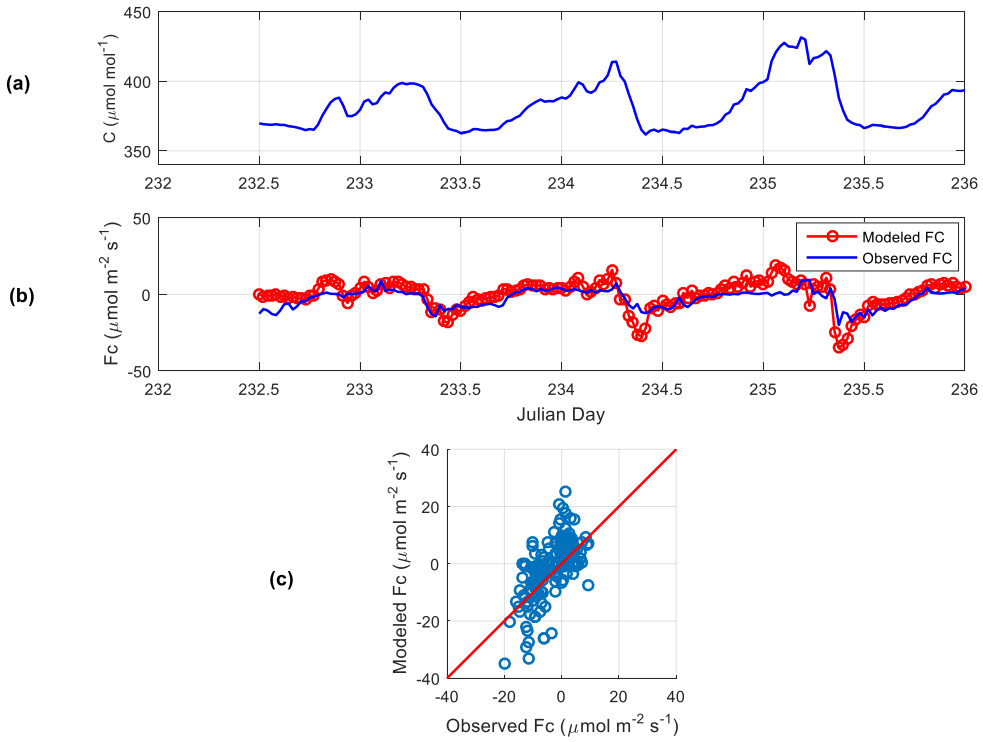


**Figure 4.2.30** (a) $CO_2$ profile, (b) Observed vs. modeled $CO_2$ fluxes, (c) Scatterplot of observed vs. modeled $CO_2$ fluxes at Cedar Bridge, New Jersey. Day 232-236, 2006.

The modeled $CO_2$ flux during test period 5 (day 232 to 237) shows reasonable agreement with the observed fluxes (Figure 4.2.30 (b)). Similar to test period 3 and 4 nighttime CO2 concentration spikes (> 420 μmol/mol) causes large values of the nighttime modeled fluxes during this time period especially day 235 (Figure 4.2.30 (a)). The scatterplot shows reasonable agreement between the modeled and observed fluxes (Figure 4.2.30 (c)) with correlation coefficient, 0.6594 and regression coefficient, 0.9473. The RMSE and the NRMSE of the modeled $CO_2$ fluxes are 5.75 $\mu molm^{-2}s^{-1}$ and 19.501 % with the $CO_2$ fluxes on the order of 29.486 μmol $m^{-2}$ $s^{-1}$. The MEP energy fluxes have correlation coefficients 0.948 and 0.92554 for sensible heat (H) and latent heat (E) fluxes respectively. The RMSE and NRMSE for this test period are 67.963 W $m^{-2}$ and 12.35 % with the sensible heat fluxes on the order of 550.37 W $m^{-2}$. The RMSE and NRMSE for this test period are 80.65 W $m^{-2}$ and 19.06 % with the latent heat fluxes on the order of 423.195 W $m^{-2}$

## Test Period 6: Day 249-255, 2006, Cedar Bridge, New Jersey

**Table 4.2.31** Result summary for MEP modeled vs. observed sensible and latent heat fluxes at Cedar Bridge, New Jersey. Day 249-255, 2006.

| Sensible Heat Flux (H) Statistics | | Latent Heat Flux (E) Statistics | |
|---|---|---|---|
| Correlation Coefficient | 0.938 | Correlation Coefficient | 0.9498 |
| RMSE (W $m^{-2}$) | 43.95 | RMSE (W $m^{-2}$) | 47.96 |
| NRMSE | 0.07019 | NRMSE | 0.07698 |
| Max HOBS (W $m^{-2}$) | 578.68 | Max EOBS (W $m^{-2}$) | 583.52 |
| Min HOBS (W $m^{-2}$) | -47.444 | Min EOBS (W $m^{-2}$) | -40.362 |
| Max HMEP (W $m^{-2}$) | 229.2 | Max EMEP (W $m^{-2}$) | 453.523 |
| Min HMEP (W $m^{-2}$) | -31.334 | Min EMEP (W $m^{-2}$) | -40.788 |

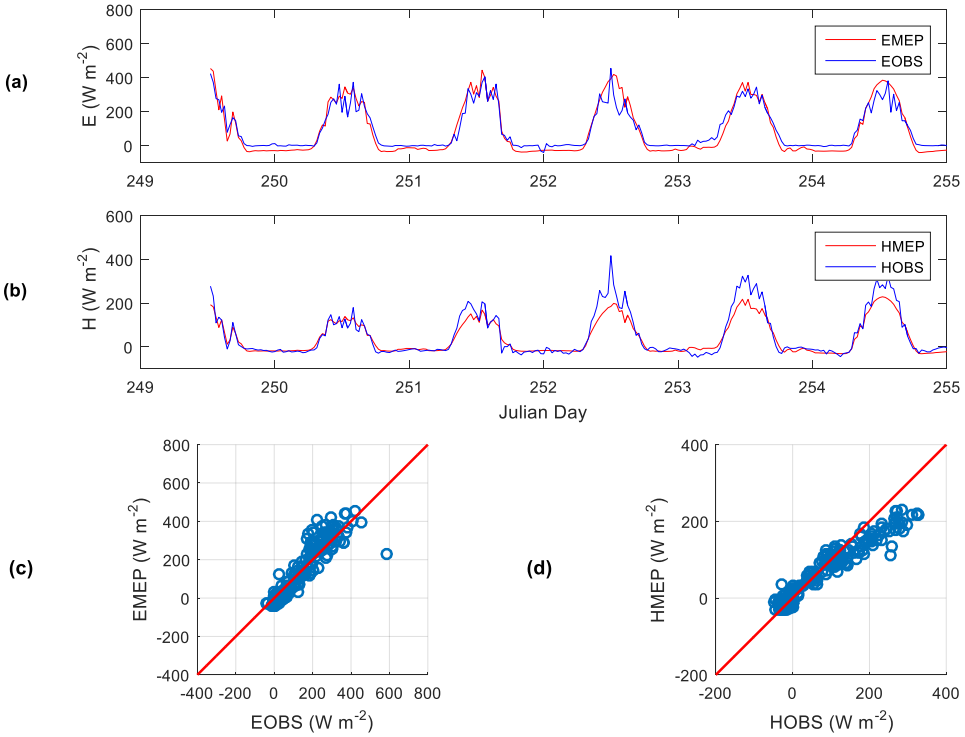


**Figure 4.2.31** (a) MEP model latent heat fluxes (EMEP) vs. observed latent heat fluxes (EOBS) (b) MEP model sensible heat fluxes (HMEP) vs. observed sensible heat fluxes (HOBS) (c) Scatter plot of EMEP vs. EOBS, (d) Scatter plot of HMEP vs. HOBS at Cedar Bridge, New Jersey. Day 249-255, 2006.

**Table 4.2.32** Result summary for modeled vs. observed $CO_2$ fluxes at Cedar Bridge, New Jersey. Day 250-256, 2006.

| $CO_2$ Flux (FC) Statistics | |
|---|---|
| RMSE ($\mu molm^{-2}s^{-1}$) | 8.054 |
| NRMSE | 0.1336 |
| Correlation Coefficient | 0.547 |
| Regression Coefficient | 0.556 |
| Max Modeled FC ($\mu molm^{-2}s^{-1}$) | 25.20 |
| Min Modeled FC ($\mu molm^{-2}s^{-1}$) | -23.362 |
| Max Observed FC ($\mu molm^{-2}s^{-1}$) | 16.131 |
| Min Observed FC ($\mu molm^{-2}s^{-1}$) | -44.17 |
| Number of Data Points | 283 |

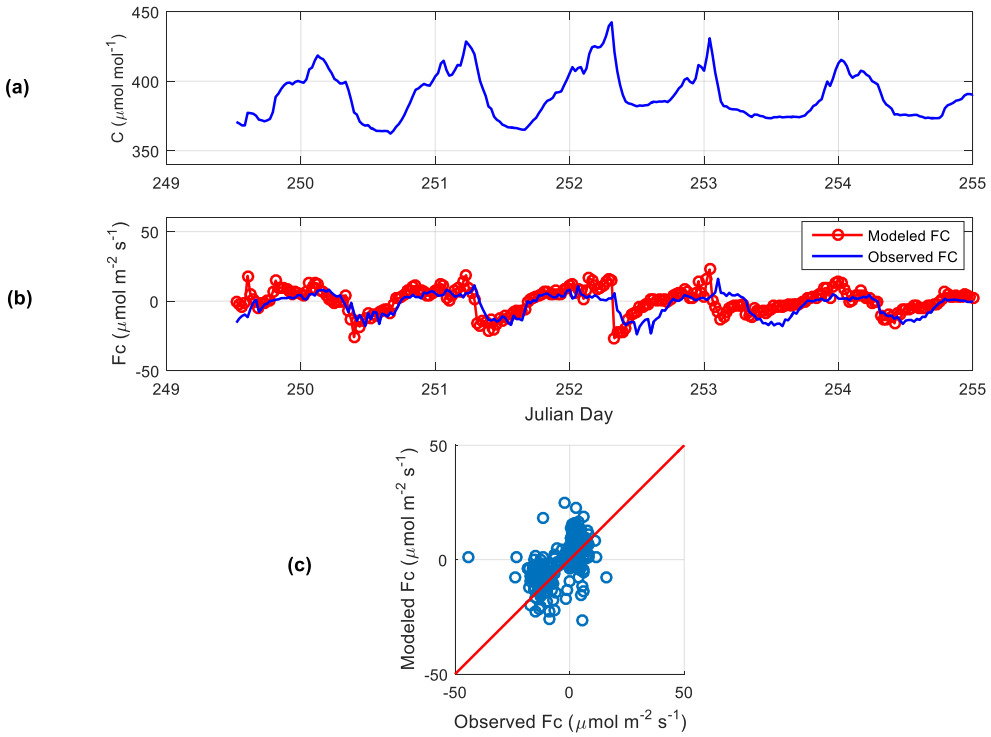


**Figure 4.2.32** (a) $CO_2$ profile, (b) Observed vs. modeled $CO_2$ fluxes, (c) Scatterplot of observed vs. modeled $CO_2$ fluxes at Cedar Bridge, New Jersey. Day 250-256, 2006.

The modeled $CO_2$ fluxed shows reasonable agreement with observed fluxes (Figure 4.2.32 (b)) during test period 6 (day 250 to 255, 2006). The scatterplot of modeled vs. observed $CO_2$ flux shows some spread (Figure 4.2.32 (c)) with the correlation coefficient, 0.547 and regression coefficient, 0.556 during this period. The RMSE and the NRMSE of the modeled $CO_2$ fluxes are 8.054 $\mu molm^{-2}s^{-1}$ and 13.36 % with the $CO_2$ fluxes on the order of 60.301 $\mu mol\ m^{-2}\ s^{-1}$. The sudden $CO_2$ concentration drop during day 252 (2:30 AM) causes relatively large numerical errors of the calculated derivative term in (3.27). The MEP energy fluxes have correlation coefficients 0.938 and 0.9498 for sensible heat (H) and latent heat (E) fluxes respectively. The RMSE and NRMSE for this test period are 43.95 W $m^{-2}$ and 7.019 % with the observed sensible heat fluxes on the order of 626.124 W $m^{-2}$. The RMSE and NRMSE for this test period are 47.96 W $m^{-2}$ and 7.698 % with the observed latent heat fluxes on the order of 623.882 W $m^{-2}$.

### 4.2.3 Site 3

Delta Junction 1920 Control site (63.89˚N, 145.74˚W) is located near Delta Junction, just to the north of the Alaska Range in interior Alaska. This evergreen needle leaf forest has a canopy overstory consisted of homogeneous stands of black spruce with a mean canopy height of 4 m with a sparse understory consisted primarily of shrubs. The site extended from the 9.5 m high eddy covariance tower for more than 1 km to the south, west, and north, with the shortest fetch to the east (approximately 200 m). The continental climate characterized by large daily and annual temperature ranges, low humidity, and relatively low precipitation. The mean annual temperature is -2.3 °C with mean annual Rainfall, 304 mm and mean annual Snowfall, 940 mm.

The model uses half-hourly time-series data of $CO_2$ concentration (μmol $mol^{-1}$), canopy surface temperature $T_s$ (˚C) and net radiation $R_n$ (W $m^{-2}$) Downward $CO_2$ flux (FC) as well as latent (E) and sensible (H) heat flux from the atmosphere to canopy surface are defined as negative. Ground heat flux (G) is defined negative from the surface into the soil layer. Due to dense canopy cover at this site the observed ground heat flux is very small. The MEP model as in (B8) – (B10) of appendix B is used to estimate H, which is used in parameterization of diffusion coefficient of $CO_2$, $D_c$. The distance above the canopy surface z is measured by the difference of mean canopy height (4 m) and height of CO2 measurement (9.5 m) is 5.5 m. Scattered missing data are filled using linear interpolation when the time interval between missing data are not very large

(< 3 hours). The dataset is re-grouped into multiple no-gap time series to avoid larger gaps (> 3hrs) of the time-series records.

The comparison of modeled $CO_2$ flux using equation (3.27) with the observed eddy-covariance flux is characterized by the root-mean-square error (RMSE), the normalized root-mean-square error (NRMSE defined as the RMSE divided by the magnitude of the observed fluxes), correlation coefficient (covariance of the observed and modeled $CO_2$ fluxes divided by the product of their standard deviations) and regression coefficient (covariance of the observed and modeled $CO_2$ fluxes divided by the variance of observed $CO_2$ fluxes). The maximum and minimum observed flux over the test period and maximum and minimum model flux over test period are reported. As the MEP modeled sensible heat flux is used in the parameterization of eddy diffusivity of $CO_2$, the MEP modeled energy fluxes are compared with observed energy fluxes from eddy covariance measurements. This includes: root-mean-square error (RMSE), normalized root-mean-square error (NRMSE), correlation coefficient, maximum and minimum flux of the observed and MEP modeled heat fluxes over the test period. The results are shown in figures and tables followed by summary tables.

## Test Period 1: Day 233-238, 2006, Delta Junction 1920-Control, Alaska

**Table 4.2.33** Result summary for MEP modeled vs. observed sensible and latent heat fluxes at Delta Junction 1920-Control, Alaska. Day 233-238, 2004.

| Sensible Heat Flux (H) Statistics | | Latent Heat Flux (E) Statistics | |
|---|---|---|---|
| Correlation Coefficient | 0.9440 | Correlation Coefficient | 0.9479 |
| RMSE (W $m^{-2}$) | 21.6844 | RMSE (W $m^{-2}$) | 65.9230 |
| NRMSE | 0.08998 | NRMSE | 0.5134 |
| Max HOBS (W $m^{-2}$) | 206.074 | Max EOBS (W $m^{-2}$) | 120.488 |
| Min HOBS (W $m^{-2}$) | -34.93 | Min EOBS (W $m^{-2}$) | -7.92 |
| Max HMEP (W $m^{-2}$) | 171.28 | Max EMEP (W $m^{-2}$) | 268.38 |
| Min HMEP (W $m^{-2}$) | -19.537 | Min EMEP (W $m^{-2}$) | -28.30 |

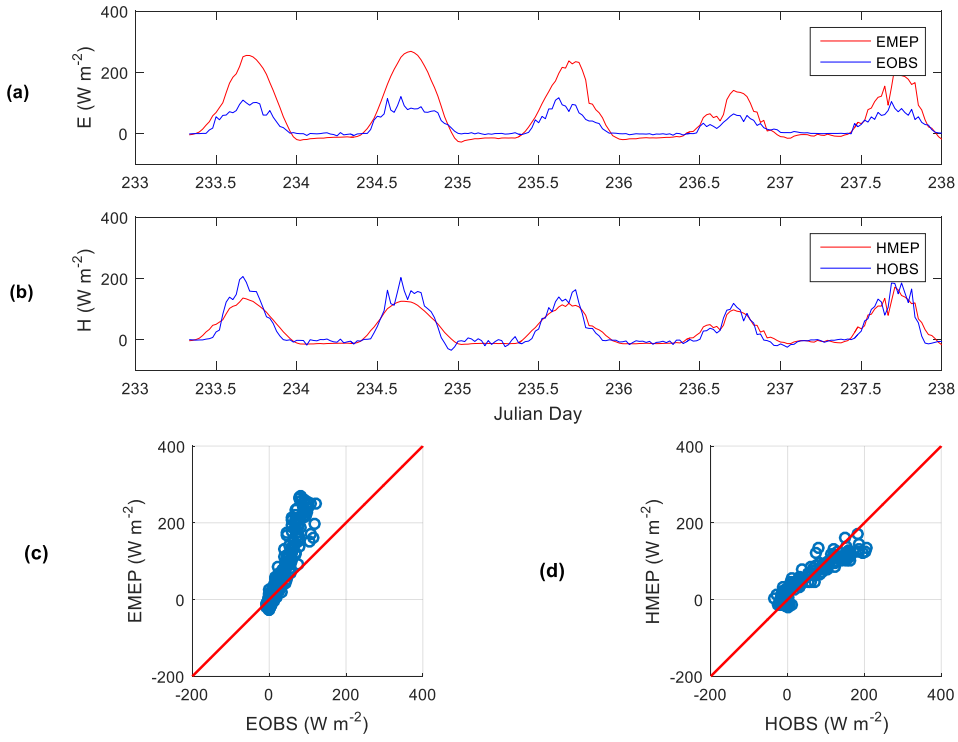


**Figure 4.2.33** (a) MEP model latent heat fluxes (EMEP) vs. observed latent heat fluxes (EOBS) (b) MEP model sensible heat fluxes (HMEP) vs. observed sensible heat fluxes (HOBS) (c) Scatter plot of EMEP vs. EOBS, (d) Scatter plot of HMEP vs. HOBS at Delta Junction 1920-Control, Alaska. Day 233-238, 2004.

**Table 4.2.34** Result summary for modeled vs. observed $CO_2$ fluxes at Delta Junction 1920-Control, Alaska. Day 233-238, 2004.

| $CO_2$ Flux (FC) Statistics | |
|---|---|
| RMSE ($\mu molm^{-2}s^{-1}$) | 2.886 |
| NRMSE | 0.15352 |
| Correlation Coefficient | 0.6795 |
| Regression Coefficient | 0.6532 |
| Max Modeled FC ($\mu molm^{-2}s^{-1}$) | 9.7029 |
| Min Modeled FC ($\mu molm^{-2}s^{-1}$) | -13.38 |
| Max Observed FC ($\mu molm^{-2}s^{-1}$) | 6.085 |
| Min Observed FC ($\mu molm^{-2}s^{-1}$) | -12.7162 |
| Number of Data Points | 226 |

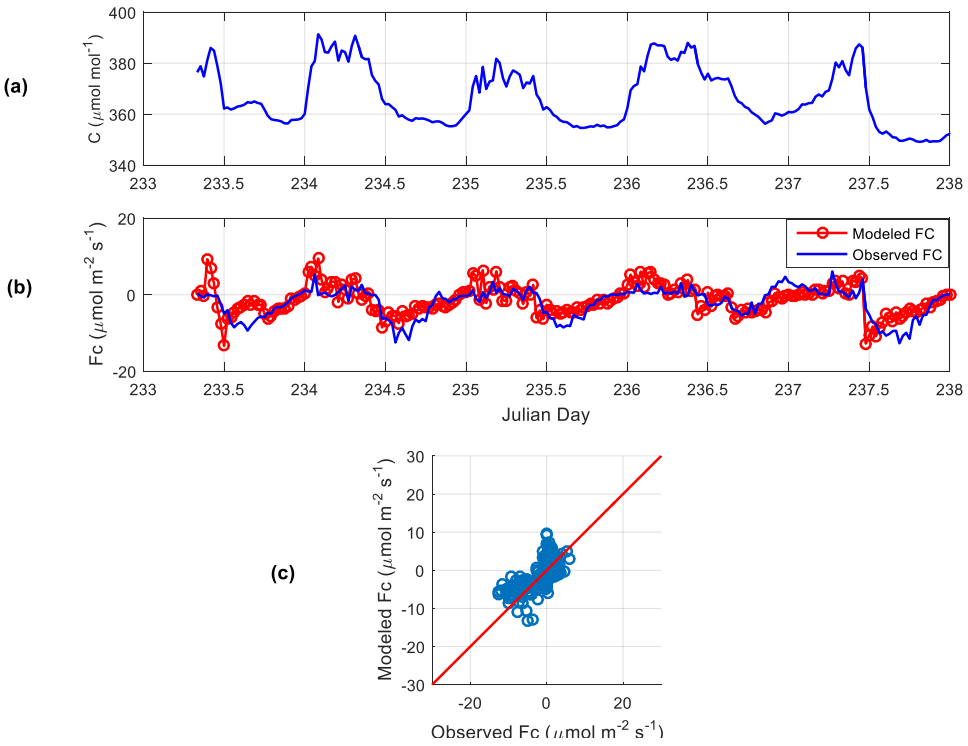


**Figure 4.2.34** (a) $CO_2$ profile, (b) Observed vs. modeled $CO_2$ fluxes, (c) Scatterplot of observed vs. modeled $CO_2$ fluxes at Delta Junction 1920-Control, Alaska. Day 233-238, 2004.

The modeled $CO_2$ fluxes using equation (3.27) capture the diurnal variation and magnitude of the observed fluxes reasonably well (Figure 4.2.34 (b)) during test period 1 (day 233 to 238, 2004). The RMSE and the NRMSE of the modeled $CO_2$ fluxes are 2.886 $\mu molm^{-2}s^{-1}$ and 15.352 % respectively, with the $CO_2$ fluxes on the order of 18.8012 $\mu mol\ m^{-2}\ s^{-1}$. The scatterplot of modeled vs. observed fluxes show good agreement (Figure 4.2.34 (c)) with correlation coefficient 0.6795 and regression coefficient, 0.6532 respectively. The maximum and minimum observed $CO_2$ fluxes are comparable to maximum and minimum modeled fluxes (Table 4.2.34). The MEP energy fluxes have correlation coefficients 0.944 and 0.9479 for sensible heat (H) and latent heat (E) fluxes, respectively. The RMSE and NRMSE for this test period are 21.6844 W $m^{-2}$ and 8.998 % with the sensible heat fluxes on the order of 190.817 W $m^{-2}$. The RMSE and NRMSE for this test period are 65.923 W $m^{-2}$ and 51.34 % with the latent heat fluxes on the order of 128.408 W $m^{-2}$. The MEP model as in (B8) – (B10) of appendix B was used to calculate the energy fluxes as ground heat flux $\approx 0$ for forested area. Due to sparse understory in this site, ground heat flux may not be zero which cannot be verified as ground heat flux were measured for only once at 12.30 AM day 235 when observed ground heat, latent heat and sensible heat fluxes were -13.6469 W $m^{-2}$, -2.525 W $m^{-2}$ and -15.873 W $m^{-2}$ respectively.

## Test Period 2: Day 247-252, 2006, Delta Junction 1920-Control, Alaska

**Table 4.2.35** Result summary for MEP modeled vs. observed sensible and latent heat fluxes at Delta Junction 1920-Control, Alaska. Day 247-252, 2004.

| Sensible Heat Flux (H) Statistics | | Latent Heat Flux (E) Statistics | |
|---|---|---|---|
| Correlation Coefficient | 0.9269 | Correlation Coefficient | 0.7734 |
| RMSE (W $m^{-2}$) | 30.344 | RMSE (W $m^{-2}$) | 63.85 |
| NRMSE | 0.1105 | NRMSE | 0.4751 |
| Max HOBS (W $m^{-2}$) | 254.1 | Max EOBS (W $m^{-2}$) | 131.25 |
| Min HOBS (W $m^{-2}$) | -20.463 | Min EOBS (W $m^{-2}$) | -3.151 |
| Max HMEP (W $m^{-2}$) | 209.29 | Max EMEP (W $m^{-2}$) | 228.18 |
| Min HMEP (W $m^{-2}$) | -32.248 | Min EMEP (W $m^{-2}$) | -22.775 |

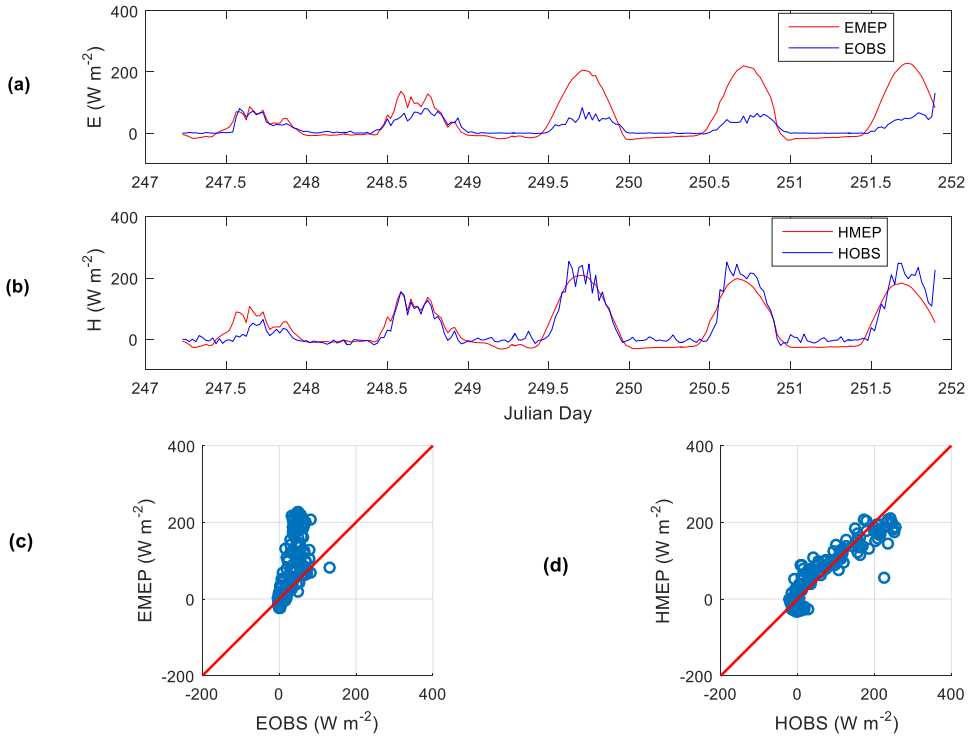


Figure 4.2.35: (a) MEP model latent heat fluxes (EMEP) vs. observed latent heat fluxes (EOBS) (b) MEP model sensible heat fluxes (HMEP) vs. observed sensible heat fluxes (HOBS) (c) Scatter plot of EMEP vs. EOBS, (d) Scatter plot of HMEP vs. HOBS at Delta Junction 1920-Control, Alaska. Day 247-252, 2004.

.

**Table 4.2.36** Result summary for modeled vs. observed $CO_2$ fluxes at Delta Junction 1920-Control, Alaska. Day 247-252, 2004.

| $CO_2$ Flux (FC) Statistics | |
|---|---|
| RMSE ($\mu molm^{-2}s^{-1}$) | 2.454 |
| NRMSE | 0.1531 |
| Correlation Coefficient | 0.524 |
| Regression Coefficient | 0.9164 |
| Max Modeled FC ($\mu molm^{-2}s^{-1}$) | 7.007 |
| Min Modeled FC ($\mu molm^{-2}s^{-1}$) | -9.581 |
| Max Observed FC ($\mu molm^{-2}s^{-1}$) | 6.021 |
| Min Observed FC ($\mu molm^{-2}s^{-1}$) | -10.0138 |
| Number of Data Points | 225 |

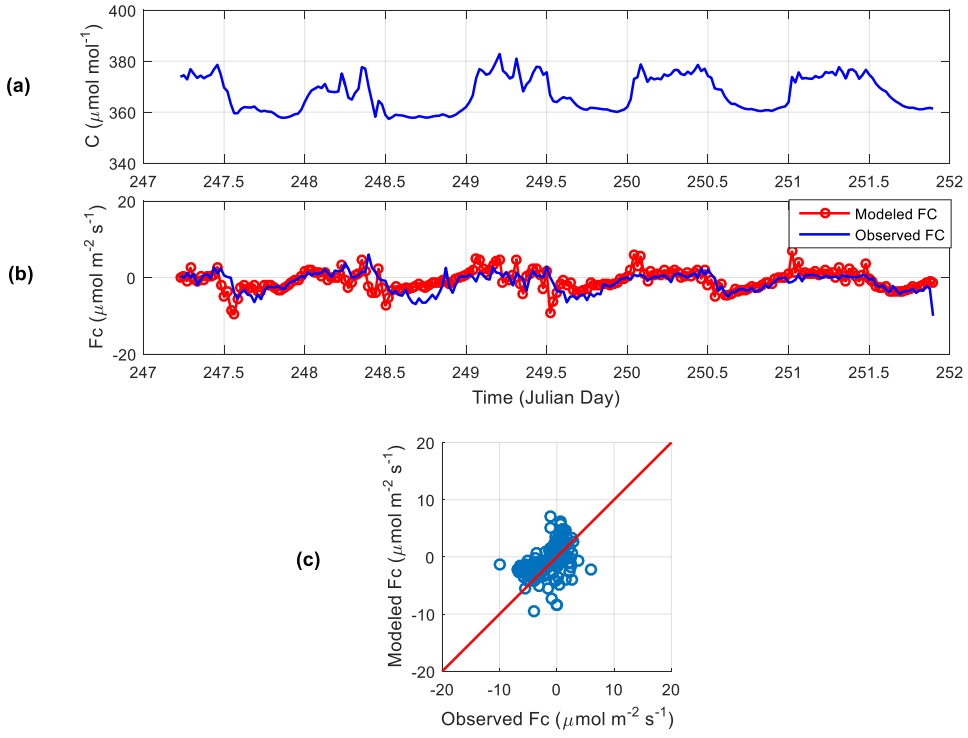


Figure 4.2.36: (a) $CO_2$ profile, (b) Observed vs. modeled $CO_2$ fluxes, (c) Scatterplot of observed vs. modeled $CO_2$ fluxes at Delta Junction 1920-Control, Alaska. Day 247-252, 2004.

Modeled $CO_2$ fluxes show reasonable agreement with observed fluxes during test period 2 (day 247 to 252, 2004) (Figure 4.2.36 (b), (c)) with correlation coefficient, 0.524 and regression coefficient, 0.9164. The RMSE and the NRMSE of the modeled $CO_2$ fluxes are 2.454 $\mu molm^{-2}s^{-1}$ and 15.31% with the $CO_2$ fluxes on the order of 16.0348 $\mu mol\ m^{-2}\ s^{-1}$. Similar to test period 1, the maximum and minimum observed $CO_2$ fluxes are comparable to maximum and minimum modeled fluxes (Table 4.2.36). The MEP energy fluxes have correlation coefficients 0.9269 and 0.7734 for sensible heat (H) and latent heat (E) fluxes respectively. The RMSE and NRMSE for this test period are 30.344 $W\ m^{-2}$ and 11.05 % with the sensible heat fluxes on the order of 274.563 $W\ m^{-2}$. The RMSE and NRMSE for this test period are 63.85 $W\ m^{-2}$ and 47.51 % with the latent heat fluxes on the order of 134.401 $W\ m^{-2}$. The large error in latent heat fluxes are due to similar causes as test period 1 (day 233 to 238, 2004) described in previous section.

### 4.2.4 Site 4

Lucky hills site (31.74°N, 110.052°W) is located on the USDA-ARS Walnut Gulch Experimental Watershed in south-eastern Arizona. The study site has a temperate semi- arid climate with mean annual temperature 17.6 °C and mean annual precipitation 320 mm. About 60% average fall during the months of July–September as part of the North American Monsoon (Adams and Comrie, 1997). The open shrubland, dominated by a diverse stand of desert shrub species with shrub heights range from 0.3 to 1 m. Most of the ground between the shrub canopies consists of bare and rocky soil (39% bare-soil cover of which 47% is composed of rock) with very small amounts of herbs and grasses. About 10% of the surface is covered with plant litter, and the canopy coverage is 51%. The eddy covariance system is located in an area with a fetch of >1 km in all directions with tower height 6.5 m (3.1 before Julian day 150, 2008).

The model uses half-hourly time-series data of $CO_2$ concentration ($\mu mol\ mol^{-1}$), canopy surface temperature $T_s$ ($^{\circ}C$) and net radiation $R_n$ ($W\ m^{-2}$) Downward $CO_2$ flux (FC) as well as latent (E) and sensible (H) heat flux from the atmosphere to canopy surface are defined as negative. Ground heat flux (G) is defined negative from the surface into the soil layer. Due to considerable percentage of bare-soil cover at this site the observed ground heat flux is substantial. The MEP model as in (B1) – (B7) of appendix B is used to estimate H, which is used in parameterization of diffusion coefficient of $CO_2$, $D_c$. The distance above the canopy surface z is measured by the difference of mean canopy height and height of $CO_2$ measurement is 4.3 m. Scattered

missing data are filled using linear interpolation when the time interval between missing data are not very large (< 3 hours). The dataset is re-grouped into multiple no-gap time series to avoid larger gaps (> 3hrs) of the time-series records.

The comparison of modeled CO2 flux using equation (3.27) with the observed eddy-covariance flux is characterized by the root-mean-square error (RMSE), the normalized root-mean-square error (NRMSE defined as the RMSE divided by the magnitude of the observed fluxes), correlation coefficient (covariance of the observed and modeled $CO_2$ fluxes divided by the product of their standard deviations) and regression coefficient (covariance of the observed and modeled $CO_2$ fluxes divided by the variance of observed $CO_2$ fluxes). The maximum and minimum observed flux over the test period and maximum and minimum model flux over test period are reported. As the MEP modeled sensible heat flux is used in the parameterization of eddy diffusivity of $CO_2$, the MEP modeled energy fluxes are compared with observed energy fluxes from eddy covariance measurements. This includes: root-mean-square error (RMSE), normalized root-mean-square error (NRMSE), correlation coefficient, maximum and minimum flux of the observed and MEP modeled heat fluxes over the test period. The results are shown in figures and tables followed by summary tables.

**Test Period 1: Day 229-238, 2006, Walnut Gulch Lucky Hills, Arizona**

**Table 4.2.37** Result summary for MEP modeled vs. observed sensible, latent and ground heat fluxes at Walnut Gulch Lucky Hills, Arizona. Day 229-238, 2008.

| Sensible Heat Flux (H) Statistics | | Latent Heat Flux (E) Statistics | | Ground Heat Flux (G) Statistics | |
|---|---|---|---|---|---|
| Correlation Coefficient | 0.9519 | Correlation Coefficient | 0.8967 | Correlation Coefficient | 0.9542 |
| RMSE ($W\ m^{-2}$) | 27.018 | RMSE ($W\ m^{-2}$) | 44.462 | RMSE ($W\ m^{-2}$) | 41.931 |
| NRMSE | 0.07344 | NRMSE | 0.1121 | NRMSE | 0.1372 |
| Max HOBS ($W\ m^{-2}$) | 291.231 | Max EOBS ($W\ m^{-2}$) | 362.232 | Max GOBS ($W\ m^{-2}$) | 198.061 |
| Min HOBS ($W\ m^{-2}$) | -76.64 | Min EOBS ($W\ m^{-2}$) | -34.23 | Min GOBS ($W\ m^{-2}$) | -107.56 |
| Max HMEP ($W\ m^{-2}$) | 233.54 | Max EMEP ($W\ m^{-2}$) | 310.59 | Max GMEP ($W\ m^{-2}$) | 227.23 |
| Min HMEP ($W\ m^{-2}$) | -22.17 | Min EMEP ($W\ m^{-2}$) | -25.96 | Min GMEP ($W\ m^{-2}$) | -60.68 |

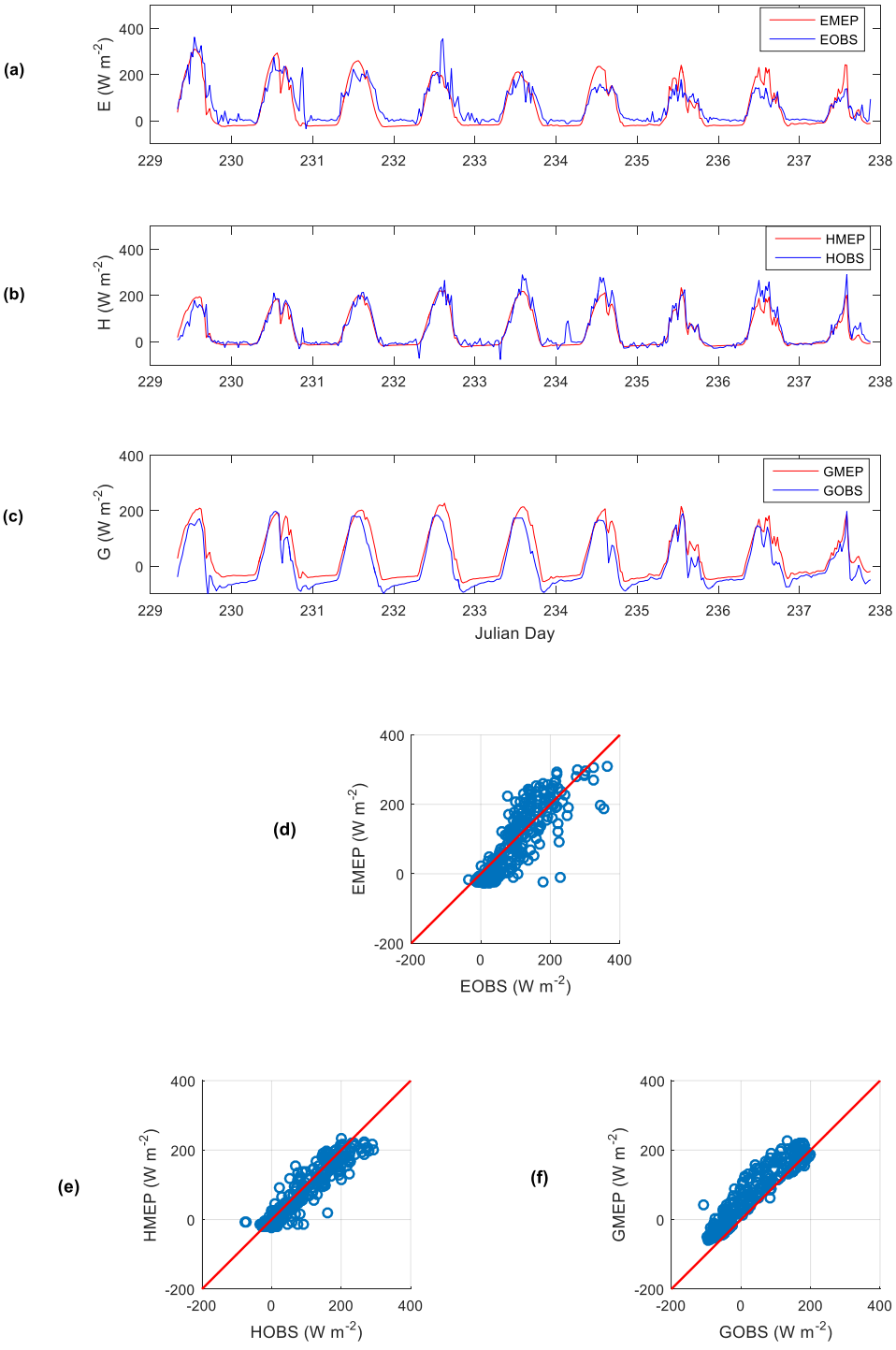


**Figure 4.2.37** (a) MEP model latent heat fluxes (EMEP) vs. observed latent heat fluxes (EOBS) (b) MEP model sensible heat fluxes (HMEP) vs. observed sensible heat fluxes (HOBS) (c) MEP model ground heat fluxes (GMEP) vs. observed ground heat fluxes (GOBS) (d) Scatter plot of EMEP vs. EOBS, (e) Scatter plot of HMEP vs. HOBS (f) Scatter plot of GMEP vs. GOBS at Walnut Gulch Lucky Hills, Arizona. Day 229-238, 2008.

**Table 4.2.38** Result summary for modeled vs. observed $CO_2$ fluxes at Walnut Gulch Lucky Hills, Arizona. Day 229-238, 2008

| $CO_2$ Flux (FC) Statistics | |
|---|---|
| RMSE ($\mu molm^{-2}s^{-1}$) | 2.584 |
| NRMSE | 0.1624 |
| Correlation Coefficient | 0.6388 |
| Regression Coefficient | 0.6451 |
| Max Modeled FC ($\mu molm^{-2}s^{-1}$) | 14.18 |
| Min Modeled FC ($\mu molm^{-2}s^{-1}$) | -12.472 |
| Max Observed FC ($\mu molm^{-2}s^{-1}$) | 5.71 |
| Min Observed FC ($\mu molm^{-2}s^{-1}$) | -10.206 |
| Number of Data Points | 410 |

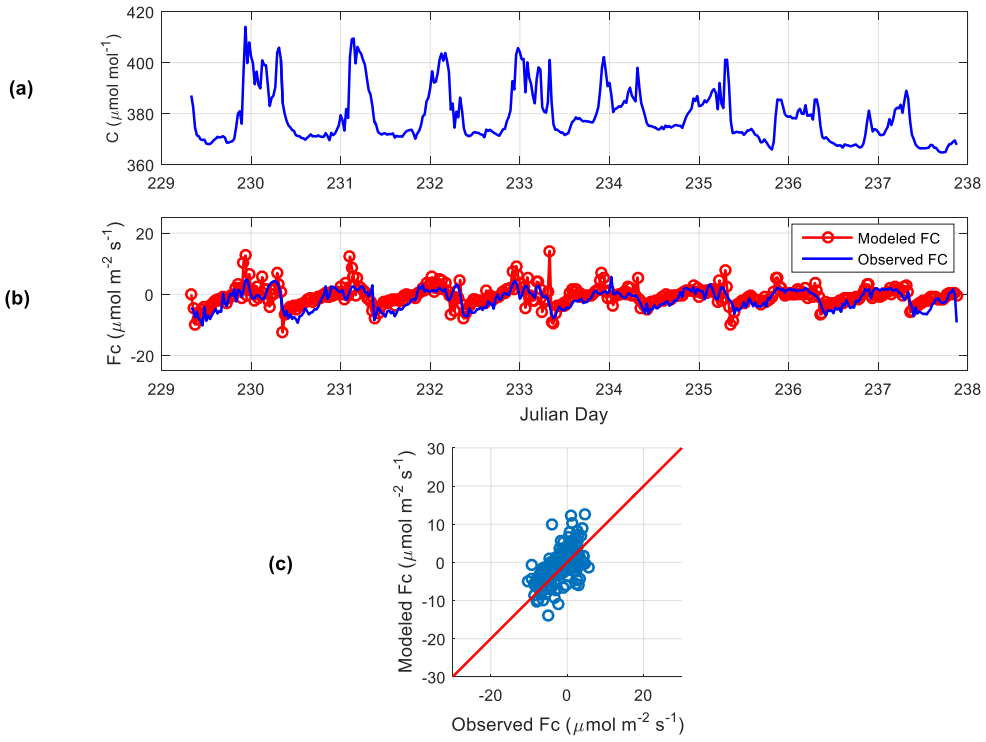


**Figure 4.2.38** (a) $CO_2$ profile, (b) Observed vs. modeled $CO_2$ fluxes, (c) Scatterplot of observed vs. modeled $CO_2$ fluxes at Walnut Gulch Lucky Hills, Arizona. Day 229-238, 2008.

The modeled $CO_2$ fluxes using equation (3.27) capture the diurnal variation and magnitude of the observed fluxes (Figure 4.2.38 (b)) reasonably well during test period 1 (day 229 to 238, 2008). The RMSE and the NRMSE of the modeled $CO_2$ fluxes are 2.584 $\mu molm^{-2}s^{-1}$ and 16.24 % respectively, with the $CO_2$ fluxes on the order of 15.916 $\mu mol\ m^{-2}\ s^{-1}$. The scatterplot of modeled vs. observed fluxes shows agreement along 1:1 line (Figure 4.2.38 (c)). The correlation coefficient was 0.6388 and regression coefficient was 0.6451 during this period. The magnitudes of modeled fluxes are comparable to the observed fluxes except for a small number of points where spikes in $CO_2$ concentration data (> 400 μmol/mol) resulted from linear interpolation of the missing $CO_2$ concentration data causing relatively large numerical errors of the calculated derivative term in (3.27) associated with large value of modeled fluxes. The correlation coefficients are 0.9519, 0.8967 and 0.9542, MEP model sensible heat (H), latent heat (E) and ground heat fluxes (G), respectively. The RMSE and NRMSE for this test period are 27.018 W $m^{-2}$ and 7.344 % with the sensible heat fluxes on the order of 367.871 W $m^{-2}$. The RMSE and NRMSE for this test period are 44.462 W $m^{-2}$ and 11.21 % with the latent heat fluxes on the order of 396.462 W $m^{-2}$. The RMSE and NRMSE for this test period are 41.931 W $m^{-2}$ and 13.72 % with the ground heat fluxes on the order of 305.621 W $m^{-2}$.

**Test Period 2: Day 245-249, 2006, Walnut Gulch Lucky Hills, Arizona**

**Table 4.2.39** Result summary for MEP modeled vs. observed sensible, latent and ground heat fluxes at Walnut Gulch Lucky Hills, Arizona. Day 245-249, 2008.

| Sensible Heat Flux (H) Statistics | | Latent Heat Flux (E) Statistics | | Ground Heat Flux (G) Statistics | |
|---|---|---|---|---|---|
| Correlation Coefficient | 0.9548 | Correlation Coefficient | 0.8943 | Correlation Coefficient | 0.9531 |
| RMSE ($W\ m^{-2}$) | 27.6134 | RMSE ($W\ m^{-2}$) | 43.652 | RMSE ($W\ m^{-2}$) | 41.129 |
| NRMSE | 0.0662 | NRMSE | 0.1635 | NRMSE | 0.1237 |
| Max OBS ($W\ m^{-2}$) | 325.302 | Max EOBS ($W\ m^{-2}$) | 229.055 | Max GOBS ($W\ m^{-2}$) | 233.89 |
| Min OBS ($W\ m^{-2}$) | -92.059 | Min EOBS ($W\ m^{-2}$) | -37.972 | Min GOBS ($W\ m^{-2}$) | -98.569 |
| Max MEP ($W\ m^{-2}$) | 265.7305 | Max EMEP ($W\ m^{-2}$) | 274.869 | Max GMEP ($W\ m^{-2}$) | 261.693 |
| Min HMEP ($W\ m^{-2}$) | -24.8721 | Min EMEP ($W\ m^{-2}$) | -25.314 | Min GMEP ($W\ m^{-2}$) | -64.556 |

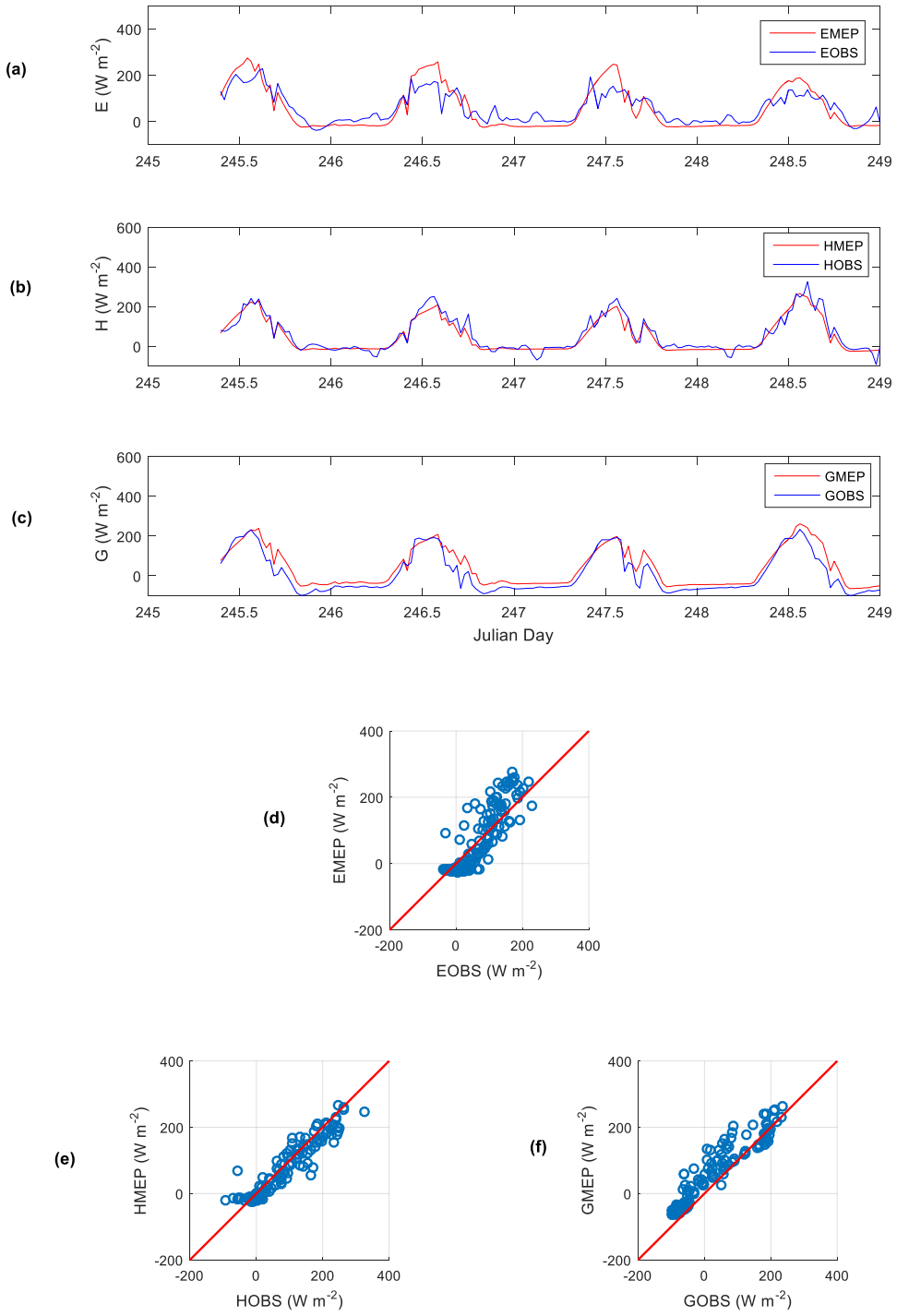


**Figure 4.2.39** (a) MEP model latent heat fluxes (EMEP) vs. observed latent heat fluxes (EOBS) (b) MEP model sensible heat fluxes (HMEP) vs. observed sensible heat fluxes (HOBS) (c) MEP model ground heat fluxes (GMEP) vs. observed ground heat fluxes (GOBS) (d) Scatter plot of EMEP vs. EOBS, (e) Scatter plot of HMEP vs. HOBS (f) Scatter plot of GMEP vs. GOBS at Walnut Gulch Lucky Hills, Arizona. Day 245-249, 2008.

**Table 4.2.40** Result summary for modeled vs. observed $CO_2$ fluxes at Walnut Gulch Lucky Hills, Arizona. Day 245-249, 2008.

| $CO_2$ Flux (FC) Statistics | |
|---|---|
| RMSE (μmolm$^{-2}$s$^{-1}$) | 2.8484 |
| NRMSE | 0.1696 |
| Correlation Coefficient | 0.5450 |
| Regression Coefficient | 0.5175 |
| Max Modeled FC (μmolm$^{-2}$s$^{-1}$) | 8.1220 |
| Min Modeled FC (μmolm$^{-2}$s$^{-1}$) | -10.9087 |
| Max Observed FC (μmolm$^{-2}$s$^{-1}$) | 8.1206 |
| Min Observed FC (μmolm$^{-2}$s$^{-1}$) | -8.679 |
| Number of Data Points | 192 |

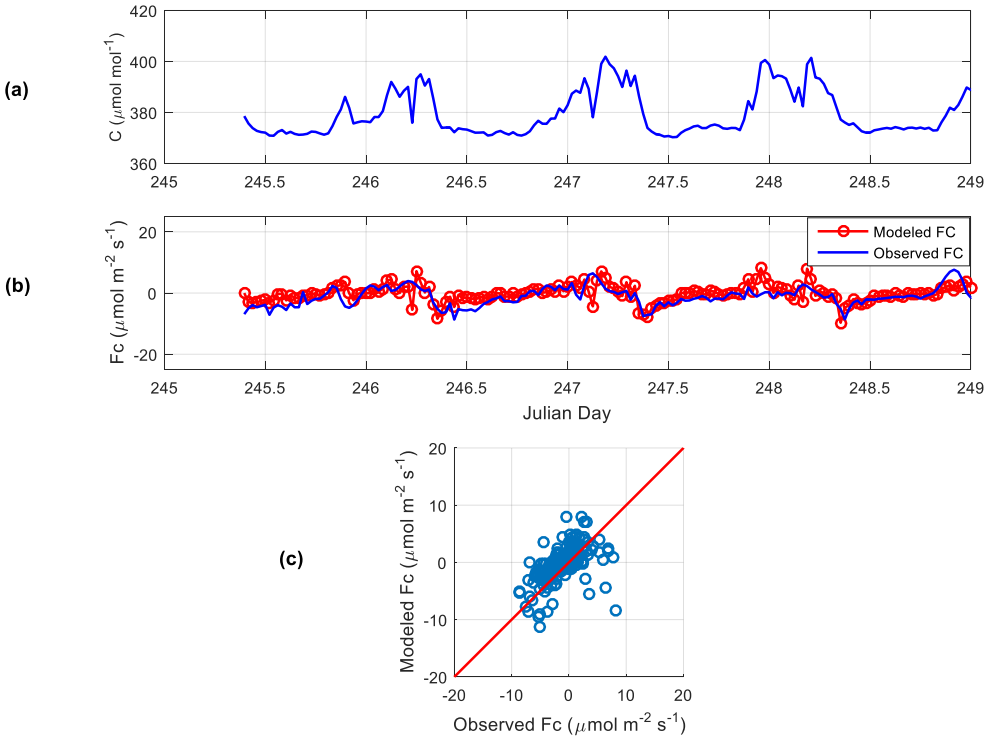


Figure 4.2.40: (a) $CO_2$ profile, (b) Observed vs. modeled $CO_2$ fluxes, (c) Scatterplot of observed vs. modeled $CO_2$ fluxes at Walnut Gulch Lucky Hills, Arizona. Day 245-249, 2008.

Similar to test period 1, the modeled $CO_2$ fluxes followed observed $CO_2$ fluxes consistently (Figure 4.2.40 (b)) during test period 2 (day 245 to 249, 2008). The scatter plot (Figure 4.2.40 (c)) shows reasonable agreement with correlation coefficient, 0.6388 and regression coefficient, 0.6451. The RMSE and the NRMSE of the modeled $CO_2$ fluxes are 2.584 $\mu molm^{-2}s^{-1}$ and 16.24 % with the $CO_2$ fluxes on the order of 15.916 $\mu mol\ m^{-2}\ s^{-1}$ for this period. The correlation coefficients are 0.9548, 0.8943 and 0.9531, MEP model sensible heat (H), latent heat (E) and ground heat fluxes (G), respectively. The RMSE and NRMSE for this test period are 27.6134 W $m^{-2}$ and 6.62 % with the sensible heat fluxes on the order of 417.361 W $m^{-2}$. The RMSE and NRMSE for this test period are 43.6516 W $m^{-2}$ and 16.35% with the latent heat fluxes on the order of 267.0273 W $m^{-2}$. The RMSE and NRMSE for this test period are 41.1285 W $m^{-2}$ and 12.37 % with the ground heat fluxes on the order of 332.458 W $m^{-2}$.

## 4.3 Result Summary

Result for sensible, latent and $CO_2$ fluxes for the four study sites are summarized in this section. Result summary for Santarem Primary Forest site in the Brazilian amazon during test period 1 to test period 10 in 2003 are presented in Tables 4.3.1, 4.3.2, 4.3.3 and 4.3.4; Summary of results for 6 test periods in 2006 at Cedar bridge site in New Jersey Pine barrens are presented in tables 4.3.5, 4.3.6 and 4.3.7; Summary of results for 2 test periods in 2004 at Delta Junction 1920 Control site north of the Alaska Range in interior Alaska are presented in tables 4.3.8 to 4.3.10; Finally summary of results for 2 test periods in 2008 in Lucky Hills site, Walnut Gulch Experimental Watershed in south-eastern Arizona are presented in tables 4.3.11, 4.3.12, 4.3.13 and 4.3.14. Table 4.3.15, 4.3.16, and 4.3.17 present the sensible heat flux, latent heat flux and $CO_2$ flux statistics averaged over testing periods for respective study sites. Due to large gaps in data only two test periods are available for Delta Junction and Lucky Hills site. The Santarem Primary forest results contain both dry (July to December) and wet seasons (January to June) in southern hemisphere while for the Cedar Bridge, Delta Junction and Lucky Hills sites results are available only during growing seasons (June-September) in northern hemisphere.

The observed vs. MEP modeled sensible heat fluxes show consistently high correlation coefficients for all the test periods for all four sites with the averaged over test periods 0.92485, 0.955333, 0.93545 and 0.95335 for Santarem Primary Forest, Cedar Bridge, Delta Junction 1920 Control and Lucky Hills respectively demonstrating the

MEP sensible modeled fluxes are capable of capturing the diurnal variation and magnitude of observed sensible heat fluxes. The NRMSE for above sites are 10.207 %, 9.7043 %, 10.024 % and 6.982 % for Santarem Primary Forest, Cedar Bridge, Delta Junction 1920 Control and Lucky Hills sites respectively. The lower (more accurate) value of NRMSE for Lucky hills site is due to using the partition of all the energy fluxes (H, E, G) in MEP model, while G is not used for Santarem Primary Forest, Cedar Bridge, Delta Junction due to forested land cover. The RMSE of MEP model sensible heat flux is about 28 W $m^{-2}$ for all the sites except cedar bridge (48.6 W $m^{-2}$) due to high standard deviation in observed sensible heat data (107.1591 W $m^{-2}$) in cedar bridge site. The mean absolute error (MAE) defined as the average of absolute differences between observed and modeled H fluxes averaged of the periods are 21.28012 W $m^{-2}$, 28.99298 W $m^{-2}$, 19.68319 W $m^{-2}$ and 18.95338 W $m^{-2}$ for Santarem Primary Forest, Cedar Bridge, Delta Junction 1920 Control and Lucky Hills site respectively. The RMSE – MAE shows there are some variability with in the errors for all the four sites although large errors are less likely to occur as the difference between RMSE and MAE is not significantly large during the test periods in the study sites. The magnitude of maximum modeled sensible heat fluxes are well comparable to observed sensible heat fluxes in all the stations except Cedar Bridge site where maximum observed sensible heat fluxes are consistently high (> 400 W $m^{-2}$) for most test periods. The modeled sensible heat fluxes during nighttime have large numerical differences with observed fluxes negative which is due to eddy covariance method tends to underestimate night time fluxes by 10-30% [Goulden et al., 1996; Twine et al., 2000]. However it has insignificant effect over $CO_2$ flux estimation using proposed method due to eddy-diffusivity parameter according to Equation (3.13)

has much reduced sensitivity to the uncertainty in model parameters due to its one third power dependence of H.

The observed vs. MEP modeled latent heat fluxes show consistently high correlation coefficients for all the test periods for all four sites with the averaged over test periods 0.93934, 0.929107, 0.86065 and 0.8955 for Santarem Primary Forest, Cedar Bridge, Delta Junction 1920 Control and Lucky Hills respectively. The NRMSE for above sites are 11.32 %, 11.88 %, 49.424 % and 13.78 % respectively for Santarem Primary Forest, Cedar Bridge, Delta Junction 1920 Control and Lucky Hills site. Relatively large error in Delta Junction site is due to The MEP model as in (B8) – (B10) of appendix B was used to calculate the energy fluxes as ground heat flux $\approx 0$ for forested area. Due to sparse understory in this site, ground heat flux may not be zero which cannot be verified as ground heat flux were measured for only once (12.30 AM day 235) during two test periods when observed ground heat was not zero. Also, latent heat fluxes are not used in computing $CO_2$ fluxes in proposed method.

The $CO_2$ flux modeled using proposed method show consistent agreement for all four test sites with average correlation coefficient in the test periods are 0.6122, 0.662, 0.602 and 0.592 for Santarem Primary Forest, Cedar Bridge, Delta Junction 1920 Control and Lucky Hills site respectively with average regression coefficient (observed flux is regressor) 0.593, 0.774, 0.785 and 0.58 respectively for above sites. The average NRMSE during the testing periods are 14.339 %, 17. 4352%, 15.331 % and 16.6 % for Santarem Primary Forest, Cedar Bridge, Delta Junction 1920 Control and Lucky Hills sites

respectively implying modeling errors are limited as for forest sites, the relative uncertainty of eddy-covariance fluxes, defined as the standard deviation of the random errors around hourly mean fluxes, may reach 50% [Vickers et al., 2010]. The average RMSE over all the test periods are 7.4596 $\mu molm^{-2}s^{-1}$, 6.382167 $\mu molm^{-2}s^{-1}$, 2.67 $\mu molm^{-2}s^{-1}$ and 2.7162 $\mu molm^{-2}s^{-1}$ with the $CO_2$ fluxes with the order of 52.9245 $\mu molm^{-2}s^{-1}$, 37.87883 $\mu molm^{-2}s^{-1}$, 17.418 $\mu molm^{-2}s^{-1}$ and 16.3578 $\mu molm^{-2}s^{-1}$ for Santarem Primary Forest, Cedar Bridge, Delta Junction 1920 Control and Lucky hills sites respectively. The standard deviation of $CO_2$ concentration data varies significantly between the test periods for the forested sites due to spikes in $CO_2$ concentration data (see Tables 4.3.4, 4.3.5, 4.3.7, 4.3.10 and 4.3.14). Due to presence of outliers in $CO_2$ concentration time series, the mean absolute error (MAE) defined as the average of absolute differences between observed and modeled $CO_2$ fluxes is calculated for the study sites which is much lower than corresponding RMSE values. The average MAE are 5.316628 $\mu molm^{-2}s^{-1}$, 4.525786 $\mu molm^{-2}s^{-1}$, 1.9216 $\mu molm^{-2}s^{-1}$ and 1.959426 $\mu molm^{-2}s^{-1}$ for Santarem Primary Forest, Cedar Bridge, Delta Junction 1920 Control and Lucky hills sites respectively. The magnitudes of the observed fluxes are well captured by modeled fluxes for all the sites except for a small number of points where spikes in $CO_2$ concentration data (> 400μmol/mol) resulted from linear interpolation of the missing $CO_2$ concentration data causing relatively large numerical errors of the calculated derivative term in (3.27) associated with large value of modeled fluxes during nighttime. Another reason for the differences in magnitude between modeled and observed fluxes during nighttime is eddy covariance method tends to underestimate night time fluxes by 10-30% [Goulden et al., 1996; Twine et al., 2000].

**Table 4.3.1** Summary of results for sensible heat fluxes at Santarem Primary Forest, Brazil, 2003

| Sensible Heat Flux (H) | Test Period 1 | Test Period 2 | Test Period 3 | Test Period 4 | Test Period 5 | Test Period 6 | Test Period 7 | Test Period 8 | Test Period 9 | Test Period 10 |
|---|---|---|---|---|---|---|---|---|---|---|
| Correlation Coefficient | 0.94 | 0.92 | 0.94 | 0.87 | 0.93 | 0.92 | 0.93 | 0.94 | 0.94 | 0.93 |
| RMSE ($W\ m^{-2}$) | 27.62 | 27.94 | 26.21 | 30.16 | 28.77 | 27.32 | 27.87 | 23.08 | 29.43 | 32.79 |
| MAE (W m-2) | 20.96 | 20.35 | 20.35 | 23.05 | 22.58 | 20.38 | 19.74 | 17.01 | 22.53 | 25.85 |
| NRMSE | 0.1209 | 0.0819 | 0.0869 | 0.1225 | 0.1093 | 0.0829 | 0.0876 | 0.0935 | 0.1159 | 0.1193 |
| RMSE-MAE ($W\ m^{-2}$) | 6.66 | 7.59 | 5.86 | 7.11 | 6.19 | 6.94 | 8.13 | 6.07 | 6.90 | 6.94 |
| SD HOBS (W m-2) | 56.02 | 62.29 | 53.65 | 42.42 | 47.87 | 52.70 | 49.21 | 46.16 | 45.83 | 46.88 |
| Max HOBS ($W\ m^{-2}$) | 189.28 | 298.95 | 239.50 | 165.77 | 212.02 | 273.78 | 246.29 | 206.28 | 193.17 | 199.56 |
| Min HOBS ($W\ m^{-2}$) | -39.07 | -42.33 | -62.09 | -80.38 | -51.26 | -55.61 | -71.90 | -40.52 | -60.66 | -75.41 |
| Max MEP ($W\ m^{-2}$) | 201.35 | 188.98 | 187.96 | 173.99 | 189.20 | 211.91 | 219.58 | 184.24 | 189.56 | 184.76 |
| Min HMEP ($W\ m^{-2}$) | -13.12 | -11.01 | -10.57 | -9.33 | -10.64 | -10.41 | -11.12 | -8.47 | -10.76 | -9.34 |

**Table 4.3.2** Summary of results for latent heat fluxes at Santarem Primary Forest, Brazil, 2003

| Latent Heat Flux (E) Statistics LBA | Test Period 1 | Test Period 2 | Test Period 3 | Test Period 4 | Test Period 5 | Test Period 6 | Test Period 7 | Test Period 8 | Test Period 9 | Test Period 10 |
|---|---|---|---|---|---|---|---|---|---|---|
| Correlation Coefficient | 0.94 | 0.95 | 0.94 | 0.94 | 0.95 | 0.93 | 0.94 | 0.94 | 0.94 | 0.94 |
| RMSE (W $m^{-2}$) | 65.64 | 62.85 | 55.30 | 44.74 | 51.43 | 57.56 | 60.22 | 49.28 | 55.46 | 52.49 |
| MAE (W m-2) | 46.87 | 45.04 | 38.67 | 29.83 | 32.62 | 37.31 | 38.28 | 32.86 | 40.37 | 39.30 |
| RMSE- MAE (W m-2) | 18.77 | 17.81 | 16.63 | 14.91 | 18.81 | 20.25 | 21.94 | 16.42 | 15.09 | 13.19 |
| NRMSE | 0.1585 | 0.1341 | 0.1381 | 0.1099 | 0.1133 | 0.1002 | 0.0961 | 0.0943 | 0.0892 | 0.0981 |
| SD EOBS (W m-2) | 127.43 | 107.84 | 104.88 | 98.91 | 104.89 | 110.52 | 119.15 | 113.20 | 141.94 | 133.77 |
| Max EOBS (W $m^{-2}$) | 404.83 | 459.99 | 382.65 | 382.65 | 439.32 | 561.86 | 594.02 | 515.28 | 581.38 | 524.40 |
| Min EOBS (W $m^{-2}$) | -9.20 | -8.74 | -17.81 | -24.47 | -14.74 | -12.91 | -32.59 | -7.35 | -28.94 | -10.42 |
| Max EMEP (W $m^{-2}$) | 552.50 | 533.57 | 499.75 | 464.48 | 487.91 | 580.99 | 594.72 | 519.24 | 537.09 | 535.84 |
| Min EMEP (W $m^{-2}$) | -33.74 | -29.17 | -27.72 | -24.95 | -26.26 | -24.39 | -28.23 | -20.32 | -40.58 | -23.63 |

**Table 4.3.3** Summary of results for $CO_2$ fluxes at Santarem Primary Forest, Brazil, Test period 1-5, 2003

| $CO_2$ Flux (FC) Statistics | Test Period 1 | Test Period 2 | Test Period 3 | Test Period 4 | Test Period 5 |
|---|---|---|---|---|---|
| RMSE ($\mu molm^{-2}s^{-1}$) | 6.36 | 8.39 | 7.52 | 7.90 | 7.57 |
| MAE ($\mu molm^{-2}s^{-1}$) | 4.48 | 5.84 | 5.61 | 5.92 | 5.59 |
| RMSE -MAE ($\mu molm^{-2}s^{-1}$) | 1.88 | 2.54 | 1.91 | 1.98 | 1.98 |
| NRMSE | 0.1285 | 0.1981 | 0.1263 | 0.1646 | 0.1267 |
| Correlation Coefficient | 0.73 | 0.42 | 0.71 | 0.55 | 0.72 |
| Regression Coefficient | 0.66 | 0.40 | 0.56 | 0.70 | 0.54 |
| Max Modeled FC ($\mu molm^{-2}s^{-1}$) | 44.30 | 59.71 | 23.26 | 71.91 | 33.84 |
| Min Modeled FC ($\mu molm^{-2}s^{-1}$) | -35.49 | -27.97 | -39.43 | -73.71 | -32.69 |
| Max Observed FC ($\mu molm^{-2}s^{-1}$) | 23.76 | 17.01 | 32.35 | 22.86 | 29.19 |
| Min Observed FC ($\mu molm^{-2}s^{-1}$) | -25.77 | -25.33 | -27.13 | -25.13 | -30.52 |
| SD Observed FC (μmolm-2s-1) | 9.72 | 9.36 | 10.54 | 10.33 | 11.05 |
| Max Observed $CO_2$ (μmol/mol) | 407.99 | 470.65 | 418.44 | 429.24 | 422.67 |
| Min Observed $CO_2$ (μmol/mol) | 367.88 | 350.48 | 367.27 | 345.65 | 366.12 |
| SD Observed $CO_2$ (μmol/mol) | 10.35 | 15.72 | 10.29 | 14.79 | 11.66 |
| Mean Observed $CO_2$ (μmol/mol) | 382.97 | 382.52 | 384.02 | 383.20 | 385.82 |
| No. of Data Points | 168 | 189 | 248 | 226 | 338 |

**Table 4.3.4** Summary of results for $CO_2$ fluxes at Santarem Primary Forest, Brazil, Test period 6-10, 2003

| $CO_2$ Flux (FC) Statistics | Test Period 6 | Test Period 7 | Test Period 8 | Test Period 9 | Test Period 10 |
|---|---|---|---|---|---|
| RMSE ($\mu molm^{-2}s^{-1}$) | 6.98 | 6.66 | 6.50 | 8.75 | 7.97 |
| MAE ($\mu molm^{-2}s^{-1}$) | 4.83 | 4.83 | 4.55 | 5.88 | 5.63 |
| RMSE -MAE ($\mu molm^{-2}s^{-1}$) | 2.15 | 1.83 | 1.95 | 2.87 | 2.34 |
| NRMSE | 0.1475 | 0.1023 | 0.1353 | 0.1525 | 0.1521 |
| Correlation Coefficient | 0.63 | 0.63 | 0.63 | 0.51 | 0.58 |
| Regression Coefficient | 0.71 | 0.75 | 0.72 | 0.45 | 0.43 |
| Max Modeled FC ($\mu molm^{-2}s^{-1}$) | 63.67 | 107.20 | 59.59 | 60.01 | 28.72 |
| Min Modeled FC ($\mu molm^{-2}s^{-1}$) | -37.83 | -59.53 | -40.33 | -62.44 | -25.90 |
| Max Observed FC ($\mu molm^{-2}s^{-1}$) | 19.93 | 29.52 | 27.31 | 23.45 | 23.94 |
| Min Observed FC ($\mu molm^{-2}s^{-1}$) | -27.38 | -35.60 | -20.73 | -33.89 | -28.45 |
| SD Observed FC (μmolm-2s-1) | 9.88 | 9.00 | 7.99 | 10.03 | 9.82 |
| Max Observed $CO_2$ (μmol/mol) | 432.59 | 439.58 | 419.47 | 425.91 | 407.13 |
| Min Observed $CO_2$ (μmol/mol) | 365.04 | 361.94 | 361.82 | 337.28 | 368.64 |
| SD Observed $CO_2$ (μmol/mol) | 13.30 | 13.16 | 10.30 | 9.94 | 8.48 |
| Mean Observed $CO_2$ (μmol/mol) | 386.32 | 384.49 | 382.43 | 383.81 | 385.03 |
| No. of Data Points | 325 | 1227 | 392 | 891 | 384 |

**Table 4.3.5** Summary of sensible heat fluxes at Cedar Bridge, New Jersey, 2006

| Sensible Heat Flux Statistics | Test Period 1 | Test Period 2 | Test Period 3 | Test Period 4 | Test Period 5 | Test Period 6 |
|---|---|---|---|---|---|---|
| Correlation Coefficient | 0.970 | 0.955 | 0.951 | 0.969 | 0.948 | 0.938 |
| RMSE (W $m^{-2}$) | 48.240 | 24.086 | 50.010 | 57.467 | 67.963 | 43.950 |
| MAE (W m-2) | 31.095 | 17.451 | 29.420 | 35.836 | 37.165 | 22.990 |
| RMSE-MAE (W $m^{-2}$) | 17.145 | 6.635 | 20.590 | 21.631 | 30.798 | 20.960 |
| NRMSE | 0.0891 | 0.0716 | 0.1080 | 0.1199 | 0.1235 | 0.0702 |
| SD HOBS (W m-2) | 117.673 | 75.348 | 104.144 | 121.697 | 121.071 | 103.023 |
| Max OBS (W $m^{-2}$) | 457.360 | 289.940 | 410.898 | 429.480 | 498.010 | 578.680 |
| Min HOBS (W $m^{-2}$) | -84.275 | -46.510 | -52.087 | -49.770 | -52.360 | -47.444 |
| Max MEP (W $m^{-2}$) | 269.420 | 197.310 | 204.110 | 222.262 | 197.510 | 229.200 |
| Min MEP (W $m^{-2}$) | -40.127 | -22.610 | -22.760 | -26.302 | -20.440 | -31.334 |

**Table 4.3.6** Summary of Latent Heat Fluxes at Cedar Bridge, New Jersey. 2006

| Latent Heat Flux Statistics | Test Period 1 | Test Period 2 | Test Period 3 | Test Period 4 | Test Period 5 | Test Period 6 |
|---|---|---|---|---|---|---|
| Correlation Coefficient | 0.938 | 0.908 | 0.929 | 0.925 | 0.926 | 0.950 |
| RMSE (W $m^{-2}$) | 61.887 | 73.811 | 82.650 | 75.851 | 80.650 | 47.960 |
| MAE (W $m^{-2}$) | 45.961 | 48.986 | 54.139 | 54.457 | 53.980 | 35.450 |
| RMSE-MAE (W $m^{-2}$) | 15.926 | 24.825 | 28.511 | 21.394 | 26.670 | 12.510 |
| NRMSE | 0.1017 | 0.0959 | 0.1167 | 0.1308 | 0.1906 | 0.0770 |
| SD EOBS (W $m^{-2}$) | 141.155 | 163.694 | 150.397 | 134.463 | 113.870 | 122.277 |
| Max EOBS (W $m^{-2}$) | 533.305 | 681.910 | 665.720 | 567.410 | 382.780 | 583.520 |
| Min EOBS (W $m^{-2}$) | -75.384 | -87.757 | -42.690 | -12.415 | -40.415 | -40.362 |
| Max EMEP (W $m^{-2}$) | 550.609 | 490.624 | 569.402 | 506.150 | 573.490 | 453.523 |
| Min EMEP (W $m^{-2}$) | -52.673 | -37.831 | -44.670 | -46.935 | -45.257 | -40.788 |

**Table 4.3.7** Summary of $CO_2$ Fluxes at Cedar Bridge, New Jersey. 2006

| $CO_2$ Flux (FC) Statistics | Test Period 1 | Test Period 2 | Test Period 3 | Test Period 4 | Test Period 5 | Test Period 6 |
|---|---|---|---|---|---|---|
| RMSE ($\mu molm^{-2}s^{-1}$) | 5.29 | 6.33 | 7.57 | 5.29 | 5.75 | 8.05 |
| MAE ($\mu molm^{-2}s^{-1}$) | 3.93 | 4.47 | 5.64 | 3.72 | 4.10 | 5.30 |
| RMSE-MAE ($\mu molm^{-2}s^{-1}$) | 1.36 | 1.86 | 1.93 | 1.58 | 1.65 | 2.76 |
| NRMSE | 0.1494 | 0.1759 | 0.1895 | 0.2027 | 0.1950 | 0.1336 |
| Correlation Coefficient | 0.80 | 0.73 | 0.66 | 0.57 | 0.66 | 0.55 |
| Regression Coefficient | 0.82 | 0.73 | 0.82 | 0.77 | 0.95 | 0.56 |
| Max Modeled FC ($\mu molm^{-2}s^{-1}$) | 27.50 | 22.97 | 39.81 | 33.74 | 25.58 | 25.20 |
| Min Modeled FC ($\mu molm^{-2}s^{-1}$) | -23.19 | -24.21 | -30.62 | -38.81 | -30.04 | -23.36 |
| Max Observed FC ($\mu molm^{-2}s^{-1}$) | 11.75 | 10.06 | 16.94 | 8.24 | 9.47 | 16.13 |
| Min Observed FC ($\mu molm^{-2}s^{-1}$) | -23.67 | -25.94 | -23.01 | -17.87 | -20.02 | -44.17 |
| SD Observed FC (μmolm-2s-1) | 8.44 | 8.79 | 8.31 | 6.61 | 6.01 | 8.08 |
| Max Observed $CO_2$ (μmol/mol) | 427.96 | 420.43 | 465.16 | 434.36 | 431.54 | 442.38 |
| Min Observed $CO_2$ (μmol/mol) | 360.61 | 348.40 | 359.04 | 355.90 | 360.55 | 362.33 |
| SD Observed $CO_2$ (μmol/mol) | 16.18 | 18.13 | 23.09 | 16.64 | 17.26 | 16.73 |
| Mean Observed $CO_2$ (μmol/mol) | 390.56 | 378.80 | 393.62 | 380.17 | 382.84 | 388.84 |
| No. of Data Points | 480 | 287 | 343 | 345 | 220 | 283 |

**Table 4.3.8** Summary of sensible heat fluxes at Delta Junction, Alaska. 2004

| Sensible Heat Flux Statistics | Test Period 1 | Test Period 2 |
|---|---|---|
| Correlation Coefficient | 0.944 | 0.9269 |
| RMSE(W $m^{-2}$) | 21.6844 | 30.344 |
| MAE (W $m^{-2}$) | 16.08 | 23.29 |
| RMSE-MAE (W $m^{-2}$) | 5.61 | 7.05 |
| NRMSE | 0.08998 | 0.1105 |
| SD HOBS (W $m^{-2}$) | 61.69 | 79.78 |
| Max HOBS (W $m^{-2}$) | 206.074 | 254.1 |
| Min HOBS (W $m^{-2}$) | -34.93 | -20.463 |
| Max HMEP (W $m^{-2}$) | 171.28 | 209.29 |
| Min HMEP (W $m^{-2}$) | -19.537 | -32.248 |

**Table 4.3.9** Summary of latent heat fluxes at Delta Junction, Alaska. 2004

| Latent Heat Flux Statistics | Test Period 1 | Test Period 2 |
|---|---|---|
| Correlation Coefficient | 0.9479 | 0.7734 |
| RMSE (W $m^{-2}$) | 65.923 | 63.85 |
| MAE (W $m^{-2}$) | 44.04 | 39.90 |
| RMSE-MAE (W $m^{-2}$) | 21.88 | 23.95 |
| NRMSE | 0.5134 | 0.4751 |
| SD EOBS (W $m^{-2}$) | 34.60 | 25.56 |
| Max EOBS (W $m^{-2}$) | 120.488 | 131.25 |
| Min EOBS (W $m^{-2}$) | -7.92 | -3.151 |
| Max EMEP (W $m^{-2}$) | 268.38 | 228.18 |
| Min EMEP (W $m^{-2}$) | -28.3 | -22.775 |

**Table 4.3.10** Summary of $CO_2$ fluxes at Delta Junction, Alaska. 2004

| $CO_2$ Flux (FC) Statistics | Test Period 1 | Test Period 2 |
|---|---|---|
| RMSE ($\mu molm^{-2}s^{-1}$) | 2.886 | 2.454 |
| MAE ($\mu molm^{-2}s^{-1}$) | 2.20 | 1.64 |
| RMSE-MAE ($\mu molm^{-2}s^{-1}$) | 0.69 | 0.81 |
| NRMSE | 0.15352 | 0.1531 |
| Correlation Coefficient | 0.6795 | 0.524 |
| Regression Coefficient | 0.6532 | 0.9164 |
| Max Modeled FC ($\mu molm^{-2}s^{-1}$) | 9.7029 | 7.007 |
| Min Modeled FC ($\mu molm^{-2}s^{-1}$) | -13.38 | -9.581 |
| Max Observed FC ($\mu molm^{-2}s^{-1}$) | 6.085 | 6.021 |
| Min Observed FC ($\mu molm^{-2}s^{-1}$) | -12.7162 | -10.014 |
| SD Observed FC (μmolm-2s-1) | 3.88 | 2.45 |
| Max Observed $CO_2$ (μmol/mol) | 391.33 | 382.81 |
| Min Observed $CO_2$ (μmol/mol) | 349.12 | 357.33 |
| SD Observed $CO_2$ (μmol/mol) | 11.54 | 6.86 |
| Mean Observed $CO_2$ (μmol/mol) | 366.64 | 367.38 |
| No. of Data Points | 226 | 225 |

**Table 4.3.11** Summary of sensible heat fluxes at Lucky Hills, Arizona. 2008

| Sensible Heat Flux (H) | Test Period 1 | Test Period 2 |
|---|---|---|
| Correlation Coefficient | 0.9519 | 0.9548 |
| RMSE(W $m^{-2}$) | 27.018 | 27.6134 |
| MAE (W $m^{-2}$) | 18.23 | 19.68 |
| RMSE-MAE (W $m^{-2}$) | 8.79 | 7.94 |
| NRMSE | 0.07344 | 0.0662 |
| SD HOBS (W $m^{-2}$) | 83.45 | 87.90 |
| Max HOBS (W $m^{-2}$) | 291.231 | 325.302 |
| Min HOBS (W $m^{-2}$) | -76.64 | -92.059 |
| Max HMEP (W $m^{-2}$) | 233.54 | 265.731 |
| Min HMEP (W $m^{-2}$) | -22.17 | -24.872 |

**Table 4.3.12** Summary of latent heat fluxes at Lucky Hills, Arizona. 2008

| Latent Heat Flux (E) Statistics | Test Period 1 | Test Period 2 |
|---|---|---|
| Correlation Coefficient | 0.8967 | 0.8943 |
| RMSE (W $m^{-2}$) | 44.462 | 43.652 |
| MAE (W m-2) | 33.94 | 34.74 |
| RMSE-MAE (W $m^{-2}$) | 10.52 | 8.91 |
| NRMSE | 0.1121 | 0.1635 |
| SD EOBS (W m-2) | 80.23 | 63.51 |
| Max EOBS (W $m^{-2}$) | 362.232 | 229.055 |
| Min EOBS (W $m^{-2}$) | -34.23 | -37.972 |
| Max EMEP (W $m^{-2}$) | 310.59 | 274.869 |
| Min EMEP (W $m^{-2}$) | -25.96 | -25.314 |

**Table 4.3.13** Summary of ground heat fluxes at Lucky Hills, Arizona. 2008

| Ground Heat Flux (G) | Test Period 1 | Test Period 2 |
|---|---|---|
| Correlation Coefficient | 0.9542 | 0.9531 |
| RMSE(W $m^{-2}$) | 41.931 | 41.129 |
| MAE (W m-2) | 33.86 | 32.31 |
| RMSE-MAE (W $m^{-2}$) | 8.07 | 8.82 |
| NRMSE | 0.1372 | 0.1237 |
| SD GOBS (W m-2) | 85.42 | 96.58 |
| Max GOBS (W $m^{-2}$) | 198.061 | 233.89 |
| Min GOBS (W $m^{-2}$) | -107.56 | -98.569 |
| Max GMEP (W $m^{-2}$) | 227.23 | 261.693 |
| Min GMEP (W $m^{-2}$) | -60.68 | -64.556 |

**Table 4.3.14** Summary of $CO_2$ fluxes at Lucky Hills, Arizona. 2008

| $CO_2$ Flux (FC) Statistics | Test Period 1 | Test Period 2 |
|---|---|---|
| RMSE ($\mu molm^{-2}s^{-1}$) | 2.584 | 2.8484 |
| MAE ($\mu molm^{-2}s^{-1}$) | 1.94 | 1.98 |
| RMSE-MAE ($\mu molm^{-2}s^{-1}$) | 0.65 | 0.86 |
| NRMSE | 0.1624 | 0.1696 |
| Correlation Coefficient | 0.6388 | 0.545 |
| Regression Coefficient | 0.6451 | 0.5175 |
| Max Modeled FC ($\mu molm^{-2}s^{-1}$) | 14.18 | 8.122 |
| Min Modeled FC ($\mu molm^{-2}s^{-1}$) | -12.472 | -10.909 |
| Max Observed FC ($\mu molm^{-2}s^{-1}$) | 5.71 | 8.1206 |
| Min Observed FC ($\mu molm^{-2}s^{-1}$) | -10.206 | -8.679 |
| SD Observed FC (µmolm-2s-1) | 3.19 | 3.05 |
| Max Observed $CO_2$ (µmol/mol) | 414.04 | 401.85 |
| Min Observed $CO_2$ (µmol/mol) | 364.78 | 368.37 |
| SD Observed $CO_2$ (µmol/mol) | 10.39 | 8.56 |
| Mean Observed $CO_2$ (µmol/mol) | 378.94 | 379.99 |
| No. of Data Points | 410 | 192 |

**Table 4.3.15** Summary results of sensible heat fluxes Averaged over test periods at Santarem Primary Forest, Brazil (2003), Cedar Bridge, New Jersey (2006), Delta Junction Control 1920, Alaska (2004) and Lucky Hills, Arizona (2008)

| Sensible Heat (H) Flux Statistics Averaged over Test Periods | Santarem Primary Forest | Cedar Bridge | Delta Junction Control | Lucky Hills |
|---|---|---|---|---|
| Correlation Coefficient | 0.92485 | 0.955333 | 0.93545 | 0.95335 |
| RMSE(W $m^{-2}$) | 28.1192 | 48.61937 | 26.0142 | 27.3157 |
| MAE (W $m^{-2}$) | 21.28012 | 28.99298 | 19.68319 | 18.95338 |
| RMSE-MAE (W $m^{-2}$) | 6.839081 | 19.62639 | 6.331009 | 8.362317 |
| NRMSE | 0.10207 | 0.097043 | 0.10024 | 0.06982 |
| SD HOBS (W $m^{-2}$) | 50.30345 | 107.1591 | 70.73488 | 85.67629 |
| Max HOBS (W $m^{-2}$) | 222.46 | 444.0613 | 230.087 | 308.2665 |
| Min HOBS (W $m^{-2}$) | -57.923 | -55.4077 | -27.6965 | -84.3495 |
| Max HMEP (W $m^{-2}$) | 193.153 | 219.9687 | 190.285 | 249.6353 |
| Min HMEP (W $m^{-2}$) | -10.4768 | -27.2622 | -25.8925 | -23.5211 |

**Table 4.3.16** Summary results of latent heat fluxes averaged over test periods at Santarem Primary Forest, Brazil (2003), Cedar Bridge, New Jersey (2006), Delta Junction Control 1920, Alaska (2004) and Lucky Hills, Arizona (2008)

| Latent Heat Flux (E) Statistics Averaged over Test Periods | Santarem Primary Forest | Cedar Bridge | Delta Junction Control | Lucky Hills |
|---|---|---|---|---|
| Correlation Coefficient | 0.93934 | 0.929107 | 0.86065 | 0.8955 |
| RMSE(W $m^{-2}$) | 55.4972 | 70.46817 | 64.8865 | 44.057 |
| MAE (W $m^{-2}$) | 38.11576 | 48.82894 | 41.97213 | 34.34375 |
| RMSE-MAE (W $m^{-2}$) | 17.38144 | 21.63923 | 22.91437 | 9.71325 |
| NRMSE | 0.11318 | 0.11878 | 0.49425 | 0.1378 |
| SD EOBS (W $m^{-2}$) | 116.255 | 137.6426 | 30.08306 | 71.86805 |
| Max EOBS (W $m^{-2}$) | 484.6378 | 569.1075 | 125.869 | 295.6435 |
| Min EOBS (W $m^{-2}$) | -16.7171 | -49.8372 | -5.5355 | -36.101 |
| Max EMEP (W $m^{-2}$) | 530.6089 | 523.9663 | 248.28 | 292.7295 |
| Min EMEP (W $m^{-2}$) | -27.8993 | -44.6923 | -25.5375 | -25.637 |

**Table 4.3.17** Summary results of $CO_2$ fluxes averaged over test periods at Santarem Primary Forest, Brazil (2003), Cedar Bridge, New Jersey (2006), Delta Junction Control 1920, Alaska (2004) and Lucky Hills, Arizona (2008)

| CO2 Flux (FC) Statistics Averaged over Test Periods | Santarem Primary Forest | Cedar Bridge | Delta Junction Control | Lucky Hills |
|---|---|---|---|---|
| RMSE ($\mu molm^{-2}s^{-1}$) | 7.4596 | 6.382167 | 2.67 | 2.7162 |
| MAE ($\mu molm^{-2}s^{-1}$) | 5.316628 | 4.525786 | 1.9216 | 1.959426 |
| RMSE-MAE ($\mu molm^{-2}s^{-1}$) | 2.142972 | 1.85638 | 0.7484 | 0.756774 |
| NRMSE | 0.14339 | 0.174352 | 0.15331 | 0.166 |
| Correlation Coefficient | 0.61218 | 0.66155 | 0.60175 | 0.5919 |
| Regression Coefficient | 0.59225 | 0.774133 | 0.7848 | 0.5813 |
| Max Modeled FC ($\mu molm^{-2}s^{-1}$) | 55.2205 | 29.13317 | 8.35495 | 11.151 |
| Min Modeled FC ($\mu molm^{-2}s^{-1}$) | -43.5316 | -28.3717 | -11.4805 | -11.6904 |
| Max Observed FC ($\mu molm^{-2}s^{-1}$) | 24.9311 | 12.10017 | 6.053 | 6.9153 |
| Min Observed FC ($\mu molm^{-2}s^{-1}$) | -27.9934 | -25.7787 | -11.365 | -9.4425 |
| SD Observed FC (μmolm-2s-1) | 9.771482 | 7.708425 | 3.166953 | 3.122375 |
| Max Observed $CO_2$ (μmol/mol) | 427.3673 | 436.9707 | 387.0725 | 407.945 |
| Min Observed $CO_2$ (μmol/mol) | 359.213 | 357.8033 | 353.2235 | 366.579 |
| SD Observed $CO_2$ (μmol/mol) | 11.79853 | 18.00399 | 9.203402 | 9.473647 |
| Mean Observed $CO_2$ (μmol/mol) | 384.0605 | 385.8048 | 367.0096 | 379.4666 |
| Total Data Points | 4388 | 1958 | 451 | 602 |

# CHAPTER 5

## CONCLUSION AND FUTURE RESEARCH

This proof-of-concept study demonstrates the feasibility of predicting surface $CO_2$ fluxes using a single level near-surface $CO_2$ concentration data. The proposed new method for estimating $CO_2$ fluxes is parameter parsimonious capturing the dynamics of $CO_2$ fluxes at sub-daily time scales. The parameterization of eddy-diffusivity based on the similarity theory of boundary layer turbulence combined with the MEP model of surface heat fluxes facilitates its application to monitoring and modeling $CO_2$ at regional to global scales using remote sensing only observations. Due to rapid improvement in satellite remote sensing technology in recent years, global $CO_2$ concentration data are becoming more abundant with improved spatial and temporal resolutions. This novel model of $CO_2$ fluxes allows direct analysis of carbon cycle in response to global climate change characterized by solar radiation, air temperature, and atmospheric water vapor in the context of coupled water-energy-carbon cycles. More independent tests of the proposed model are anticipated to further evaluate its performance and explore more applications in the study of regional and global carbon budgets. On-going work is on assessing the usefulness of the proposed model in assessing regional and global $CO_2$ fluxes only using remote sensing data. The proposed model may also be used for estimating other GHGS fluxes such as methane (CH4), Water vapor flux. The field scale tests confirm that the proposed model is a promising modeling tool for the study of regional and global GHGS budget since:

1. $CO_2$ fluxes are derived using near-surface $CO_2$ concentration time-series to avoid concentration gradient data subject to relatively large measurement errors of remote sensing observation. Use of single level $CO_2$ data facilitates the estimation of $CO_2$ fluxes using remote sensing data as accurate measurement of $CO_2$ concentration at two levels separated by a short distance (on the order of $10^0 – 10^1$ meter) required by bulk transfer models is difficult, if possible at all, from remote platforms.

2. The reduced sensitivity of the modeled fluxes to model parameters (i.e. eddy diffusivity), due to the one-sixth power dependence on sensible heat flux, could substantially reduce the uncertainties of the current estimates of regional and global carbon budget.

3. The parameterization of eddy-diffusivity using the MEP model of surface heat fluxes directly links the change of carbon fluxes in response to climate change characterized by radiative forcing, surface temperature warming and greenhouse gas (water vapor) increase as the sensible heat flux is expressed analytically as a function of the three climatic variables.

The uncertainty in eddy-covariance measurements of $CO_2$ fluxes is largely caused by intermittent turbulence, low wind velocity conditions, temperature inversions, inhomogeneous landscapes, and other random measurement errors (Aubinet, 2008; Baldocchi, 2003; Hollinger and Richardson, 2005; Post et al., 2015; Vickers et al., 2010). For forest sites, the relative uncertainty of eddy-covariance fluxes, defined as the standard

deviation of the random errors around hourly mean fluxes, may reach 50% (Vickers et al., 2010). The errors of the modeled fluxes for both sites are no more than 16%, implying that the modeling errors are limited. The modeled $CO_2$ fluxes have reduced sensitivity to the measurement error of $CO_2$ concentration at single level compared to that of the corresponding bulk gradient. The sensitivity of the modeled $CO_2$ fluxes to the model parameters (i.e. eddy-diffusivity) is also reduced due to its one-sixth power dependence on sensible heat flux. While the uncertainty of the sensible heat flux is 20% (Vickers et al., 2010), the corresponding uncertainties of the eddy-diffusivity and the modeled fluxes are only 6% and 3%, respectively. The model is expected to perform well under all-sky conditions due also to the one-sixth power dependence of the eddy-diffusivity on sensible heat flux as well as net radiation, implying much reduced sensitivity of the modeled $CO_2$ fluxes to the uncertainties of net radiation using the MEP model of heat fluxes. In fact, eddy-diffusivity parameterized according to Eq. (3.13) well characterizes the diurnal variability of turbulent mixing intensity of the surface layer even using the climatology of diurnal variations of net radiation and surface temperature.

This proof-of-concept study justifies the proposed model as a practical solution for monitoring and modeling global GHGS budget over remote areas and oceans where ground observations of GHGS fluxes are limited or non-existent. Due to rapid improvement in remote sensing technology in recent years, global $CO_2$ concentration data are available from satellites and other resources with improved spatial and temporal resolutions. Data from NASA Orbiting Carbon Observatory (OCO-2) to be launched in 2014 combined with this model could produce improved regional and global distributions

of carbon fluxes than existing ones (Marland et al., 2009) for identification $CO_2$ of sinks and sources. The new parameterization of eddy-diffusivity as in Eq (3.13) allows direct analysis of carbon cycle and budget in response to global climate change characterized by solar radiation, warming trend of temperature, atmospheric water vapor in the context of water-energy carbon cycle. More independent tests of the proposed model are anticipated to further evaluate its usefulness and explore more applications in monitoring and modeling regional and global carbon cycle and budget.

We have demonstrated the usefulness and potential of the proposed gradient independent model of $CO_2$ fluxes for the study of regional and global GHGS budget. The parsimony of model input makes it ideal for estimating fluxes of GHGS including $CO_2$ and methane given limited data availability and space-time coverage and resolution. Further field scale tests of the proposed model at daily and longer time scales are underway. One focus of the on-going research is to investigate its application to producing regional and global distributions of carbon fluxes for identifying sinks and sources of carbon and re-evaluating the regional and global carbon budget at monthly and annual time scales.

# APPENDIX A

## FRACTIONAL INTEGRAL AND DERIVATIVE

As a generalization of integration of integer order, the integral of a function of non-integer order $0 < \alpha < 1$ is defined as (Miller and Ross, 1993),

$$\frac{d^{-\alpha}f(t)}{dt^{-\alpha}} = \frac{1}{\Gamma(\alpha)}\int_0^t \frac{f(s)}{(t-s)^{1-\alpha}}ds \quad , \tag{A1}$$

The minus sign in front of $\alpha$ on the left hand side stands for integration operation. This definition is referred as Reimann-Liouville fractional integral of order $\alpha$ in mathematical literature.

The fractional derivative f(t) of order $0 < \alpha < 1$ can be defined accordingly

$$\frac{d^{\alpha}f(t)}{dt^{\alpha}} = \frac{1}{\Gamma(1-\alpha)}\frac{d}{dt}\int_0^t \frac{f(s)}{(t-s)^{\alpha}}ds \, , \tag{A2}$$

when f(0) = 0, (A2) is equivalent to

$$\frac{d^{\alpha}f(t)}{dt^{\alpha}} = \frac{1}{\Gamma(1-\alpha)}\int_0^t \frac{\acute{f}(s)}{(t-s)^{\alpha}}ds \, , \tag{A3}$$

For example, fractional integral/derivative of a liner function f (t) = t, are shown to be based on (A2) and (A3)

$$\frac{d^{-\alpha}f(t)}{dt^{-\alpha}} = \frac{t^{1+\alpha}}{\Gamma(2+\alpha)} \ , \tag{A4}$$

$$\frac{d^{\alpha}f(t)}{dt^{\alpha}} = \frac{t^{1-\alpha}}{\Gamma(2-\alpha)} \ , \tag{A5}$$

Where, the prime symbol ( ´ ) stands for derivative and Γ stands for gamma function. As $\alpha \to 0$ and 1, the results are given by ordinary calculus.

# APPENDIX B

## MEP MODEL OF HEAT FLUXES

The Maximum Entropy Production (MEP) model (Wang and Bras, 2011) predicts the surface heat fluxes by partitioning land surface net radiation flux into the surface turbulent and conductive heat fluxes

$$E + H + G = R_n \tag{B1}$$

Where, $E$ (W m$^{-2}$) is the latent heat flux, $H$ (W m$^{-2}$) is the sensible heat flux, $G$ (W m$^{-2}$) is the ground heat flux and $R_n$ (W m$^{-2}$) is the net radiation. Following the MEP formalism, the surface heat fluxes are expressed as

$$G = \frac{B(\sigma)}{\sigma}\frac{I_S}{I_0}H|H|^{-\frac{1}{6}} \tag{B2}$$

$$E = B(\sigma)\,H \tag{B3}$$

$$B(\sigma) = 6\left(\sqrt{1+\frac{11}{36}\sigma} - 1\right) \tag{B4}$$

$$\sigma = \frac{\lambda^2 q_s}{c_p R_v T_s^2} \tag{B5}$$

Where, $I_s$ (W m$^{-2}$ K$^{-1}$ s$^{1/2}$) is the thermal inertia of soil varying with moisture content (e.g., Verhoef, 2004). A convenient method for estimating $I_s$ is based on an

analytic solution of diffusion equation (Wang et al., 2010). $I_0$ (W m$^{-2}$ K$^{-1}$ s$^{1/2}$) is the "apparent thermal inertia of the air" parameterized based on Monin-Obukhov Similarity Theory (MOST) (Wang and Bras, 2009). $T_s$ is the temperature at soil skin (or canopy) surface (K), $\lambda$ is the latent heat of vaporization of liquid water (2.5 $\times 10^6$ J kg$^{-1}$ K$^{-1}$), $c_p$ is the specific heat of air at constant pressure ($10^3$ J kg$^{-1}$K$^{-1}$) and $R_v$ is the gas constant of water vapor (461 J kg$^{-1}$K$^{-1}$). $q_s$ is the specific humidity at ground (or canopy) surface (kg kg$^{-1}$). $q_s$ may be directly measured or estimated from meteorological and/or hydrological variables. The most convenient method to compute $q_s$ from relative humidity (RH) and surface temperature ($T_s$) using Clausius-Clapeyron equation according to (B6).

$$q_s(T_s) = 0.62 \left(\frac{e_0}{P_s}\right) \exp\left[\frac{\lambda}{R_v}\left(\frac{1}{T_0} - \frac{1}{T_s}\right)\right] \quad \text{(B6)}$$

Alternately $q_s$ may be derived from surface temperature ($T_s$) and surface soil water potential ($\psi_s$) if the retention curve in known given by (B7) (Edelfsen and Anderson, 1943, p.141).

$$q_s(T_s, \psi_s) = \frac{e_0}{P_s} \exp\left[\frac{\lambda}{R_v}\left(\frac{1}{T_0} - \frac{1}{T_s}\right)\right] \exp\left(\frac{g\,\psi_s}{R_v T_s}\right) \quad \text{(B7)}$$

Where, $e_0$ is the saturation vapor pressure at (an arbitrary reference temperature $T_0$, $P_s$ is the surface atmospheric pressure ($10^5$ Pa) and g is the gravitational constant (9.81 m s$^{-2}$). At $T_0 = 273K, e_0 = 611\ Pa$.

Over land surfaces covered with close canopy $I_s \cong 0$. The surface heat fluxes are expressed using (B1) - (B3) reduces to

$$G = 0 \tag{B8}$$

$$H = \frac{R_n}{1+B(\sigma)} \tag{B9}$$

$$E = \frac{R_n}{1+B^{-1}(\sigma)} \tag{B10}$$

Where, $B(\sigma)$ and $\sigma$ are given by (B4) and (B5) respectively except $T_s$ and $q_s$ represent leaf temperature and specific humidity at leaf surface (Wang and Bras, 2011).

# APPENDIX C

## MATLAB CODES

The procedures to compute $F_c$ using HOD method consist of the following steps:

1) Load $CO_2$ concentration, $CO_2$ flux, net radiation, and canopy surface temperature data from **.csv file**. 2) Find a period with most available data and fill the missing points using **linear interpolation**. 3) Compute H in terms of $R_n$ and $T_s$ using **MEP model**. 4) Compute $D_c$ in terms of H and z using Eq. (3.13). 5) Compute $F_c$ in terms of $D_c$ and C using Eq. (3.27). 6) Compare the modeled $F_c$ to the observed $F_c$. Steps 1-6 are illustrated by Figure C.1

The procedures to run the numerical model are as follows:

1) Run **readme.m** (MATLAB Code) to upload **input data** (Santarem_KM67_Pramary_2003.csv) in **MATLAB**. 2) Run the **Interpolation.m** (MATLAB Code) to fill the missing data points, if any, using linear interpolation.
3) Run **MEP.m** (MATLAB Code) to calculate H, variable MEP_H, using input data of $R_n$ and $T_s$, saved in file **MEP_40_50.mat**. for Forested Areas. Use **MEP_New.m** (MATLAB Code) and **FMEP.m** (MATLAB Code) for less vegetated areas.
4) Run the **HOD.m** (MATLAB Code) to calculate $D_c$ according to Eq. (3.13) followed by $F_c$ according to Eq. (3.27), and plot the results in Figure 1. The input data and model output are shown in Appendix D.

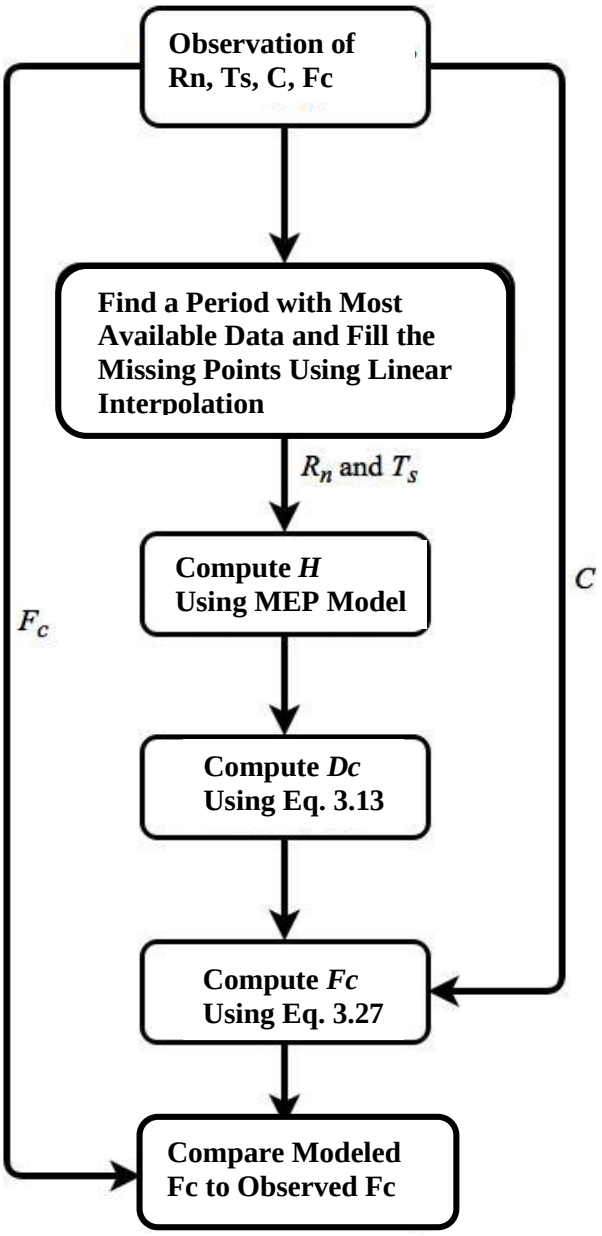


**Figure C1:** Flow Chart of Proposed Model

**CODE 1: readdata.m**

```
%Reads data from .csv file to .mat file
clc
clear
filename = 'Santarem_KM67_Pramary_2003.csv';
Rn = xlsread(filename,'BJ2:BJ8761'); %Rn, Net Radiation (W m-2)
RH = xlsread(filename,'AO2:AO8761'); %RH, Relative Humidity of Air
Ts = xlsread(filename,'BW2:BW8761'); %Ts, Canopy Surface Temperature
P = xlsread(filename,'BE2:BE8761');%P, Pressure (Kpa)
CO2 = xlsread(filename,'T2:T8761');%CO2,CO2 Concentration (µmol/mol)
LE = xlsread(filename,'AV2:AV8761'); % LE, Observed Latent Heat Flux(W m-2)
H =  xlsread(filename,'AU2:AU8761'); % Observed Sensible Heat Flux(W m-2)
FC = xlsread(filename,'AW2:AW8761'); %FC, Observed CO2 Flux (µmol m-2s-1)
WS = xlsread(filename,'BF2:BF8761'); % WS, Wind Speed (m/s)
TA = xlsread(filename,'BP2:BP8761'); % TA, Air Temperature
UST = xlsread(filename,'BK2:BK8761');% UST, Friction Velocity (m/s)
save('Santarem_KM67_Pramary_2003.mat','Rn',
'RH','Ts','P','CO2','LE','H','FC','WS','TA','UST'); % Saving Excel data to Matlab Files
N = length(Rn);  % Length of Net Radiation Data
X = 1:N; % Counts Time steps 1 to N
figure(1); plot(X, Rn); % Plotting Net Radiation
figure(2); plot(X, RH); % Plotting Relative Humidity of Air
```

```
figure(3); plot(X, Ts); % Plotting Canopy Surface Temperature

figure(4); plot(X, P); % Plotting Pressure

figure(5); plot(X, CO2); % Plotting CO2 Concentration

figure(6); plot(X, LE); % Plotting Observed Latent Heat Flux

figure(7); plot(X, H); % Plotting Observed Sensible Heat Flux

figure(8); plot(X, FC); % Plotting Observed CO2 Flux

figure(9); plot(X, WS); % Plotting Wind Speed

figure(10); plot(X, TA); % Plotting Air Temperature

figure(12); plot(X, UST); % Plotting Friction Velocity
```

**CODE 2: Interpolation.m**

```
% Finds a period with available data, fill the missing points using linear interpolation
clear
clc
close all
load('Santarem_KM67_Pramary_2003.mat','Rn',
'RH','Ts','P','CO2','LE','H','FC','WS','TA','UST'); % Load saved .matlab file.
N = length(Rn); % Length of Rn Data
X = 1:N; % Counts Time steps 1 to N
figure(1); plot(X, Rn); % Plotting Net Radiation
figure(2); plot(X, RH); % Plotting Relative Humidity of Air
figure(3); plot(X, Ts); % Plotting Canopy Surface Temperature
figure(4); plot(X, P); % Plotting Pressure
figure(5); plot(X, CO2); % Plotting CO2 Concentration
figure(6); plot(X, LE); % Plotting Observed Latent Heat Flux
figure(7); plot(X, H); % Plotting Observed Sensible Heat Flux
figure(8); plot(X, FC); % Plotting Observed CO2 Flux
figure(9); plot(X, WS); % Plotting Wind Speed
figure(10); plot(X, TA); % Plotting Air Temperature
figure(12); plot(X, UST); % Plotting Friction Velocity
```

```
% Identify missing variable (NAN)

Rn1 = Rn;

RH1 = RH;

Ts1 = Ts;

P1 = P;

CO21 = CO2;

LE1 = LE;

H1 = H;

FC1 = FC;

WS1 = WS;

TA1 = TA;

UST1 = UST;

N = length(Rn);

X = (1:N)./24;

Rn1(Rn == -9999) = NaN;

RH1(RH == -9999) = NaN;

Ts1(Ts == -9999) = NaN;

P1(P == -9999) = NaN;

CO21(CO2== -9999) = NaN;

LE1(LE == -9999) = NaN;

H1(H == -9999) = NaN;

FC1(FC == -9999) = NaN;

WS1(WS == -9999) = NaN;
```

```
TA1(TA == -9999) = NaN;
UST1(UST == -9999) = NaN;
figure(1); plot(X, Rn1); % Plotting Net Radiation with No Data
figure(2); plot(X, RH1); %Plotting Relative Humidity of Air with No Data
figure(3); plot(X, Ts1); %Plotting Canopy Surface Temperature with No Data
figure(4); plot(X, P1); % Plotting Pressure with No Data
figure(5); plot(X, CO21); % Plotting CO2 Concentration with No Data
figure(6); plot(X, LE1); % Plotting Observed Latent Heat Flux with No Data
figure(7); plot(X, H1); % Plotting Observed Sensible Heat Flux with No Data
figure(8); plot(X, FC1); % Plotting Observed CO2 Flux with No Data
xlabel('Julian Day');
ylabel('CO2 Flux (umol/(m2s))');
figure(9); plot(X, WS1); % Plotting Wind Speed with No Data
figure(10); plot(X, TA1); % Plotting Air Temperature with No Data
figure(12); plot(X, UST1); % Plotting Friction Velocity with No Data
% Selection of data for interpolation missing few data points
T1 = 960; % Starting Point
T2 = 1200; % End Point
X1 = T1:T2; % Length
X = 1:length(X1); % Counts Time steps 1 to X1
```

```
Rn2 = Rn1(X1);

RH2 = RH1(X1);

Ts2 = Ts1(X1);

P2 = P1(X1);

CO22 = CO21(X1);

LE2 = LE1(X1);

H2 = H1(X1);

FC2 = FC1(X1);

WS2 = WS1(X1);

TA2 = TA1(X1);

UST2 = UST1(X1);

Rn3 = Rn2;

RH3 = RH2;

Ts3 = Ts2;

P3 = P2;

CO23 = CO22;

LE3 = LE2;

H3 = H2;

FC3 = FC2;

WS3 = WS2;

TA3 = TA2;

UST3 = UST2;
```

```
% Interpolate missing data
Rn4 = find(~isnan(Rn3));
Rn5 = interp1(Rn4, Rn3(Rn4),X,'spline');
RH4 = find(~isnan(RH3));
RH5 = interp1(RH4, RH3(RH4),X,'spline');
Ts4 = find(~isnan(Ts3));
Ts5 = interp1(Ts4, Ts3(Ts4),X,'spline');
P4 = find(~isnan(P3));
P5 = interp1(P4, P3(P4),X,'spline');
CO24 = find(~isnan(CO23));
CO25 = interp1(CO24, CO23(CO24),X,'spline');
LE4 = find(~isnan(LE3));
LE5 = interp1(LE4, LE3(LE4),X,'spline');
H4 = find(~isnan(H3));
H5 = interp1(H4, H3(H4),X,'spline');
FC4 = find(~isnan(FC3));
FC5 = interp1(FC4, FC3(FC4),X,'spline');
WS4 = find(~isnan(WS3));
WS5 = interp1(WS4, WS3(WS4),X,'spline');
TA4 = find(~isnan(TA3));
TA5 = interp1(TA4, TA3(TA4),X,'spline');
UST4 = find(~isnan(UST3));
UST5 = interp1(UST4, UST3(UST4),X,'spline');
```

```
save('Santarem_KM67_Pramary_2003_40_50.mat','Rn5','RH5','Ts5','P5','CO25','LE5','H
5','FC5','WS5','TA5','UST5'); %Saving interpolated variables
X = (X+T1)./24;   % Changing hourly to daily (for half hourly ./48)
figure(1); plot(X, Rn5); % Plotting interpolated Net Radiation
figure(2); plot(X, RH5); %Plotting interpolated Relative Humidity of Air
figure(4); plot(X, P5); % Plotting interpolated Pressure
figure(5); plot(X, CO25); % Plotting interpolated CO2 Concentration
figure(6); plot(X, LE5); % Plotting interpolated Observed Latent Heat Flux
figure(7); plot(X, H5); % Plotting interpolated Observed Sensible Heat Flux
figure(8); plot(X, FC5); %Plotting interpolated Observed CO2 Flux
figure(9); plot(X, WS5); %Plotting interpolated Wind Speed
figure(10); plot(X, TA5); %Plotting interpolated Air Temperature
figure(12); plot(X, UST5); %Plotting interpolated Friction Velocity
figure(3); plot(X, Ts5); %Plotting interpolated Canopy surface Temperature
```

## CODE 3: MEP.m

```
%Calculates H in terms of Rn and Ts using MEP model Forested/Vegetated Areas
clear
clc
close all
load('Santarem_KM67_Pramary_2003_40_50.mat','Rn5','RH5','Ts5','P5','CO25','LE5','H5
','FC5','WS5','TA5','UST5'); %Loads Interpolated Variable Data from Code 2
% Transposed Variables
Rn = Rn5';
RH = RH5';
Ts = Ts5';
P = P5';
CO2 = CO25';
LE = LE5';
H = H5';
FC = FC5';
WS = WS5';
TA = TA5';
UST = UST5';
esT0 = 6.11; % Saturation Vapor Pressure at 273K
Lv = 2.5E6; % Latent Heat of Vaporization
Rv = 461; % Gas Constant
```

```
T0 = 273; % Reference Temperature = 273K

Rd = 287; % Gas Constant for Dry Air

KA = T0 + TA;

KS = T0 + Ts;

Length = length(Rn);

I0 = zeros(Length,1);

Julian = ((1:Length)+960)./24;

RH = 1; % Saturated as Canopy surface is saturated

P = 100; % Pressure (Kpa)

e = RH .* esT0 .* exp(Lv ./ Rv .*(1./T0 - 1./KA)); % Water Vapor Pressure

rhov = e .* 100 ./ (Rv .* KA); % Water Vapor Density

rhod = (1000 .* P - e .* 100) ./ (Rd .* KA);   % Dry Air Density

rho = rhov + rhod; % Moist Air Density

qa = rhov ./ rho; % Specific Humidity of Moist Air

qs = qa;   % Assumption Specific Humidity at Canopy Surface equals

           %Specific Humidity of Moist Air

alpha = 1; % Aerodynamic Constants

beta = 5; % Aerodynamic Constants

gamma2 = 9 % Aerodynamic Constants

kappa = 0.41;  %Von Karman Constant

cp = 1000; % Specific Gas Constant at Constant Pressure

g = 9.81; % Gravitational Constant
```

```
% MEP Equations for Latent Heat and Sensible Heat for Forested Landcover
sigma = Lv .^ 2 ./ cp ./ Rv .* qs ./ KS .^2;
B = 6 .* (sqrt(1+11./36.* sigma)-1);
EMEP = B .* Rn./(1+B);
HMEP = Rn ./ (1+B);
figure(1);
subplot(2,1,1); % Plotting Modeled  vs. Observed Latent Heat fluxes
plot(Julian, EMEP','r-',Julian, LE,'b-');
axis([40,50,-100,500]);
legend('EMEP','EOBS');
title('MEP VS OBS, 2003');
xlabel('Julian Day');
ylabel('E (W m-2)');
subplot(2,1,2); % Plotting Modeled vs. Observed Sensible Heat fluxes
plot(Julian, HMEP','r-',Julian, H,'b-');
axis([40,50,-100,300]);
legend('HMEP','HOBS');
xlabel('Julian Day');
ylabel('H (W m-2)');
save('MEP_40_50.mat','HMEP'); % Saving Modeled Sensible Heat fluxes (HMEP)
```

**CODE 3A: MEP_New.m**

```
%Calculates H in terms of Rn and Ts using MEP model for Non-Vegetated Areas

clear

clc

close all

%Loads Interpolated Variable Data from Code 2

load('Santarem_KM67_Pramary_2003_40_50.mat

','Rn5','RH5','Ts5','P5','CO25','LE5','H5','FC5','WS5','TA5','FG5','UST5','SWC5');

% Transposed Variables

Rn = Rn5';

RH = RH5';

Ts = Ts5';

P = P5';

CO2 = CO25';

LE = LE5';

H = H5';
```

```
FC = FC5';

WS = WS5';

TA = TA5';

FG = FG5';

UST = UST5';

SWC = SWC5';

 esT0 = 6.11; % Saturation Vapor Pressure at 273K

Lv = 2.5E6; % Latent Heat of Vaporization

Rv = 461; % Gas Constant

T0 = 273; % Reference Temperature

Rd = 287; % Gas Constant for Dry Air

KA = T0 + TA;

KS = T0 + Ts;

 Length = length(Rn);

HMEP = zeros(Length, 1);

EMEP = zeros(Length, 1);

GMEP = zeros(Length, 1);

I0 = zeros(Length,1);

Julian = ((1:Length)+11778)./48;

RH = RH ./ 100; % percent

e = RH .* esT0 .* exp(Lv ./ Rv .*(1./T0 - 1./KA)); % water vapor pressure

rhov = e .* 100 ./ (Rv .* KA); % water vapor density

rhod = (1000 .* P - e .* 100) ./ (Rd .* KA);
```

```
rho = rhov + rhod;

qa = rhov ./ rho;

 %MEP Assumption qs = qa

qs = qa;

alpha = 1;

beta = 5;

gamma2 = 9;

kappa = 0.41;

cp = 1000;

g = 9.81;

z = 4.3;

 % MEP Model

 sigma = Lv .^ 2 ./ cp ./ Rv .* qs ./ KS .^2;

B = 6 .* (sqrt(1+11./36.* sigma)-1);

Ids = 870; %Thermal Inertia of Dry Soil

rhow = 1000;   % Density of Water Kg/m3

cw = 4.18E3;   %Specific Heat of Liquid Water

kw = 0.58; %Heat Conductivity of Liquid Water

Iw =sqrt(rhow*cw*kw); % Thermal Inertia of water

Is = Ids + sqrt(SWC./100).*Iw; % Thermal Inertia of Moist Soil
```

```
% MEP Energy Fluxes
syms x
 for i=1:Length
   [EMEP(i),HMEP(i),GMEP(i),I0(i)]=FMEP(Rn(i),rho(i),KA(i),B(i),sigma(i),z,Is(i));
end
 % Statistical analysis

Errors1 = bsxfun(@minus, H, HMEP);  % Errors of Modeled H
SquareEs1 = Errors1.^2; % Squared Error of Modeled H
MSE1=mean(SquareEs1);  % MSE of Modeled H
RMSE1 = sqrt(mean(SquareEs1)); %RMSE of Modeled H
NRMSE1 = RMSE1/(max(H)-min(H)); % NRMSE of Modeled H
MAE1=mean(abs(Errors1));   % Mean Absolute Error
stdObsH=std(H); % Standard Deviation of Observed H
maxHMEP=max(HMEP); % Maximum Modeled H
minHMEP=min(HMEP); % Minimum Modeled H
minH=min(H); % Minimum Observed H
maxH=max(H); % Maximum Observed H
 Errors2 = bsxfun(@minus, LE, EMEP); % Errors of Modeled E
SquareEs2 = Errors2.^2;% Squared Error of Modeled E
MSE2=mean(SquareEs2); % MSE of Modeled E
RMSE2 = sqrt(mean(SquareEs2)); %RMSE of Modeled E
NRMSE2 = RMSE2/(max(LE)-min(LE)); % NRMSE of Modeled E
```

```
MAE2=mean(abs(Errors2)); % Mean Absolute Error E

stdObsE=std(LE); % Standard Deviation of Observed E

maxEMEP=max(EMEP); % Maximum Modeled E

minEMEP=min(EMEP); % Minimum Modeled E

maxE=max(LE); % Minimum Observed E

minE=min(LE); % Minimum Observed E

Errors3 = bsxfun(@minus, FG, GMEP); % Errors of Modeled G

SquareEs3 = Errors3.^2; % Squared Error of Modeled G

MSE3=mean(SquareEs3); % MSE of Modeled G

RMSE3 = sqrt(mean(SquareEs3)); %RMSE of Modeled G

NRMSE3 = RMSE3/(max(FG)-min(FG)); % NRMSE of Modeled G

MAE3=mean(abs(Errors3)); % Mean Absolute Error G

stdObsG=std(FG); % Standard Deviation of Observed G

maxGMEP=max(GMEP); % Maximum Modeled G

minGMEP=min(GMEP); % Minimum Modeled G

maxG=max(FG); % Minimum Observed G

minG=min(FG); % Minimum Observed G

CorrcoefH = corrcoef(HMEP',H);% Correlation Coefficient Observed and Modeled H

CorrcoefE = corrcoef(EMEP',LE); % Correlation Coefficient Observed and Modeled E

CorrcoefG = corrcoef(GMEP',FG); % Correlation Coefficient Observed and Modeled G
```

```
figure(1);
 subplot('position',[0.15 0.75 0.7 0.2]);
plot(Julian, EMEP,'r-',Julian, LE,'b-'); % Plotting Observed vs. Modeled E
axis([245,249,-100,500])
legend('EMEP','EOBS');
title('(a)')
ylabel('E (W m^{-2})');
subplot('position',[0.15 0.43 0.7 0.2]);
plot(Julian, HMEP,'r-',Julian, H,'b-'); % Plotting Observed vs. Modeled H
axis([245,249,-100,600])
legend('HMEP','HOBS');
%xlabel('Julian Day');
ylabel(' H (W m^{-2})');
title('(b)')
subplot('position',[0.15 0.1 0.7 0.2]);
plot(Julian, GMEP,'r-',Julian, FG,'b-'); % Plotting Observed vs. Modeled G
axis([245,249,-100,600])
legend('GMEP','GOBS');
xlabel('Julian Day');
ylabel(' G (W m^{-2})');
title('(c)')
```

```
figure(2);
subplot('position',[0.35 0.6 0.3 0.3]);
 scatter(LE,EMEP','LineWidth',1.5);hold on; % Scatterplot of Observed vs. Modeled E
plot(-800:1:800,-800:1:800,'r','LineWidth',1.5);hold off
xlabel('EOBS (W m^{-2})','FontSize',11);
ylabel('EMEP (W m^{-2})','FontSize',11);
grid on;
title('(d)','FontSize',12);
 axis([-200,400,-200,400])
axis('square');
subplot('position',[0.6 0.1 0.3 0.3]);
scatter(FG,GMEP','LineWidth',1.5);hold on; % Scatterplot of Observed vs. Modeled G
plot(-800:1:800,-800:1:800,'r','LineWidth',1.5);hold off
xlabel('GOBS (W m^{-2})','FontSize',11);
ylabel('GMEP (W m^{-2})','FontSize',11);
grid on;
title('(f)','FontSize',12);
axis([-200,400,-200,400])
axis('square');
subplot('position',[0.15 0.1 0.3 0.3]);
 scatter(H,HMEP','LineWidth',1.5);hold on; % Scatterplot of Observed vs. Modeled H
plot(-800:1:800,-800:1:800,'r','LineWidth',1.5);hold off
xlabel('HOBS (W m^{-2})','FontSize',11);
```

```
ylabel('HMEP (W m^{-2})','FontSize',11);
grid on;
title('(e)','FontSize',12);
 axis([-200,400,-200,400])
axis('square');
 save('MEP_245_249.mat','HMEP'); % Saving Variable HMEP
```

**CODE 3B: FMEP.m**

```
%Function FMEP.m uses Rn and other variables to calculate H in Dry land Area
%MEP Model %output EMEP, HMEP, GMEP and I0
function [ EMEP, HMEP, GMEP, I0 ] = FMEP( Rn, rho, KA, B, sigma, z, Is )
alpha = 1; beta = 5; gamma2 = 9;  kappa = 0.41; cp = 1000; g = 9.81;
 if Rn>0
        C1 = sqrt(3) / alpha;
        C2 = gamma2 / 2;
        else
        C1 = 1/(1+2*alpha);
        C2 = 2*beta;
end
I0 = rho * cp * sqrt(C1 * kappa * z) * ( C2 * kappa * z * g / (rho * cp * KA))^(1/6);
% Apparent Thermal Inertia of Air
HMEP = fzero(@(x) B*x*abs(x)^(1/6) + x*abs(x)^(1/6)+ B/sigma*Is/I0*x -
abs(x)^(1/6)*Rn, Rn*0.5); % Calculates HMEP
        EMEP = B*HMEP;    % Calculates EMEP
        GMEP = Rn - EMEP - HMEP; % Calculates GMEP
end
```

**CODE 4: HOD.m**

```
%Calculates Dc in terms of H and z, then calculate Fc in terms of Dc and C
clear
clc
close all
load('Santarem_KM67_Pramary_2003_40_50.mat','Rn5','RH5','Ts5','P5','CO25','LE5','H5
','FC5','WS5','TA5','UST5'); %Loads Interpolated Variable Data from Code 2
load('MEP_40_50.mat','HMEP'); % Loading Modeled Sensible Heat fluxes (HMEP)
%Interpolated Variable Data from Code 2
Rn = Rn5';
RH = RH5';
Ts = Ts5';
P = P5';
CO2 = CO25';
LE = LE5';
H = HMEP;
FC = FC5';
WS = WS5';
TA = TA5';
UST = UST5';
Length = length(H);% Length of H Data
N = Length;
```

```
t = (((1:N))+960)./24; % Starting Time (Julian Day)

rho = 1.2; % Density of Air

CO2MolMass = 44.01; % Molar Mass of CO2 Gas

AirMolMass = 28.97; % Molar Mass of Air

CO2New = 1E-6 * CO2MolMass * rho / AirMolMass * CO2; % CO2 Mass in Kg/m3

CO2FluxOBS = FC .* CO2MolMass*1E-9;  % Observed CO2 flux in Kg/m3

zb = 19; % Distance between Canopy Surface and CO2 Measurement

kappa = 0.41;

cp = 1000;

T0 = 300; % Reference Temperature

g = 9.81;

alpha =1;

beta = 5;

gamma2 = 9;

H13 = abs(H.^(1/3));

Dc3 = zeros(N,1);

Fc3 = zeros(N,1);

Dk = zeros(N,1);
```

```
for i = 1:N       % Calculation of Diffusion Coefficient
        if H(i)>0  %Unstable Condition
            Value_Under_Sqrt = gamma2*kappa*g*H(i)*zb/(2*rho*cp*T0);
            u_star = (Value_Under_Sqrt)^(1/3);
            Ck = sqrt(3)/alpha;  % Empirical Coefficient based on MOSE Eq 3.9
            Value_Under_Sqrt_New = gamma2*kappa*g/(2*rho*cp*T0);
        else      %Stable  Condition
            Value_Under_Sqrt = -2*beta*kappa*g*H(i)*zb/(rho*cp*T0);
            u_star = (Value_Under_Sqrt)^(1/3);
            Ck = 2/(1+2*alpha); % Empirical Coefficient based on MOSE Eq 3.10
            Value_Under_Sqrt_New = -2*beta*kappa*g/(rho*cp*T0);
        end
        Dc3(i) = Ck*kappa*zb*u_star; % Diffusion Coefficient Eq 3.13
        Dk(i) = abs(Ck*kappa*(Value_Under_Sqrt_New)^(1/3)); % Eq 3.14 and 3.15
End
for i = 1:N
        if Dc3(i) == 0
            Dc3(i) = 1;
        end
        if Dk(i) == 0
            Dk(i) = 1;
            end
end
```

```
% Calculation of Model Flux Eq3.27
dt = 60*60; % Time Interval between Observations
for n = 1:N
        a = 0;   %a = summation of total
        b1 = 0;
        b2 = 0;
                for i = 1:n-1
                b1 = sum(Dc3(i:(n-1))); % b1 = sumation of Dc(i+1) to Dc(N)
                b2 = sum(Dc3(i+1:(n-1))); % b2 = sumation of Dc(i) to Dc(N)
                bb1 = sqrt(b1);
                bb2 = sqrt(b2);
                bb = bb1 - bb2;
                a = a + (CO2New(i+1)-CO2New(i))/Dc3(i)*bb;
        end
        Fc3(n) = 2*Dc3(n)/sqrt(pi*dt)*a; %Model Flux Eq3.27 (Kg/m2/s)
end
Fc3u = Fc3 .* 1E9 ./ CO2MolMass;   %Model Flux Eq3.27 (µmol/m2/s)
```

```
% Calculation of Model Flux Eq2
Fc2 = zeros(N,1);
for n = 1:N
        a = 0;
        c2 = 0;
        c1 = 0;
    for i =1:n-1
                c1 = CO2New(i+1)-CO2New(i);
                c2 = sqrt(n-i)-sqrt(n-i-1);
                a = a + c1*c2;
    end
  Fc2(n) = 2*sqrt(Dc3(n)/pi/dt)*a; %Model Flux Eq2 (Kg/m2/s)
end
Fc2u = Fc2 .* 1E9 ./ CO2MolMass; %Model Flux Eq2 (μmol/m2/s)
```

```
% Calculation of Model Flux Eq4
Fc4 = zeros(N,1);
for n = 1:N
        a = 0; b1 = 0; b2 = 0; %a = summation of total
        for i = 1:n-1
        b1 = sum(H13(i:(n-1))); % b1 = sumation of Dc(i+1) to Dc(N)
        b2 = sum(H13(i+1:(n-1))); % b2 = sumation of Dc(i) to Dc(N)
        bb1 = sqrt(b1);
        bb2 = sqrt(b2);
        bb = bb1 - bb2;
        a = a + (CO2New(i+1)-CO2New(i))/H13(i)*bb;
   end
Fc4(n) = 2*sqrt(Dk(n)*zb^(4/3)*H13(n)^2)/sqrt(pi*dt)*a;   %Model Flux Eq4 (Kg/m2/s)
end
Fc4u = Fc4 .* 1E9 ./ CO2MolMass;  % Model Flux Eq4 μmol/(m^2s)
```

```
% Statistical Analysis
min2 = min(min(FC),min(Fc2u)); % Minimum of Observed and Model2
max2 = max(max(FC),max(Fc2u));   % Maximum of Observed and Model2
min3 = min(min(FC),min(Fc3u)); % Minimum of Observed and Model3
max3 = max(max(FC),max(Fc3u));   % Maximum of Observed and Model2
Corrcoef2 = corrcoef(Fc2u,FC); %Correlation Coefficient Model2, Observed
Corrcoef3 = corrcoef(Fc3u,FC); %Correlation Coefficient Model3, Observed
P2 = polyfit(FC, Fc2u,1); %Regression Coefficient Model2, Observed
slope2 = P2(1);
P3 = polyfit(FC, Fc3u,1); %Correlation Coefficient Model3, Observed
slope3 = P3(1);
Number = find(Fc4u>min(FC) & Fc4u<max(FC)); % range between Max and min FC
Errors = Fc4u(Number) - FC(Number); %Error within range
SquareEs = Errors.^2; % Squared Error
RMSE = sqrt(mean(SquareEs))  % RMSE
RelativeE=abs(Errors./FC(Number)); % Relative Error
RMSRE = sqrt(mean(RelativeE.^2))  %Relative rooted mean square error
NRMSE = RMSE/(max(FC)-min(FC)) %Normalized RMSE
P4 = polyfit(FC(Number), Fc4u(Number),1);   %Regression Coefficient Model4, Observed
% Plotting CO2 Profile
subplot('position',[0.15 0.75 0.7 0.2]);
plot(t,CO2,'-b','LineWidth',1.5); axis([40,50,340,440])
ylabel('C (\mumol mol^{-1})','FontSize',11);
```

```
grid on
title('(a)','FontSize',12);
% Plotting Observed vs. Modeled CO2 Flux
subplot('position',[0.15 0.5 0.7 0.2]);
plot(t, Fc4u,'-or',t, FC,'b','LineWidth',1.5,'MarkerSize',6);
AX = legend('Eq (3)','Obs');
LEG = findobj(AX,'type','text');
xlabel('Time (Julian Day)','FontSize',11);
ylabel('Fc (\mumol m^{-2} s^{-1})','FontSize',11);
set(LEG,'FontSize',15)
axis([40,50,-80,60]);
grid on
title('(b)','FontSize',12);
% Plotting Scatterplot of Observed vs. modeled CO2 Flux
subplot('position',[0.325 0.07 0.35 0.35]);
scatter(FC, Fc4u,'LineWidth',1.5);hold on;
plot(-80:1:80,-80:1:80,'r','LineWidth',1.5);hold off
xlabel('Observed Fc (\mumol m^{-2} s^{-1})','FontSize',11);
ylabel('Modeled Fc (\mumol m^{-2} s^{-1})','FontSize',11);
grid on;
title('(c)','FontSize',12);
axis([-40,40,-40,40])
axis('square');
```

## Appendix D: Input Data and Model Output

**Table D1:** Input data and model output at the Santarem Forest site shown in Figure 4.2.8

| Julian Day | $C$ ($\mu$mol mol$^{-1}$) | Observed $F_c$ ($\mu$mol m$^{-2}$ s$^{-1}$) | $R_n$ (W m$^{-2}$) | $T_s$ (°C) | $H$_MEP (W m$^{-2}$) | Modeled $F_c$ ($\mu$mol m$^{-2}$ s$^{-1}$) |
|---|---|---|---|---|---|---|
| 40.96 | 388.70 | 7.397 | -27.226 | 25.266 | -8.643 | 0.000 |
| 41.00 | 388.32 | 8.717 | -26.710 | 25.005 | -8.464 | -0.347 |
| 41.04 | 390.61 | 5.168 | -22.482 | 24.837 | -7.087 | 1.828 |
| 41.08 | 396.12 | 7.959 | -27.071 | 24.355 | -8.478 | 5.923 |
| 41.13 | 401.62 | 8.314 | -16.861 | 24.150 | -5.266 | 6.542 |
| 41.17 | 404.34 | 3.557 | -8.044 | 24.058 | -2.501 | 4.663 |
| 41.21 | 407.21 | 9.495 | -15.779 | 23.928 | -4.884 | 6.719 |
| 41.25 | 402.27 | 7.975 | 86.886 | 24.169 | 26.713 | 0.756 |
| 41.29 | 388.97 | 0.311 | 219.046 | 25.331 | 67.203 | -21.116 |
| 41.33 | 382.84 | -8.994 | 178.414 | 25.730 | 55.631 | -14.293 |
| 41.38 | 378.15 | -10.737 | 242.561 | 25.884 | 76.208 | -16.428 |
| 41.42 | 377.77 | -14.550 | 327.747 | 26.052 | 103.919 | -10.603 |
| 41.46 | 373.22 | -23.904 | 434.599 | 26.972 | 139.897 | -18.442 |
| 41.50 | 373.65 | -14.207 | 470.378 | 27.698 | 151.524 | -10.382 |
| 41.54 | 372.61 | -6.893 | 333.215 | 26.993 | 104.599 | -9.802 |
| 41.58 | 373.81 | -2.359 | 124.015 | 24.974 | 37.840 | -3.920 |
| 41.63 | 375.73 | 0.618 | 100.708 | 23.679 | 31.232 | -1.119 |
| 41.67 | 377.78 | 1.789 | 21.606 | 24.055 | 6.551 | 0.346 |
| 41.71 | 382.30 | 0.306 | -6.033 | 24.293 | -1.833 | 2.253 |
| 41.75 | 390.49 | -0.375 | -15.624 | 24.373 | -4.765 | 9.067 |
| 41.79 | 390.03 | 6.893 | -17.223 | 24.874 | -5.282 | 3.277 |
| 41.83 | 392.09 | 5.415 | -18.822 | 24.503 | -5.766 | 4.326 |
| 41.88 | 389.89 | 4.717 | -17.842 | 24.679 | -5.448 | 0.858 |
| 41.92 | 393.10 | 9.751 | -14.078 | 24.670 | -4.334 | 3.847 |
| 41.96 | 400.53 | 9.007 | -10.932 | 24.132 | -3.350 | 7.628 |
| 42.00 | 399.24 | 19.225 | -17.739 | 23.854 | -5.484 | 3.700 |
| 42.04 | 394.04 | 11.554 | -25.474 | 23.669 | -7.936 | -1.085 |
| 42.08 | 389.26 | 11.084 | -19.853 | 23.531 | -6.211 | -2.698 |
| 42.13 | 390.56 | 9.305 | -22.019 | 23.319 | -6.932 | 0.814 |
| 42.17 | 390.04 | 7.986 | -20.214 | 23.245 | -6.392 | 0.039 |
| 42.21 | 392.41 | 8.360 | -14.181 | 23.189 | -4.491 | 2.132 |

**Table D1 (continued)**

| | | | | | | |
|---|---|---|---|---|---|---|
| 42.25 | 391.80 | 8.951 | 54.455 | 23.411 | 17.168 | 1.396 |
| 42.29 | 387.24 | -1.438 | 125.928 | 23.788 | 39.399 | -6.511 |
| 42.33 | 382.30 | -7.330 | 220.452 | 24.295 | 68.654 | -11.415 |
| 42.38 | 377.77 | -13.252 | 302.446 | 24.762 | 94.024 | -14.192 |
| 42.42 | 374.57 | -25.128 | 495.259 | 26.117 | 157.556 | -15.898 |
| 42.46 | 372.00 | -17.766 | 399.292 | 26.343 | 126.817 | -13.700 |
| 42.50 | 372.38 | -16.116 | 293.165 | 26.439 | 92.181 | -7.676 |
| 42.54 | 369.21 | -15.542 | 354.533 | 27.150 | 112.643 | -13.853 |
| 42.58 | 367.27 | -13.100 | 274.499 | 27.514 | 87.799 | -12.013 |
| 42.63 | 369.20 | -12.821 | 308.277 | 27.939 | 98.302 | -5.513 |
| 42.67 | 371.82 | -3.565 | 92.360 | 27.602 | 29.808 | -1.095 |
| 42.71 | 374.25 | 0.608 | 6.756 | 27.336 | 2.186 | 0.465 |
| 42.75 | 379.43 | 1.616 | -31.767 | 26.745 | -10.207 | 5.911 |
| 42.79 | 382.14 | 3.244 | -32.901 | 26.125 | -10.407 | 4.026 |
| 42.83 | 389.55 | 4.756 | -32.746 | 25.378 | -10.238 | 8.756 |
| 42.88 | 385.97 | 6.189 | -20.576 | 25.470 | -6.469 | 0.645 |
| 42.92 | 382.06 | 6.710 | -9.850 | 25.657 | -3.087 | -1.482 |
| 42.96 | 384.35 | 3.472 | -10.984 | 25.378 | -3.417 | 1.681 |
| 43.00 | 386.60 | 2.549 | -12.170 | 25.061 | -3.744 | 2.609 |
| 43.04 | 390.92 | 1.217 | -23.258 | 24.819 | -7.051 | 5.956 |
| 43.08 | 391.04 | 7.446 | -29.704 | 24.670 | -8.933 | 3.338 |
| 43.13 | 392.83 | 2.744 | -31.613 | 24.503 | -9.561 | 4.324 |
| 43.17 | 398.84 | 6.750 | -15.162 | 24.188 | -4.627 | 6.664 |
| 43.21 | 406.36 | 19.433 | -5.518 | 23.891 | -1.703 | 7.278 |
| 43.25 | 407.80 | 14.827 | 47.290 | 23.836 | 14.679 | 16.045 |
| 43.29 | 406.55 | 8.956 | 136.662 | 23.973 | 41.974 | 12.896 |
| 43.33 | 393.20 | -9.225 | 231.192 | 24.816 | 69.986 | -13.145 |
| 43.38 | 381.23 | -17.480 | 493.276 | 26.053 | 151.307 | -27.010 |
| 43.42 | 375.89 | -18.706 | 399.005 | 26.785 | 124.632 | -17.771 |
| 43.46 | 374.23 | -18.546 | 394.595 | 27.174 | 120.102 | -12.419 |
| 43.50 | 372.40 | -24.425 | 535.310 | 27.623 | 169.391 | -13.495 |
| 43.54 | 373.06 | -20.118 | 651.192 | 28.436 | 212.021 | -8.416 |
| 43.58 | 374.93 | -10.318 | 528.763 | 29.295 | 175.594 | -3.320 |
| 43.63 | 375.39 | -7.464 | 333.927 | 29.340 | 112.545 | -3.270 |
| 43.67 | 375.24 | -0.368 | 217.014 | 29.451 | 73.140 | -3.384 |
| 43.71 | 376.71 | 3.664 | -7.375 | 28.793 | -2.484 | -0.107 |
| 43.75 | 380.02 | 2.822 | -35.327 | 27.708 | -11.636 | 3.505 |
| 43.79 | 383.88 | 3.830 | -29.963 | 27.027 | -9.524 | 4.089 |
| 43.83 | 385.74 | 2.639 | -23.775 | 26.651 | -7.408 | 3.187 |
| 43.88 | 390.10 | 2.378 | -12.429 | 26.144 | -3.839 | 4.579 |

**Table D1 (continued)**

| | | | | | | |
|---|---|---|---|---|---|---|
| 43.92 | 395.56 | 0.930 | -13.976 | 25.583 | -4.312 | 7.196 |
| 43.96 | 403.48 | 15.411 | -6.911 | 25.005 | -2.124 | 8.239 |
| 44.00 | 393.73 | 16.900 | -11.346 | 23.725 | -3.530 | -2.482 |
| 44.04 | 383.69 | 11.386 | -7.272 | 23.282 | -2.291 | -5.524 |
| 44.08 | 381.25 | 6.846 | -5.673 | 22.839 | -1.817 | -3.075 |
| 44.13 | 380.21 | 8.035 | -4.848 | 22.894 | -1.555 | -2.171 |
| 44.17 | 383.20 | 14.015 | -2.888 | 22.968 | -0.924 | 0.579 |
| 44.21 | 381.01 | 16.392 | -5.054 | 22.526 | -1.634 | -1.873 |
| 44.25 | 380.46 | 1.131 | 5.261 | 22.351 | 1.717 | -1.805 |
| 44.29 | 383.67 | 2.072 | 42.342 | 22.293 | 13.798 | 3.843 |
| 44.33 | 384.91 | 4.101 | 48.376 | 22.427 | 15.611 | 2.006 |
| 44.38 | 381.15 | 0.723 | 125.686 | 22.521 | 40.163 | -6.280 |
| 44.42 | 375.11 | -13.793 | 323.060 | 23.239 | 100.281 | -16.380 |
| 44.46 | 370.09 | -20.684 | 549.369 | 25.106 | 170.288 | -19.927 |
| 44.50 | 368.45 | -18.741 | 280.668 | 25.659 | 87.840 | -11.406 |
| 44.54 | 367.84 | -10.558 | 284.175 | 24.876 | 86.088 | -9.554 |
| 44.58 | 367.58 | -4.746 | 176.385 | 24.898 | 53.796 | -7.058 |
| 44.63 | 368.33 | -1.639 | 79.528 | 24.496 | 24.111 | -3.729 |
| 44.67 | 371.40 | 1.081 | 45.283 | 24.149 | 13.645 | 0.581 |
| 44.71 | 373.55 | 3.691 | 4.900 | 24.432 | 1.476 | 0.713 |
| 44.75 | 375.00 | 5.924 | -23.364 | 24.503 | -7.075 | 1.607 |
| 44.79 | 383.67 | 7.512 | -16.195 | 24.188 | -4.954 | 6.947 |
| 44.83 | 390.14 | 8.189 | -8.510 | 23.836 | -2.636 | 6.664 |
| 44.88 | 392.34 | 7.686 | -3.507 | 23.780 | -1.092 | 3.976 |
| 44.92 | 387.06 | 6.030 | -2.115 | 23.669 | -0.661 | -0.465 |
| 44.96 | 392.38 | 4.228 | -2.424 | 23.503 | -0.761 | 4.189 |
| 45.00 | 385.45 | 2.822 | -2.991 | 23.060 | -0.952 | -2.065 |
| 45.04 | 383.62 | 2.168 | -3.868 | 22.802 | -1.240 | -0.980 |
| 45.08 | 388.56 | 2.871 | -4.075 | 22.636 | -1.317 | 3.333 |
| 45.13 | 388.56 | 6.543 | -5.570 | 22.820 | -1.789 | 1.725 |
| 45.17 | 395.24 | 11.305 | -5.622 | 22.820 | -1.804 | 6.129 |
| 45.21 | 396.75 | 6.645 | -3.095 | 22.857 | -0.994 | 3.510 |
| 45.25 | 398.32 | 1.963 | 65.657 | 22.931 | 21.036 | 14.127 |
| 45.29 | 391.40 | -0.516 | 171.957 | 23.086 | 54.152 | -2.271 |
| 45.33 | 383.91 | -13.020 | 199.190 | 23.516 | 62.860 | -9.503 |
| 45.38 | 378.06 | -14.165 | 269.645 | 24.074 | 84.607 | -13.278 |
| 45.42 | 372.64 | -20.684 | 457.283 | 25.227 | 141.876 | -18.290 |
| 45.46 | 368.80 | -16.339 | 425.617 | 25.871 | 132.865 | -16.476 |
| 45.50 | 367.79 | -17.927 | 327.774 | 26.241 | 102.634 | -11.115 |
| 45.54 | 368.36 | -13.608 | 337.678 | 26.752 | 106.499 | -7.490 |

**Table D1 (continued)**

| | | | | | | |
|---|---|---|---|---|---|---|
| 45.58 | 367.85 | -6.268 | 232.203 | 26.870 | 73.078 | -7.078 |
| 45.63 | 366.79 | -7.575 | 193.056 | 26.952 | 61.035 | -7.545 |
| 45.67 | 370.38 | -5.428 | 192.231 | 27.450 | 60.765 | 0.332 |
| 45.71 | 371.79 | -0.410 | 12.688 | 27.365 | 4.022 | -0.152 |
| 45.75 | 374.36 | 0.660 | -24.964 | 27.037 | -7.848 | 1.973 |
| 45.79 | 379.20 | 2.479 | -13.875 | 26.650 | -4.387 | 3.776 |
| 45.83 | 382.76 | 1.548 | -26.357 | 26.388 | -8.377 | 5.540 |
| 45.88 | 382.35 | 2.151 | -29.193 | 26.181 | -9.318 | 2.334 |
| 45.92 | 381.80 | 3.353 | -31.154 | 25.928 | -9.959 | 1.351 |
| 45.96 | 380.54 | 4.176 | -24.758 | 25.676 | -7.927 | 0.078 |
| 46.00 | 380.59 | 4.757 | -30.689 | 25.024 | -9.863 | 0.610 |
| 46.04 | 386.22 | 6.054 | -23.778 | 24.503 | -7.591 | 5.289 |
| 46.08 | 390.75 | 3.340 | -20.425 | 24.002 | -6.430 | 6.166 |
| 46.13 | 394.92 | 3.194 | -9.284 | 23.669 | -2.889 | 5.434 |
| 46.17 | 410.19 | 2.996 | -14.339 | 23.540 | -4.477 | 17.487 |
| 46.21 | 419.60 | 19.725 | -10.883 | 23.374 | -3.422 | 14.931 |
| 46.25 | 416.60 | 18.625 | 45.648 | 23.411 | 14.359 | 16.215 |
| 46.29 | 407.39 | 0.990 | 120.697 | 23.557 | 37.852 | 2.701 |
| 46.33 | 393.71 | -5.451 | 218.235 | 24.351 | 68.302 | -14.786 |
| 46.38 | 377.28 | -18.374 | 394.845 | 25.416 | 123.554 | -35.053 |
| 46.42 | 366.74 | -15.799 | 536.176 | 26.804 | 170.647 | -35.500 |
| 46.46 | 361.32 | -12.598 | 560.833 | 27.346 | 179.858 | -28.847 |
| 46.50 | 358.60 | -15.503 | 509.253 | 28.003 | 163.008 | -22.731 |
| 46.54 | 357.74 | -14.163 | 487.127 | 26.960 | 151.728 | -17.671 |
| 46.58 | 355.66 | -8.938 | 496.000 | 27.742 | 159.802 | -18.947 |
| 46.63 | 353.83 | -7.091 | 345.746 | 28.360 | 111.865 | -16.369 |
| 46.67 | 351.91 | -0.589 | 141.332 | 28.212 | 45.254 | -12.512 |
| 46.71 | 349.36 | -0.133 | -6.138 | 28.010 | -1.958 | -3.628 |
| 46.75 | 346.93 | 0.157 | -25.017 | 27.859 | -8.132 | -7.734 |
| 46.79 | 345.65 | 0.151 | -14.752 | 27.726 | -4.795 | -5.577 |
| 46.83 | 346.55 | 7.538 | -15.784 | 27.291 | -5.116 | -4.006 |
| 46.88 | 350.66 | 6.340 | -10.265 | 26.482 | -3.243 | -0.571 |
| 46.92 | 359.01 | 19.499 | -8.098 | 25.322 | -2.491 | 3.992 |
| 46.96 | 369.29 | 15.579 | -4.384 | 24.225 | -1.342 | 6.564 |
| 47.00 | 371.44 | 20.634 | -3.250 | 23.780 | -1.007 | 3.738 |
| 47.04 | 372.99 | 7.903 | -3.972 | 23.411 | -1.250 | 3.491 |
| 47.08 | 379.01 | 2.003 | -4.384 | 23.171 | -1.391 | 6.435 |
| 47.13 | 385.34 | 4.218 | -3.456 | 23.134 | -1.098 | 7.144 |
| 47.17 | 392.33 | 14.551 | -2.218 | 23.152 | -0.704 | 7.556 |
| 47.21 | 397.53 | 16.245 | -4.591 | 23.078 | -1.462 | 10.038 |

**Table D1 (continued)**

| | | | | | | |
|---|---|---|---|---|---|---|
| 47.25 | 403.50 | 11.177 | 0.103 | 23.171 | 0.033 | 4.146 |
| 47.29 | 409.78 | 3.862 | 39.409 | 23.030 | 12.493 | 47.518 |
| 47.33 | 414.95 | -2.185 | 133.290 | 23.368 | 41.668 | 41.266 |
| 47.38 | 411.24 | -3.956 | 108.324 | 23.944 | 33.400 | 18.390 |
| 47.42 | 406.12 | -4.578 | 207.726 | 23.850 | 63.806 | 11.172 |
| 47.46 | 402.15 | -13.225 | 270.400 | 24.602 | 82.954 | 7.731 |
| 47.50 | 396.27 | -12.852 | 291.859 | 25.359 | 89.958 | -0.266 |
| 47.54 | 392.15 | -18.026 | 371.660 | 25.680 | 113.483 | -2.318 |
| 47.58 | 386.92 | -15.555 | 359.384 | 26.059 | 109.982 | -7.227 |
| 47.63 | 382.01 | -4.523 | 131.848 | 25.916 | 40.525 | -7.396 |
| 47.67 | 375.06 | -0.917 | 15.011 | 24.847 | 4.565 | -7.066 |
| 47.71 | 364.99 | 5.447 | 0.516 | 23.460 | 0.161 | -5.169 |
| 47.75 | 357.77 | 10.168 | -4.746 | 23.208 | -1.503 | -12.312 |
| 47.79 | 351.51 | 1.065 | -6.087 | 23.115 | -1.938 | -11.385 |
| 47.83 | 352.68 | 8.380 | -2.682 | 23.152 | -0.854 | -4.900 |
| 47.88 | 356.52 | 14.454 | -2.682 | 23.115 | -0.854 | -2.141 |
| 47.92 | 362.15 | 14.629 | -2.373 | 23.078 | -0.757 | 0.361 |
| 47.96 | 367.45 | 11.994 | -1.702 | 22.894 | -0.546 | 1.549 |
| 48.00 | 372.15 | 9.638 | -1.805 | 22.636 | -0.583 | 2.489 |
| 48.04 | 377.79 | 8.876 | -2.992 | 22.443 | -0.972 | 4.513 |
| 48.08 | 383.55 | 6.796 | -3.817 | 22.268 | -1.246 | 5.685 |
| 48.13 | 389.73 | 7.103 | -3.559 | 22.305 | -1.162 | 6.525 |
| 48.17 | 395.41 | 5.467 | -5.004 | 22.360 | -1.631 | 8.062 |
| 48.21 | 401.47 | 3.493 | -2.992 | 22.342 | -0.976 | 7.401 |
| 48.25 | 407.48 | 7.309 | 13.206 | 22.323 | 4.317 | 19.795 |
| 48.29 | 412.37 | 0.410 | 63.966 | 22.256 | 20.814 | 28.729 |
| 48.33 | 416.53 | -4.309 | 199.173 | 22.630 | 63.666 | 34.097 |
| 48.38 | 418.69 | -7.633 | 281.093 | 23.462 | 88.343 | 28.943 |
| 48.42 | 419.01 | -8.984 | 358.702 | 24.361 | 112.827 | 23.976 |
| 48.46 | 373.01 | -22.812 | 361.620 | 25.162 | 115.967 | -71.578 |
| 48.50 | 368.07 | -12.575 | 248.131 | 25.603 | 80.616 | -26.616 |
| 48.54 | 368.98 | -10.973 | 204.077 | 25.380 | 64.740 | -13.197 |
| 48.58 | 366.72 | -8.736 | 185.351 | 25.608 | 59.804 | -14.554 |
| 48.63 | 370.04 | -9.223 | 156.411 | 25.130 | 47.721 | -4.311 |
| 48.67 | 370.20 | 0.078 | 74.388 | 25.154 | 22.884 | -4.567 |
| 48.71 | 374.69 | 0.223 | -6.190 | 24.795 | -1.873 | 0.725 |
| 48.75 | 378.73 | 1.967 | -14.135 | 24.893 | -4.322 | 3.498 |
| 48.79 | 376.01 | 2.395 | -26.774 | 25.005 | -8.280 | -1.688 |
| 48.83 | 407.07 | 0.726 | -23.679 | 24.002 | -7.296 | 26.322 |
| 48.88 | 384.83 | 0.095 | -24.246 | 24.392 | -7.463 | -9.122 |

**Table D1 (continued)**

| | | | | | | |
|---|---|---|---|---|---|---|
| 48.92 | 375.72 | 0.294 | -30.179 | 24.503 | -9.383 | -8.915 |
| 48.96 | 387.78 | 12.764 | -27.961 | 23.790 | -8.666 | 7.823 |
| 49.00 | 384.38 | 6.486 | -25.794 | 23.669 | -8.031 | -0.694 |
| 49.04 | 381.10 | 5.053 | -24.195 | 23.595 | -7.583 | -2.451 |
| 49.08 | 382.78 | 3.170 | -22.131 | 23.632 | -6.958 | 0.703 |
| 49.13 | 386.81 | 7.542 | -12.742 | 23.521 | -4.043 | 3.036 |
| 49.17 | 395.76 | 10.539 | -7.222 | 23.226 | -2.295 | 7.076 |
| 49.21 | 414.69 | 11.117 | -5.262 | 22.950 | -1.676 | 15.640 |
| 49.25 | 429.24 | 17.214 | 42.251 | 22.968 | 13.510 | 50.996 |
| 49.29 | 407.23 | 8.515 | 142.024 | 23.547 | 44.368 | -8.766 |
| 49.33 | 394.20 | -5.524 | 225.702 | 24.481 | 70.060 | -13.625 |
| 49.38 | 379.66 | -4.010 | 202.848 | 24.148 | 62.553 | -24.459 |
| 49.42 | 374.49 | -23.528 | 605.039 | 24.976 | 187.219 | -25.446 |
| 49.46 | 373.90 | -12.213 | 472.146 | 25.424 | 145.076 | -12.064 |
| 49.50 | 370.96 | -21.837 | 565.111 | 26.035 | 170.223 | -15.489 |
| 49.54 | 373.84 | -16.643 | 523.428 | 26.753 | 159.343 | -3.769 |
| 49.58 | 375.38 | -9.367 | 448.986 | 26.983 | 134.599 | -2.250 |
| 49.63 | 371.56 | -12.013 | 306.857 | 26.915 | 91.893 | -10.027 |
| 49.67 | 374.15 | -2.445 | 58.245 | 26.769 | 17.654 | -0.658 |
| 49.71 | 380.45 | 1.982 | -15.735 | 25.747 | -4.679 | 3.341 |
| 49.75 | 379.84 | 0.051 | -28.014 | 25.975 | -8.385 | 0.784 |
| 49.79 | 379.55 | 0.038 | -23.422 | 26.200 | -7.073 | 0.276 |
| 49.83 | 381.00 | -0.077 | -13.723 | 26.294 | -4.161 | 1.250 |
| 49.88 | 378.77 | 0.621 | -11.144 | 26.388 | -3.411 | -1.149 |
| 49.92 | 398.00 | 5.042 | -5.881 | 24.968 | -1.765 | 11.791 |
| 49.96 | 402.42 | 4.065 | -8.925 | 24.708 | -2.681 | 9.502 |
| 50.00 | 412.05 | 22.864 | -3.302 | 23.817 | -1.019 | 9.474 |
| 50.04 | 386.36 | 15.392 | -3.044 | 23.189 | -0.964 | -10.165 |
| 50.08 | 385.15 | 7.767 | -3.663 | 23.078 | -1.166 | -2.609 |
| 50.13 | 388.19 | 9.001 | -6.088 | 23.097 | -1.937 | 1.134 |
| 50.17 | 390.50 | 9.946 | -6.913 | 22.987 | -2.206 | 2.093 |
| 50.21 | 389.71 | 7.172 | -5.314 | 23.041 | -1.694 | 0.547 |
| 50.25 | 391.39 | 6.639 | 41.480 | 23.208 | 13.150 | 5.357 |
| 50.29 | 391.92 | 4.109 | 47.774 | 23.307 | 14.985 | 3.992 |
| 50.33 | 390.55 | 1.630 | 96.993 | 23.590 | 30.049 | 1.528 |
| 50.38 | 384.03 | -2.308 | 106.177 | 24.037 | 32.267 | -7.976 |
| 50.42 | 380.13 | -10.853 | 329.210 | 23.925 | 100.821 | -11.862 |
| 50.46 | 372.24 | -21.604 | 416.645 | 24.694 | 134.230 | -21.722 |
| 50.50 | 372.81 | -20.038 | 408.664 | 25.565 | 122.573 | -8.618 |
| 50.54 | 373.37 | -16.842 | 391.949 | 25.306 | 117.238 | -5.858 |

**Table D1 (continued)**

| | | | | | | |
|---|---|---|---|---|---|---|
| 50.58 | 379.85 | -6.157 | 217.825 | 24.376 | 65.691 | 6.115 |
| 50.63 | 376.66 | -5.400 | 190.223 | 24.533 | 57.349 | -4.913 |
| 50.67 | 374.41 | -1.027 | 54.276 | 24.930 | 16.170 | -4.173 |
| 50.71 | 379.14 | -0.730 | -6.552 | 24.944 | -1.938 | 1.415 |
| 50.75 | 384.10 | 6.510 | -13.982 | 25.098 | -4.152 | 4.999 |
| 50.79 | 393.18 | 13.897 | -14.085 | 24.355 | -4.273 | 9.287 |
| 50.83 | 389.23 | 7.182 | -15.323 | 23.762 | -4.752 | 1.224 |
| 50.88 | 386.01 | 6.462 | -19.606 | 23.595 | -6.125 | -0.581 |
| 50.92 | 388.24 | 7.367 | -13.466 | 23.558 | -4.221 | 2.445 |
| 50.96 | 389.74 | 6.555 | -8.152 | 23.577 | -2.555 | 2.303 |

**Table D2:** Input data and model output at the Cedar Bridge New Jersey site shown in Figure 4.2.22

| Julian Day | $C$ ($\mu$mol mol$^{-1}$) | Observed $F_c$ ($\mu$mol m$^{-2}$ s$^{-1}$) | $R_n$ (W m$^{-2}$) | $T_s$ (°C) | $H$_MEP (W m$^{-2}$) | Modeled $F_c$ ($\mu$mol m$^{-2}$ s$^{-1}$) |
|---|---|---|---|---|---|---|
| 160.98 | 409.85 | 5.972 | -61.520 | 14.140 | -27.052 | 0.000 |
| 161.00 | 410.94 | 5.608 | -60.760 | 13.810 | -27.001 | 1.228 |
| 161.02 | 408.33 | 7.833 | -62.950 | 13.580 | -28.215 | -2.466 |
| 161.04 | 407.36 | 5.189 | -65.710 | 13.440 | -29.691 | -1.972 |
| 161.06 | 407.18 | 5.364 | -67.260 | 13.220 | -30.557 | -1.298 |
| 161.08 | 407.82 | 3.902 | -71.400 | 13.160 | -32.514 | -0.226 |
| 161.10 | 405.72 | 2.303 | -92.800 | 13.260 | -42.463 | -3.234 |
| 161.13 | 403.82 | 3.525 | -89.000 | 13.430 | -41.027 | -3.872 |
| 161.15 | 406.48 | 6.617 | -69.880 | 12.920 | -32.156 | 0.897 |
| 161.17 | 406.49 | 3.980 | -71.500 | 12.820 | -33.218 | -0.482 |
| 161.19 | 405.64 | 6.328 | -62.450 | 12.730 | -29.286 | -1.501 |
| 161.21 | 400.71 | 3.317 | -42.700 | 13.200 | -20.410 | -5.848 |
| 161.23 | 395.65 | -1.881 | 16.140 | 13.930 | 7.852 | -8.608 |
| 161.25 | 394.07 | -3.291 | 107.400 | 14.590 | 52.285 | -13.524 |
| 161.27 | 391.87 | -5.329 | 197.800 | 15.170 | 98.028 | -15.348 |
| 161.29 | 389.10 | -10.508 | 253.600 | 15.540 | 128.848 | -17.308 |
| 161.31 | 387.38 | -12.687 | 279.800 | 15.550 | 145.261 | -16.041 |
| 161.33 | 386.91 | -13.029 | 276.400 | 15.820 | 144.361 | -13.009 |
| 161.35 | 386.39 | -12.019 | 402.800 | 16.150 | 210.188 | -13.674 |
| 161.38 | 385.17 | -18.035 | 432.900 | 16.460 | 224.024 | -14.574 |
| 161.40 | 384.44 | -15.347 | 518.200 | 16.850 | 268.151 | -14.322 |
| 161.42 | 383.78 | -15.438 | 409.000 | 17.170 | 211.829 | -12.563 |
| 161.44 | 383.82 | -17.817 | 560.600 | 17.210 | 291.411 | -11.974 |
| 161.46 | 383.04 | -16.729 | 590.000 | 17.790 | 308.252 | -13.139 |
| 161.48 | 382.13 | -19.326 | 689.500 | 18.410 | 360.496 | -14.209 |
| 161.50 | 382.28 | -15.467 | 733.000 | 18.400 | 383.954 | -11.871 |
| 161.52 | 382.20 | -15.709 | 584.000 | 18.220 | 304.438 | -10.527 |
| 161.54 | 382.29 | -12.845 | 572.100 | 18.330 | 299.432 | -9.629 |
| 161.56 | 381.94 | -14.802 | 500.200 | 18.880 | 261.733 | -9.677 |
| 161.58 | 382.02 | -12.655 | 486.500 | 18.880 | 257.862 | -8.652 |
| 161.60 | 381.42 | -12.487 | 433.700 | 19.000 | 233.234 | -9.462 |
| 161.63 | 380.57 | -15.026 | 467.100 | 19.100 | 249.641 | -10.570 |
| 161.65 | 380.47 | -10.021 | 360.500 | 19.290 | 195.773 | -8.519 |
| 161.67 | 380.72 | -7.188 | 249.100 | 18.970 | 135.566 | -6.585 |

**Table D2 (continued)**

| | | | | | | |
|---|---|---|---|---|---|---|
| 161.69 | 380.81 | -4.954 | 238.200 | 19.330 | 129.962 | -6.320 |
| 161.71 | 380.62 | -3.695 | 124.300 | 19.320 | 67.420 | -5.348 |
| 161.73 | 380.72 | -1.336 | 86.300 | 19.430 | 46.873 | -4.335 |
| 161.75 | 381.00 | -0.025 | 7.850 | 19.070 | 4.251 | -1.733 |
| 161.77 | 382.18 | 1.065 | -42.360 | 18.200 | -22.482 | -0.545 |
| 161.79 | 383.85 | 1.573 | -58.540 | 17.280 | -30.722 | 0.152 |
| 161.81 | 387.24 | 1.460 | -63.660 | 15.900 | -33.096 | 2.759 |
| 161.83 | 386.92 | 0.947 | -63.340 | 15.570 | -32.913 | -0.242 |
| 161.85 | 393.33 | 0.252 | -59.010 | 14.800 | -30.347 | 6.753 |
| 161.88 | 391.48 | -0.406 | -57.380 | 14.480 | -29.405 | 0.161 |
| 161.90 | 394.01 | -0.808 | -58.000 | 13.730 | -29.839 | 3.469 |
| 161.92 | 394.85 | -0.734 | -64.420 | 14.020 | -33.424 | 2.557 |
| 161.94 | 401.63 | 0.034 | -65.620 | 13.020 | -34.222 | 9.454 |
| 161.96 | 409.38 | 1.715 | -67.280 | 12.330 | -36.059 | 13.685 |
| 161.98 | 410.32 | 4.227 | -66.400 | 11.550 | -36.508 | 8.306 |
| 162.00 | 407.79 | 6.278 | -63.390 | 11.460 | -35.877 | 3.101 |
| 162.02 | 410.98 | 6.275 | -66.710 | 10.740 | -38.065 | 7.796 |
| 162.04 | 409.28 | 3.697 | -69.000 | 10.980 | -39.765 | 3.160 |
| 162.06 | 409.30 | 1.511 | -67.530 | 10.460 | -38.965 | 3.631 |
| 162.08 | 412.97 | 0.539 | -65.730 | 9.560 | -37.902 | 7.651 |
| 162.10 | 410.52 | 0.803 | -64.290 | 9.730 | -37.385 | 1.894 |
| 162.13 | 413.16 | 2.322 | -62.950 | 9.090 | -36.524 | 6.060 |
| 162.15 | 411.55 | 5.115 | -65.600 | 9.050 | -38.135 | 2.215 |
| 162.17 | 411.76 | 7.019 | -64.950 | 8.760 | -37.736 | 3.113 |
| 162.19 | 410.23 | 2.465 | -58.090 | 8.840 | -33.799 | 0.980 |
| 162.21 | 403.25 | 0.557 | -34.390 | 9.800 | -20.003 | -5.324 |
| 162.23 | 395.40 | -2.129 | 23.590 | 11.330 | 13.671 | -12.280 |
| 162.25 | 391.89 | -8.291 | 102.400 | 12.220 | 59.762 | -17.296 |
| 162.27 | 389.65 | -7.602 | 188.000 | 12.800 | 110.605 | -15.759 |
| 162.29 | 388.74 | -9.770 | 275.600 | 13.040 | 163.917 | -13.147 |
| 162.31 | 387.70 | -10.821 | 352.800 | 13.440 | 210.386 | -12.683 |
| 162.33 | 386.73 | -11.880 | 432.100 | 13.990 | 257.096 | -12.387 |
| 162.35 | 385.70 | -19.529 | 499.000 | 14.570 | 294.600 | -12.460 |
| 162.38 | 385.16 | -12.414 | 569.100 | 15.220 | 334.408 | -11.420 |
| 162.40 | 384.98 | -14.705 | 617.900 | 15.860 | 359.470 | -10.153 |
| 162.42 | 384.93 | -15.547 | 655.200 | 16.350 | 377.911 | -9.191 |
| 162.44 | 384.08 | -18.360 | 635.100 | 17.220 | 359.216 | -10.308 |
| 162.46 | 383.62 | -15.204 | 669.400 | 17.500 | 377.020 | -9.826 |
| 162.48 | 382.48 | -18.167 | 652.700 | 18.230 | 362.360 | -11.187 |
| 162.50 | 382.11 | -16.016 | 659.700 | 18.700 | 363.314 | -9.911 |

**Table D2 (continued)**

| | | | | | | |
|---|---|---|---|---|---|---|
| 162.52 | 381.52 | -16.968 | 469.000 | 18.690 | 256.490 | -9.029 |
| 162.54 | 380.33 | -12.960 | 390.700 | 19.010 | 210.420 | -9.933 |
| 162.56 | 379.50 | -17.440 | 577.400 | 19.750 | 307.842 | -11.239 |
| 162.58 | 379.74 | -11.304 | 526.400 | 20.220 | 280.989 | -8.417 |
| 162.60 | 378.72 | -12.557 | 547.000 | 20.630 | 289.185 | -10.612 |
| 162.63 | 378.12 | -9.895 | 483.100 | 21.150 | 254.282 | -9.782 |
| 162.65 | 377.18 | -8.733 | 422.900 | 21.500 | 220.967 | -10.186 |
| 162.67 | 376.92 | -5.972 | 342.300 | 21.710 | 178.718 | -8.492 |
| 162.69 | 376.35 | -5.599 | 265.200 | 21.820 | 137.831 | -8.222 |
| 162.71 | 376.15 | -2.373 | 148.700 | 21.750 | 76.679 | -6.287 |
| 162.73 | 376.41 | -1.199 | 56.800 | 21.250 | 28.927 | -3.876 |
| 162.75 | 376.59 | -1.137 | 53.780 | 21.350 | 27.380 | -3.579 |
| 162.77 | 377.50 | 1.482 | -21.530 | 20.970 | -10.789 | -1.157 |
| 162.79 | 380.09 | 2.861 | -53.120 | 19.350 | -26.006 | 1.277 |
| 162.81 | 384.77 | 3.006 | -62.310 | 17.960 | -30.320 | 4.548 |
| 162.83 | 390.14 | 3.210 | -57.960 | 17.340 | -28.378 | 6.936 |
| 162.85 | 392.87 | 3.674 | -50.810 | 16.350 | -24.857 | 5.601 |
| 162.88 | 396.27 | 4.323 | -49.780 | 15.840 | -24.342 | 6.751 |
| 162.90 | 398.27 | 5.084 | -53.900 | 15.350 | -26.348 | 6.149 |
| 162.92 | 395.09 | 5.884 | -53.310 | 15.510 | -26.148 | 0.349 |
| 162.94 | 395.69 | 6.650 | -52.830 | 15.500 | -25.904 | 2.345 |
| 162.96 | 399.60 | 7.308 | -50.050 | 15.040 | -24.481 | 6.064 |
| 162.98 | 401.65 | 7.785 | -51.120 | 14.580 | -25.041 | 5.639 |
| 163.00 | 397.24 | 8.008 | -52.100 | 14.580 | -25.690 | -1.251 |
| 163.02 | 399.18 | 7.903 | -51.450 | 14.310 | -25.260 | 3.200 |
| 163.04 | 408.30 | 7.397 | -52.570 | 13.570 | -25.785 | 12.281 |
| 163.06 | 411.58 | 6.417 | -53.670 | 13.170 | -26.329 | 9.761 |
| 163.08 | 409.80 | 4.889 | -53.300 | 13.050 | -26.251 | 4.396 |
| 163.10 | 408.82 | 2.740 | -54.580 | 12.730 | -26.929 | 3.476 |
| 163.13 | 410.40 | -0.006 | -54.810 | 12.490 | -27.032 | 5.465 |
| 163.15 | 412.51 | -2.938 | -53.650 | 12.390 | -26.457 | 6.492 |
| 163.17 | 415.40 | -5.547 | -51.410 | 12.200 | -25.326 | 7.842 |
| 163.19 | 416.20 | -7.324 | -41.550 | 12.170 | -20.463 | 5.912 |
| 163.21 | 410.94 | -7.760 | -13.420 | 13.020 | -6.583 | -0.553 |
| 163.23 | 402.86 | -6.347 | 86.400 | 14.310 | 42.064 | -15.530 |
| 163.25 | 394.05 | -4.805 | 103.900 | 15.110 | 50.654 | -18.350 |
| 163.27 | 392.12 | -7.194 | 76.000 | 15.020 | 36.896 | -9.375 |
| 163.29 | 393.62 | -3.252 | 65.200 | 14.900 | 31.549 | -3.076 |
| 163.31 | 391.36 | -6.304 | 73.300 | 15.040 | 35.051 | -7.207 |
| 163.33 | 388.19 | -7.879 | 81.600 | 15.370 | 38.888 | -10.035 |

**Table D2 (continued)**

| | | | | | | |
|---|---|---|---|---|---|---|
| 163.35 | 383.17 | -6.748 | 96.200 | 15.780 | 45.654 | -15.288 |
| 163.38 | 383.50 | -5.715 | 126.200 | 16.190 | 60.760 | -9.090 |
| 163.40 | 383.22 | -7.177 | 147.000 | 16.390 | 69.992 | -8.573 |
| 163.42 | 380.79 | -11.891 | 172.600 | 16.690 | 81.810 | -12.350 |
| 163.44 | 380.31 | -17.934 | 311.600 | 17.060 | 146.603 | -11.621 |
| 163.46 | 381.15 | -18.002 | 448.400 | 17.760 | 210.362 | -8.654 |
| 163.48 | 380.13 | -15.331 | 499.100 | 18.860 | 231.645 | -11.213 |
| 163.50 | 380.84 | -11.186 | 249.400 | 18.240 | 116.177 | -5.953 |
| 163.52 | 385.31 | -8.667 | 180.800 | 17.780 | 82.707 | 2.625 |
| 163.54 | 391.75 | -5.464 | 94.300 | 16.850 | 43.108 | 8.520 |
| 163.56 | 392.62 | -23.666 | 500.000 | 17.860 | 226.928 | 7.129 |
| 163.58 | 388.33 | -13.519 | 427.900 | 19.590 | 193.411 | -6.892 |
| 163.60 | 383.55 | -22.998 | 289.200 | 19.130 | 131.327 | -11.745 |
| 163.63 | 382.76 | -13.715 | 503.000 | 19.990 | 228.340 | -9.560 |
| 163.65 | 379.35 | -15.873 | 420.800 | 20.280 | 189.862 | -13.928 |
| 163.67 | 378.04 | -11.344 | 242.200 | 20.110 | 109.252 | -9.912 |
| 163.69 | 378.16 | -7.326 | 260.000 | 20.650 | 118.053 | -7.689 |
| 163.71 | 378.34 | -6.190 | 176.800 | 20.800 | 80.079 | -5.862 |
| 163.73 | 379.13 | -2.509 | 88.300 | 20.710 | 39.933 | -3.295 |
| 163.75 | 380.70 | 1.490 | -3.442 | 20.030 | -1.540 | -0.268 |
| 163.77 | 383.85 | 4.497 | -29.820 | 18.980 | -13.115 | 3.403 |
| 163.79 | 388.08 | 6.060 | -26.820 | 18.170 | -11.715 | 4.184 |
| 163.81 | 390.67 | 5.724 | -27.270 | 17.690 | -11.883 | 3.978 |
| 163.83 | 390.56 | 4.361 | -34.230 | 17.330 | -14.797 | 1.897 |
| 163.85 | 391.72 | 5.124 | -35.710 | 16.900 | -15.395 | 2.528 |
| 163.88 | 394.03 | 4.156 | -35.560 | 16.500 | -15.340 | 3.830 |
| 163.90 | 395.51 | 5.060 | -37.870 | 16.280 | -16.343 | 3.659 |
| 163.92 | 398.34 | 2.816 | -42.750 | 15.970 | -18.464 | 5.423 |
| 163.94 | 403.06 | 4.477 | -37.590 | 15.700 | -16.211 | 7.772 |
| 163.96 | 407.43 | 5.813 | -53.670 | 15.180 | -23.237 | 10.116 |
| 163.98 | 409.39 | 2.973 | -55.170 | 14.850 | -23.960 | 8.261 |
| 164.00 | 409.85 | 4.227 | -54.210 | 14.520 | -23.712 | 6.377 |
| 164.02 | 411.02 | 3.488 | -51.610 | 14.270 | -22.823 | 6.415 |
| 164.04 | 413.04 | 4.934 | -52.210 | 14.000 | -23.172 | 7.311 |
| 164.06 | 413.58 | 7.213 | -52.040 | 13.730 | -23.350 | 6.038 |
| 164.08 | 408.41 | 3.104 | -51.390 | 13.680 | -23.382 | -0.628 |
| 164.10 | 408.21 | 4.825 | -51.170 | 13.740 | -23.441 | 1.982 |
| 164.13 | 407.90 | 2.721 | -51.800 | 13.650 | -23.792 | 1.966 |
| 164.15 | 409.28 | 2.505 | -50.990 | 13.380 | -23.486 | 3.697 |
| 164.17 | 411.40 | 3.260 | -47.680 | 13.190 | -22.010 | 5.007 |

**Table D2 (continued)**

| | | | | | | |
|---|---|---|---|---|---|---|
| 164.19 | 412.44 | 4.003 | -38.060 | 13.130 | -17.571 | 4.288 |
| 164.21 | 409.95 | 3.706 | -13.370 | 13.930 | -6.144 | 0.525 |
| 164.23 | 405.74 | -0.259 | 39.160 | 14.710 | 17.992 | -4.772 |
| 164.25 | 397.84 | -3.748 | 114.900 | 15.910 | 52.788 | -16.621 |
| 164.27 | 393.54 | -5.705 | 195.000 | 17.020 | 89.321 | -14.829 |
| 164.29 | 390.17 | -9.363 | 274.700 | 17.890 | 125.174 | -14.897 |
| 164.31 | 386.55 | -10.413 | 355.500 | 18.970 | 160.790 | -16.978 |
| 164.33 | 383.27 | -8.784 | 438.900 | 20.360 | 196.687 | -18.193 |
| 164.35 | 380.78 | -13.649 | 512.300 | 21.230 | 228.935 | -17.921 |
| 164.38 | 378.65 | -13.816 | 574.300 | 21.930 | 256.140 | -17.807 |
| 164.40 | 376.37 | -10.611 | 637.400 | 22.950 | 282.514 | -18.714 |
| 164.42 | 375.74 | -9.332 | 691.100 | 23.090 | 309.669 | -15.635 |
| 164.44 | 370.88 | -11.310 | 544.200 | 23.860 | 244.197 | -22.680 |
| 164.46 | 370.63 | -14.369 | 597.600 | 24.220 | 268.480 | -16.446 |
| 164.48 | 370.48 | -10.889 | 414.600 | 24.280 | 185.841 | -12.791 |
| 164.50 | 369.70 | -7.577 | 382.700 | 24.860 | 170.767 | -12.913 |
| 164.52 | 370.23 | -9.390 | 354.600 | 24.860 | 159.212 | -9.822 |
| 164.54 | 371.23 | -14.545 | 401.600 | 24.880 | 171.775 | -7.794 |
| 164.56 | 371.81 | -11.307 | 461.900 | 24.950 | 196.977 | -7.706 |
| 164.58 | 371.88 | -14.075 | 323.600 | 24.290 | 135.136 | -7.152 |
| 164.60 | 372.46 | -11.575 | 696.700 | 25.800 | 296.759 | -7.684 |
| 164.63 | 376.48 | -10.692 | 543.700 | 25.110 | 227.153 | 1.018 |
| 164.65 | 379.02 | -6.565 | 341.800 | 24.660 | 141.487 | 1.615 |
| 164.67 | 380.53 | -8.419 | 237.200 | 23.740 | 97.513 | 1.291 |
| 164.69 | 379.86 | -5.462 | 278.300 | 24.160 | 114.184 | -2.339 |
| 164.71 | 379.81 | -0.404 | 106.500 | 23.740 | 43.459 | -1.636 |
| 164.73 | 380.59 | -1.020 | 67.300 | 22.820 | 27.252 | -0.330 |
| 164.75 | 380.61 | -0.283 | 27.240 | 22.700 | 10.957 | -0.757 |
| 164.77 | 382.27 | 0.895 | -15.870 | 21.660 | -6.385 | 0.827 |
| 164.79 | 384.92 | 2.822 | -42.430 | 20.490 | -17.154 | 3.333 |
| 164.81 | 388.37 | 2.850 | -54.090 | 19.310 | -22.010 | 4.985 |
| 164.83 | 391.74 | 2.492 | -53.310 | 18.410 | -21.812 | 5.798 |
| 164.85 | 392.97 | 3.732 | -52.060 | 17.940 | -21.526 | 4.328 |
| 164.88 | 398.22 | 4.786 | -52.140 | 17.660 | -21.744 | 8.570 |
| 164.90 | 399.73 | 4.076 | -53.630 | 17.260 | -22.553 | 6.365 |
| 164.92 | 402.64 | 3.840 | -52.000 | 16.780 | -22.022 | 7.584 |
| 164.94 | 405.31 | 4.350 | -47.470 | 16.330 | -20.181 | 7.700 |
| 164.96 | 405.92 | 5.101 | -46.570 | 16.010 | -19.836 | 5.931 |
| 164.98 | 404.50 | 5.588 | -43.920 | 16.110 | -18.729 | 3.216 |
| 165.00 | 403.79 | 5.411 | -43.500 | 16.110 | -18.617 | 2.785 |

**Table D2 (continued)**

| | | | | | | |
|---|---|---|---|---|---|---|
| 165.02 | 403.06 | 4.600 | -38.920 | 15.880 | -16.673 | 2.119 |
| 165.04 | 404.44 | 3.288 | -40.620 | 15.710 | -17.408 | 3.898 |
| 165.06 | 405.43 | 1.613 | -39.800 | 15.510 | -17.100 | 3.960 |
| 165.08 | 412.96 | -0.291 | -35.280 | 14.750 | -15.333 | 10.602 |
| 165.10 | 412.19 | -2.288 | -32.420 | 14.590 | -14.047 | 4.988 |
| 165.13 | 412.11 | -4.244 | -30.110 | 14.670 | -12.971 | 4.356 |
| 165.15 | 411.47 | -6.022 | -27.330 | 14.910 | -11.647 | 3.231 |
| 165.17 | 411.25 | -7.488 | -25.730 | 15.190 | -10.859 | 3.018 |
| 165.19 | 412.01 | -8.505 | -17.190 | 14.950 | -7.305 | 3.256 |
| 165.21 | 417.78 | -8.939 | -0.627 | 14.810 | -0.267 | 2.666 |
| 165.23 | 421.90 | -8.654 | 23.710 | 15.210 | 9.956 | 19.167 |
| 165.25 | 410.47 | -7.515 | 49.960 | 16.220 | 20.377 | -7.375 |
| 165.27 | 402.86 | -5.387 | 78.100 | 17.480 | 31.075 | -10.429 |
| 165.29 | 399.73 | -6.356 | 134.500 | 18.260 | 53.318 | -7.982 |
| 165.31 | 392.97 | -16.786 | 195.700 | 19.900 | 76.526 | -16.280 |
| 165.33 | 390.60 | -9.154 | 230.600 | 20.790 | 90.483 | -11.634 |
| 165.35 | 382.51 | -9.216 | 255.600 | 21.430 | 99.903 | -23.089 |
| 165.38 | 376.80 | -13.194 | 269.300 | 22.190 | 105.476 | -23.524 |
| 165.40 | 375.35 | -17.183 | 329.700 | 22.720 | 128.844 | -18.208 |
| 165.42 | 372.87 | -16.255 | 385.600 | 23.020 | 151.285 | -19.619 |
| 165.44 | 369.26 | -19.081 | 303.300 | 23.100 | 119.930 | -20.245 |
| 165.46 | 371.61 | -16.854 | 302.500 | 22.800 | 115.843 | -9.587 |
| 165.48 | 370.06 | -14.376 | 301.000 | 22.940 | 115.932 | -13.713 |
| 165.50 | 367.26 | -19.449 | 419.200 | 22.780 | 159.413 | -18.721 |
| 165.52 | 367.85 | -13.920 | 312.400 | 22.770 | 120.205 | -11.383 |
| 165.54 | 368.87 | -16.620 | 251.900 | 22.080 | 98.993 | -8.197 |
| 165.56 | 368.81 | -14.546 | 263.600 | 21.640 | 105.788 | -9.019 |
| 165.58 | 369.84 | -10.317 | 198.300 | 21.120 | 81.210 | -5.986 |
| 165.60 | 371.65 | -10.254 | 155.100 | 20.090 | 63.654 | -3.051 |
| 165.63 | 374.06 | -10.559 | 156.800 | 19.330 | 65.010 | -0.387 |
| 165.65 | 378.06 | -8.449 | 130.100 | 18.800 | 55.699 | 3.969 |
| 165.67 | 379.72 | -5.413 | 86.400 | 18.330 | 37.615 | 2.183 |
| 165.69 | 380.20 | -2.149 | 51.660 | 18.050 | 22.364 | 0.689 |
| 165.71 | 381.48 | -1.387 | 28.090 | 17.650 | 11.988 | 1.462 |
| 165.73 | 382.70 | 0.652 | 7.940 | 17.280 | 3.352 | 1.327 |
| 165.75 | 384.44 | 3.076 | -11.300 | 16.960 | -4.765 | 2.036 |
| 165.77 | 388.12 | 5.290 | -23.510 | 16.680 | -9.919 | 5.120 |
| 165.79 | 392.15 | 7.250 | -25.970 | 16.240 | -10.945 | 6.289 |
| 165.81 | 395.28 | 8.915 | -24.790 | 15.890 | -10.473 | 6.244 |
| 165.83 | 397.88 | 10.240 | -24.150 | 15.570 | -10.237 | 6.240 |

**Table D2 (continued)**

| | | | | | | |
|---|---|---|---|---|---|---|
| 165.85 | 399.73 | 11.184 | -17.690 | 15.440 | -7.498 | 5.266 |
| 165.88 | 402.80 | 11.703 | -8.510 | 15.540 | -3.604 | 5.150 |
| 165.90 | 408.88 | 11.754 | -13.420 | 15.590 | -5.702 | 9.918 |
| 165.92 | 409.85 | 11.295 | -16.950 | 15.610 | -7.214 | 7.210 |
| 165.94 | 413.02 | 10.283 | -13.580 | 15.680 | -5.784 | 7.870 |
| 165.96 | 416.50 | 8.674 | -17.230 | 15.640 | -7.339 | 9.465 |
| 165.98 | 415.37 | 6.427 | -19.550 | 15.550 | -8.302 | 5.912 |
| 166.00 | 411.25 | 4.139 | -9.170 | 15.900 | -3.866 | 1.407 |
| 166.02 | 411.54 | 4.051 | -6.986 | 16.300 | -2.906 | 2.701 |
| 166.04 | 401.92 | 5.252 | -26.460 | 16.710 | -10.972 | -7.586 |
| 166.06 | 396.87 | 5.486 | -42.700 | 16.630 | -17.900 | -5.989 |
| 166.08 | 397.02 | 3.561 | -52.610 | 16.310 | -22.178 | -1.329 |
| 166.10 | 400.83 | 2.301 | -54.620 | 15.970 | -23.141 | 3.798 |
| 166.13 | 405.17 | 3.026 | -56.040 | 15.550 | -23.866 | 6.614 |
| 166.15 | 405.31 | 5.047 | -55.000 | 15.200 | -23.593 | 3.742 |
| 166.17 | 406.26 | 5.126 | -51.380 | 14.970 | -22.246 | 4.077 |
| 166.19 | 406.77 | 5.839 | -44.370 | 14.740 | -19.323 | 3.574 |
| 166.21 | 405.05 | 2.255 | -22.530 | 14.920 | -9.843 | 0.912 |
| 166.23 | 402.34 | 1.586 | -11.660 | 15.260 | -5.093 | -0.824 |
| 166.25 | 396.95 | -6.464 | 101.400 | 16.570 | 43.927 | -12.360 |
| 166.27 | 392.71 | -7.820 | 184.200 | 18.030 | 80.010 | -11.831 |
| 166.29 | 388.99 | -10.854 | 267.300 | 19.080 | 116.893 | -13.250 |
| 166.31 | 385.85 | -13.519 | 327.200 | 19.830 | 143.274 | -13.787 |
| 166.33 | 382.24 | -13.861 | 424.600 | 20.630 | 186.407 | -16.882 |
| 166.35 | 380.19 | -16.778 | 487.000 | 21.250 | 213.074 | -15.184 |
| 166.38 | 378.18 | -14.522 | 540.200 | 21.880 | 236.636 | -15.431 |
| 166.40 | 377.07 | -9.738 | 536.200 | 22.280 | 237.956 | -13.524 |
| 166.42 | 376.07 | -16.553 | 547.600 | 22.690 | 244.726 | -12.910 |
| 166.44 | 375.15 | -16.233 | 655.400 | 23.390 | 297.632 | -13.255 |
| 166.46 | 374.60 | -16.797 | 639.200 | 23.600 | 290.116 | -11.924 |
| 166.48 | 375.23 | -12.796 | 699.400 | 23.810 | 326.480 | -8.995 |
| 166.50 | 374.72 | -9.108 | 611.100 | 23.860 | 287.257 | -9.803 |
| 166.52 | 374.53 | -13.630 | 462.100 | 23.950 | 219.823 | -8.325 |
| 166.54 | 373.45 | -13.917 | 321.700 | 24.020 | 153.063 | -8.932 |
| 166.56 | 375.10 | -14.634 | 599.800 | 24.950 | 299.498 | -4.858 |
| 166.58 | 376.27 | -9.299 | 145.500 | 23.670 | 72.113 | -2.547 |
| 166.60 | 375.18 | -13.265 | 289.900 | 23.610 | 145.123 | -6.922 |
| 166.63 | 376.01 | -10.906 | 346.500 | 25.050 | 179.079 | -4.026 |
| 166.65 | 376.51 | -7.816 | 145.500 | 24.190 | 74.380 | -2.844 |
| 166.67 | 376.51 | -8.782 | 299.900 | 24.950 | 160.649 | -4.267 |

**Table D2 (continued)**

| | | | | | | |
|---|---|---|---|---|---|---|
| 166.69 | 376.94 | -11.465 | 218.600 | 24.880 | 118.965 | -3.110 |
| 166.71 | 377.14 | -5.712 | 206.000 | 24.910 | 116.069 | -3.161 |
| 166.73 | 378.09 | -2.607 | 90.200 | 24.720 | 50.190 | -1.151 |
| 166.75 | 379.28 | -0.651 | 26.030 | 24.470 | 14.245 | 0.084 |
| 166.77 | 378.76 | 2.295 | -4.263 | 24.090 | -2.213 | -0.559 |
| 166.79 | 379.44 | 3.848 | -43.060 | 20.580 | -18.571 | 0.081 |
| 166.81 | 383.22 | 2.523 | -47.670 | 19.170 | -20.492 | 3.488 |
| 166.83 | 386.82 | 2.324 | -38.200 | 18.570 | -16.455 | 4.459 |
| 166.85 | 389.82 | 2.688 | -54.740 | 17.810 | -23.593 | 5.742 |
| 166.88 | 389.27 | 3.111 | -54.220 | 17.450 | -23.542 | 2.300 |
| 166.90 | 393.00 | 3.533 | -57.890 | 17.780 | -25.740 | 6.224 |
| 166.92 | 398.42 | 3.892 | -55.800 | 16.910 | -25.118 | 9.333 |
| 166.94 | 403.21 | 4.125 | -56.800 | 17.660 | -28.346 | 10.896 |
| 166.96 | 406.57 | 4.172 | -61.010 | 17.880 | -31.587 | 10.748 |
| 166.98 | 408.57 | 4.004 | -57.390 | 17.230 | -29.719 | 9.292 |
| 167.00 | 411.24 | 3.732 | -54.900 | 16.720 | -28.423 | 9.782 |
| 167.02 | 413.91 | 3.499 | -54.330 | 16.210 | -28.038 | 10.116 |
| 167.04 | 414.93 | 3.450 | -53.180 | 15.450 | -27.488 | 8.551 |
| 167.06 | 415.80 | 3.530 | -53.320 | 15.330 | -27.750 | 7.995 |
| 167.08 | 418.91 | 3.153 | -52.580 | 15.140 | -27.326 | 10.165 |
| 167.10 | 423.06 | 2.589 | -52.110 | 14.560 | -26.966 | 12.135 |
| 167.13 | 425.01 | 2.375 | -50.570 | 14.540 | -26.218 | 10.713 |
| 167.15 | 424.08 | 2.975 | -55.000 | 14.560 | -28.748 | 7.644 |
| 167.17 | 422.25 | 4.144 | -52.870 | 14.820 | -27.688 | 5.232 |
| 167.19 | 421.70 | 3.837 | -43.960 | 14.950 | -23.019 | 4.998 |
| 167.21 | 419.45 | 1.123 | -20.130 | 15.490 | -10.486 | 2.050 |
| 167.23 | 415.75 | -0.581 | 32.480 | 16.850 | 16.795 | -0.942 |
| 167.25 | 411.18 | -2.946 | 107.800 | 18.260 | 55.254 | -5.845 |
| 167.27 | 408.40 | -6.180 | 187.900 | 19.530 | 96.448 | -4.150 |
| 167.29 | 401.29 | -8.910 | 272.700 | 20.950 | 141.057 | -14.726 |
| 167.31 | 394.74 | -12.139 | 336.400 | 21.660 | 175.951 | -18.883 |
| 167.33 | 390.09 | -14.615 | 421.700 | 22.430 | 221.249 | -19.258 |
| 167.35 | 387.94 | -15.783 | 484.900 | 23.190 | 254.228 | -15.467 |
| 167.38 | 383.65 | -17.341 | 550.000 | 24.130 | 287.595 | -20.454 |
| 167.40 | 381.11 | -14.734 | 595.400 | 24.820 | 311.793 | -18.689 |
| 167.42 | 378.37 | -15.796 | 622.900 | 25.590 | 323.094 | -19.394 |
| 167.44 | 376.81 | -11.761 | 612.600 | 26.050 | 324.073 | -17.184 |
| 167.46 | 376.46 | -14.390 | 703.000 | 26.680 | 376.243 | -14.563 |
| 167.48 | 377.52 | -12.207 | 699.000 | 27.160 | 383.611 | -9.675 |
| 167.50 | 377.86 | -12.137 | 670.800 | 27.420 | 373.084 | -8.995 |

**Table D2 (continued)**

| | | | | | | |
|---|---|---|---|---|---|---|
| 167.52 | 377.83 | -12.665 | 549.100 | 27.350 | 312.227 | -8.358 |
| 167.54 | 377.32 | -12.752 | 614.600 | 27.900 | 349.372 | -9.445 |
| 167.56 | 377.46 | -11.962 | 677.600 | 28.440 | 392.911 | -8.208 |
| 167.58 | 376.65 | -9.369 | 620.300 | 28.340 | 357.304 | -9.589 |
| 167.60 | 376.76 | -7.972 | 572.800 | 28.500 | 329.797 | -7.610 |
| 167.63 | 376.74 | -8.988 | 492.200 | 28.670 | 283.915 | -6.987 |
| 167.65 | 376.69 | -9.375 | 427.600 | 28.660 | 247.849 | -6.477 |
| 167.67 | 376.68 | -7.825 | 363.600 | 29.000 | 207.446 | -5.825 |
| 167.69 | 375.93 | -6.116 | 269.500 | 28.700 | 142.868 | -6.461 |
| 167.71 | 376.45 | -6.466 | 184.200 | 27.580 | 93.569 | -3.806 |
| 167.73 | 377.63 | -2.874 | 72.500 | 26.700 | 36.605 | -1.339 |
| 167.75 | 378.37 | -0.075 | 12.550 | 25.320 | 6.175 | -0.549 |
| 167.77 | 380.40 | 1.500 | -29.720 | 24.300 | -14.322 | 1.497 |
| 167.79 | 385.79 | 1.968 | -57.000 | 23.030 | -26.915 | 6.625 |
| 167.81 | 388.34 | 1.666 | -62.500 | 21.510 | -29.037 | 5.072 |
| 167.83 | 392.13 | 1.099 | -60.360 | 20.680 | -27.949 | 6.742 |
| 167.85 | 396.63 | 0.772 | -58.530 | 19.890 | -27.007 | 8.540 |
| 167.88 | 396.59 | 1.190 | -56.100 | 19.280 | -25.757 | 4.659 |
| 167.90 | 397.75 | 2.859 | -56.750 | 19.590 | -26.333 | 5.074 |
| 167.92 | 403.04 | 5.897 | -57.470 | 19.390 | -27.060 | 9.741 |
| 167.94 | 403.89 | 8.878 | -54.760 | 19.380 | -26.105 | 6.555 |
| 167.96 | 407.03 | 9.990 | -56.370 | 19.280 | -27.128 | 8.697 |
| 167.98 | 417.69 | 8.167 | -53.470 | 17.170 | -25.201 | 17.522 |
| 168.00 | 422.43 | 5.325 | -54.470 | 16.670 | -25.601 | 15.259 |
| 168.02 | 424.87 | 4.686 | -53.700 | 16.750 | -25.377 | 13.167 |
| 168.04 | 426.33 | 7.693 | -55.530 | 16.230 | -26.390 | 11.866 |
| 168.06 | 427.00 | 6.473 | -53.890 | 16.030 | -25.927 | 10.333 |
| 168.08 | 422.88 | 8.874 | -52.740 | 16.180 | -25.652 | 4.281 |
| 168.10 | 427.96 | 10.908 | -52.580 | 15.460 | -25.402 | 11.834 |
| 168.13 | 422.82 | 11.113 | -54.290 | 16.060 | -26.196 | 2.652 |
| 168.15 | 424.27 | 9.903 | -55.490 | 16.020 | -26.822 | 6.942 |
| 168.17 | 422.22 | 7.145 | -54.330 | 16.310 | -26.246 | 3.657 |
| 168.19 | 422.82 | 2.906 | -41.370 | 16.280 | -19.855 | 4.908 |
| 168.21 | 421.02 | 2.021 | -15.390 | 16.630 | -7.305 | 1.875 |
| 168.23 | 418.23 | -0.552 | 22.420 | 17.250 | 10.491 | 0.012 |
| 168.25 | 413.00 | -0.397 | 81.300 | 18.660 | 37.329 | -6.943 |
| 168.27 | 410.04 | -3.939 | 49.210 | 19.230 | 22.338 | -3.514 |
| 168.29 | 408.62 | -7.472 | 105.500 | 19.300 | 47.042 | -3.170 |
| 168.31 | 402.60 | -13.048 | 144.400 | 20.380 | 63.353 | -11.784 |
| 168.33 | 395.28 | -14.871 | 268.100 | 21.870 | 116.909 | -21.120 |

**Table D2 (continued)**

| | | | | | | |
|---|---|---|---|---|---|---|
| 168.35 | 387.09 | -16.480 | 343.200 | 23.470 | 153.123 | -27.686 |
| 168.38 | 381.35 | -19.305 | 426.500 | 24.780 | 192.751 | -27.957 |
| 168.40 | 378.83 | -17.713 | 497.600 | 25.620 | 224.221 | -22.997 |
| 168.42 | 377.27 | -16.461 | 639.300 | 27.060 | 290.851 | -21.128 |
| 168.44 | 376.66 | -8.592 | 184.900 | 26.190 | 83.718 | -11.312 |
| 168.46 | 376.09 | -14.937 | 335.200 | 26.510 | 149.266 | -13.091 |
| 168.48 | 374.92 | -14.133 | 337.500 | 27.060 | 151.771 | -13.533 |
| 168.50 | 372.18 | -10.444 | 260.800 | 26.970 | 114.753 | -15.284 |
| 168.52 | 370.17 | -12.947 | 235.100 | 27.020 | 104.278 | -14.957 |
| 168.54 | 368.31 | -17.603 | 423.300 | 27.700 | 187.423 | -18.569 |
| 168.56 | 369.68 | -10.776 | 343.200 | 27.860 | 157.851 | -10.530 |
| 168.58 | 369.25 | -12.277 | 370.800 | 27.970 | 170.528 | -12.052 |
| 168.60 | 370.01 | -12.894 | 214.600 | 27.700 | 98.285 | -7.638 |
| 168.63 | 369.56 | -13.247 | 427.900 | 28.240 | 194.350 | -11.054 |
| 168.65 | 369.08 | -8.204 | 403.600 | 28.800 | 183.953 | -10.817 |
| 168.67 | 367.78 | -6.852 | 325.300 | 28.950 | 146.698 | -11.639 |
| 168.69 | 368.34 | -5.627 | 211.200 | 28.460 | 96.370 | -7.378 |
| 168.71 | 368.49 | -6.304 | 196.600 | 28.270 | 90.742 | -7.034 |
| 168.73 | 369.88 | -1.862 | 67.340 | 27.720 | 31.044 | -2.985 |
| 168.75 | 373.03 | 1.273 | -21.580 | 26.530 | -10.034 | 0.605 |
| 168.77 | 376.45 | 0.834 | -20.260 | 25.340 | -9.330 | 2.458 |
| 168.79 | 380.67 | 3.878 | -42.480 | 24.200 | -19.755 | 5.558 |
| 168.81 | 385.94 | 2.732 | -54.530 | 23.050 | -25.496 | 7.995 |
| 168.83 | 390.24 | 3.377 | -51.450 | 22.080 | -24.063 | 8.055 |
| 168.85 | 391.79 | 4.489 | -50.940 | 21.720 | -23.967 | 5.972 |
| 168.88 | 394.32 | 6.406 | -53.990 | 21.470 | -25.791 | 6.882 |
| 168.90 | 395.95 | 4.520 | -51.760 | 20.920 | -25.001 | 6.121 |
| 168.92 | 398.43 | 2.781 | -49.970 | 20.270 | -24.312 | 6.961 |
| 168.94 | 400.34 | 3.843 | -49.140 | 19.620 | -24.095 | 6.765 |
| 168.96 | 402.68 | 4.822 | -48.470 | 19.370 | -24.121 | 7.393 |
| 168.98 | 405.95 | 4.212 | -45.210 | 18.830 | -22.638 | 8.617 |
| 169.00 | 406.49 | 6.443 | -40.880 | 18.760 | -20.363 | 6.221 |
| 169.02 | 406.00 | 5.592 | -46.680 | 18.720 | -22.979 | 4.793 |
| 169.04 | 405.69 | 5.975 | -40.670 | 18.420 | -19.778 | 3.955 |
| 169.06 | 405.33 | 4.737 | -35.830 | 18.360 | -17.284 | 3.266 |
| 169.08 | 407.46 | 3.568 | -40.740 | 18.080 | -19.514 | 5.695 |
| 169.10 | 408.54 | 4.995 | -39.730 | 17.630 | -18.853 | 5.231 |
| 169.13 | 408.54 | 6.336 | -40.830 | 17.510 | -19.205 | 4.195 |
| 169.15 | 409.05 | 3.632 | -41.330 | 17.340 | -19.378 | 4.365 |
| 169.17 | 412.64 | 6.026 | -36.490 | 16.800 | -17.041 | 7.294 |

**Table D2 (continued)**

| | | | | | | |
|---|---|---|---|---|---|---|
| 169.19 | 412.01 | 8.140 | -29.470 | 16.650 | -13.653 | 3.950 |
| 169.21 | 408.05 | 3.383 | -10.800 | 17.350 | -4.935 | -0.120 |
| 169.23 | 404.47 | -1.842 | 37.550 | 18.430 | 16.820 | -3.777 |
| 169.25 | 400.38 | -5.537 | 104.100 | 19.580 | 45.517 | -7.217 |
| 169.27 | 393.64 | -9.976 | 174.900 | 20.890 | 73.878 | -14.740 |
| 169.29 | 386.76 | -6.400 | 254.900 | 22.530 | 104.174 | -20.071 |
| 169.31 | 381.99 | -9.726 | 333.100 | 23.570 | 133.179 | -20.175 |
| 169.33 | 378.09 | -14.030 | 378.900 | 24.730 | 148.623 | -20.056 |
| 169.35 | 374.79 | -13.723 | 472.400 | 25.870 | 182.887 | -20.868 |
| 169.38 | 372.25 | -11.135 | 540.700 | 26.840 | 208.331 | -20.239 |
| 169.40 | 368.81 | -14.896 | 586.300 | 28.040 | 224.905 | -22.675 |
| 169.42 | 366.38 | -18.641 | 629.200 | 29.060 | 243.889 | -21.956 |
| 169.44 | 365.44 | -11.452 | 673.300 | 30.070 | 264.977 | -19.061 |
| 169.46 | 364.24 | -11.589 | 679.200 | 30.640 | 271.301 | -18.587 |
| 169.48 | 364.29 | -13.913 | 692.500 | 31.170 | 278.191 | -15.325 |
| 169.50 | 364.83 | -9.417 | 720.000 | 31.860 | 297.284 | -12.975 |
| 169.52 | 365.15 | -8.759 | 713.000 | 32.120 | 300.086 | -11.940 |
| 169.54 | 363.55 | -7.539 | 514.000 | 31.950 | 210.226 | -13.747 |
| 169.56 | 363.92 | -12.686 | 504.600 | 31.860 | 204.977 | -10.473 |
| 169.58 | 364.00 | -9.743 | 605.100 | 32.310 | 252.198 | -10.787 |
| 169.60 | 362.61 | -11.599 | 516.400 | 32.350 | 212.099 | -12.850 |
| 169.63 | 362.47 | -9.509 | 445.400 | 32.130 | 184.132 | -10.533 |
| 169.65 | 362.92 | -8.287 | 412.500 | 32.440 | 167.294 | -8.514 |
| 169.67 | 362.14 | -4.738 | 290.700 | 32.140 | 114.635 | -9.133 |
| 169.69 | 360.70 | -5.069 | 234.600 | 31.380 | 88.573 | -10.102 |
| 169.71 | 360.61 | -3.571 | 141.800 | 31.070 | 53.402 | -7.157 |
| 169.73 | 361.30 | -0.648 | 87.200 | 30.600 | 32.950 | -4.667 |
| 169.75 | 363.80 | 1.847 | 26.180 | 29.750 | 9.928 | -0.640 |
| 169.77 | 371.91 | 2.477 | -20.280 | 28.350 | -7.491 | 5.708 |
| 169.79 | 378.64 | 2.789 | -46.920 | 26.230 | -16.900 | 10.053 |
| 169.81 | 384.55 | 3.272 | -55.230 | 24.800 | -20.039 | 10.571 |
| 169.83 | 389.96 | 3.679 | -54.930 | 23.610 | -20.189 | 11.102 |
| 169.85 | 394.15 | 5.719 | -53.400 | 22.620 | -19.883 | 10.762 |
| 169.88 | 397.66 | 3.965 | -50.050 | 22.030 | -18.751 | 10.332 |
| 169.90 | 400.15 | 4.625 | -49.270 | 21.570 | -18.529 | 9.555 |
| 169.92 | 402.86 | 4.309 | -46.850 | 20.880 | -17.721 | 9.610 |
| 169.94 | 404.86 | 3.871 | -46.020 | 20.400 | -17.459 | 9.043 |
| 169.96 | 406.43 | 3.400 | -45.930 | 20.070 | -17.423 | 8.512 |
| 169.98 | 408.03 | 2.662 | -45.210 | 19.840 | -17.164 | 8.347 |
| 170.00 | 409.18 | 2.773 | -44.010 | 19.550 | -16.754 | 7.763 |

**Table D2 (continued)**

| | | | | | | |
|---|---|---|---|---|---|---|
| 170.02 | 409.54 | 3.588 | -43.200 | 19.250 | -16.498 | 6.716 |
| 170.04 | 408.52 | 4.534 | -43.240 | 19.020 | -16.551 | 4.827 |
| 170.06 | 407.82 | 5.038 | -43.980 | 19.090 | -16.787 | 4.263 |
| 170.08 | 408.07 | 4.686 | -46.770 | 19.090 | -17.819 | 4.760 |
| 170.10 | 411.38 | 5.066 | -48.080 | 18.950 | -18.343 | 7.958 |
| 170.13 | 408.42 | 8.456 | -48.340 | 18.920 | -18.369 | 2.526 |
| 170.15 | 408.47 | 5.498 | -48.160 | 18.970 | -18.294 | 3.851 |
| 170.17 | 410.74 | 5.189 | -43.870 | 18.600 | -16.749 | 5.984 |
| 170.19 | 410.07 | 7.621 | -37.020 | 18.630 | -14.095 | 3.599 |
| 170.21 | 404.14 | 8.519 | -21.900 | 19.450 | -8.229 | -1.961 |
| 170.23 | 399.12 | 1.865 | 32.150 | 20.480 | 11.992 | -6.271 |
| 170.25 | 393.34 | -9.899 | 105.200 | 21.560 | 39.003 | -13.515 |
| 170.27 | 383.17 | -6.238 | 190.400 | 23.270 | 70.671 | -25.941 |
| 170.29 | 377.52 | -10.600 | 231.300 | 24.550 | 87.023 | -22.655 |
| 170.31 | 374.07 | -9.391 | 314.400 | 25.530 | 118.604 | -21.247 |
| 170.33 | 371.68 | -15.599 | 409.300 | 26.070 | 155.496 | -20.012 |
| 170.35 | 369.35 | -17.566 | 466.500 | 26.820 | 178.307 | -19.675 |
| 170.38 | 367.99 | -16.578 | 509.100 | 27.650 | 195.515 | -17.611 |
| 170.40 | 367.13 | -17.353 | 618.300 | 28.300 | 238.097 | -16.628 |
| 170.42 | 366.04 | -16.815 | 597.600 | 28.830 | 234.299 | -15.916 |
| 170.44 | 365.56 | -17.765 | 557.000 | 29.320 | 225.263 | -13.903 |
| 170.46 | 365.78 | -15.728 | 569.300 | 29.550 | 236.026 | -11.714 |
| 170.48 | 366.18 | -16.904 | 637.700 | 30.060 | 267.026 | -10.493 |
| 170.50 | 365.65 | -12.666 | 659.500 | 30.260 | 270.789 | -11.558 |
| 170.52 | 367.17 | -16.171 | 510.600 | 30.100 | 210.280 | -6.205 |
| 170.54 | 366.36 | -19.241 | 574.700 | 30.360 | 243.356 | -9.856 |
| 170.56 | 364.81 | -14.423 | 507.500 | 30.430 | 210.488 | -11.598 |
| 170.58 | 364.81 | -12.591 | 503.100 | 30.460 | 211.285 | -9.318 |
| 170.60 | 365.26 | -11.474 | 417.000 | 30.080 | 177.183 | -7.264 |
| 170.63 | 364.63 | -11.938 | 453.200 | 30.200 | 190.836 | -9.024 |
| 170.65 | 365.68 | -11.039 | 402.200 | 30.420 | 165.274 | -5.401 |
| 170.67 | 367.72 | -9.738 | 286.000 | 29.440 | 111.585 | -1.753 |
| 170.69 | 369.35 | -6.713 | 228.600 | 27.980 | 87.384 | -0.573 |
| 170.71 | 370.51 | -6.072 | 136.100 | 26.930 | 51.405 | -0.290 |
| 170.73 | 372.97 | 0.131 | 43.730 | 26.050 | 16.499 | 1.868 |
| 170.75 | 376.44 | 3.395 | 0.736 | 24.490 | 0.278 | 1.330 |
| 170.77 | 379.66 | 3.603 | -13.680 | 23.500 | -5.191 | 5.977 |
| 170.79 | 382.55 | 3.734 | -21.140 | 22.850 | -8.065 | 5.375 |
| 170.81 | 385.53 | 4.880 | -23.850 | 22.370 | -9.123 | 5.835 |
| 170.83 | 388.17 | 3.782 | -30.520 | 22.050 | -11.678 | 6.391 |

**Table D2 (continued)**

| | | | | | | |
|---|---|---|---|---|---|---|
| 170.85 | 391.14 | 5.295 | -23.450 | 21.730 | -8.963 | 6.305 |
| 170.88 | 392.53 | 5.588 | -15.190 | 21.680 | -5.786 | 4.698 |
| 170.90 | 393.54 | 4.546 | -11.630 | 21.680 | -4.405 | 4.032 |
| 170.92 | 396.05 | 6.574 | -22.330 | 21.400 | -8.413 | 6.540 |
| 170.94 | 397.49 | 6.227 | -17.890 | 21.160 | -6.740 | 5.334 |
| 170.96 | 398.53 | 4.374 | -21.340 | 21.180 | -8.012 | 5.312 |
| 170.98 | 401.00 | 4.334 | -19.530 | 21.030 | -7.293 | 6.274 |

## REFERENCES


Aubinet, M. (2008), Eddy covariance CO2 flux measurements in nocturnal conditions: an analysis of the problem, *Ecological Applications*, *18*(6), 1368-1378, doi: 10.1890/06-1336.1.

Baldocchi, D. D. (2003), Assessing the eddy covariance technique for evaluating carbon dioxide exchange rates of ecosystems: past, present and future, *Global Change Biology*, *9*(4), 479-492, doi: 10.1046/j.1365-2486.2003.00629.x.

Beltrami, H., J. Wang, and R. L. Bras (2000), Energy balance at the Earth's surface: Heat flux history in eastern Canada, *Geophysical Research Letters*, *27*(20), 3385-3388, doi: 10.1029/2000GL008483.

Bennett, W. B., J. Wang, and R. L. Bras (2008), Estimation of global ground heat flux, *Journal of Hydrometeorology*, *9*(4), 744-759, doi: 10.1175/2008JHM940.1.

Bounoua, L., J. Masek, and Y. M. Tourre (2006), Sensitivity of surface climate to land surface parameters: A case study using the simple biosphere model SiB2, *Journal of Geophysical Research: Atmospheres*, *111*(D22), n/a-n/a, doi: 10.1029/2006JD007309.

Businger, J. A., J. C. Wyngaard, Y. Izumi, and E. F. Bradley (1971), Flux-Profile relationships in the atmospheric surface layer, *Journal of the Atmospheric Sciences*, *28*(2), 181-189, doi: 10.1175/1520-0469(1971)028<0181:FPRITA>2.0.CO;2.

Clark, K. L., Skowronski, J Hom. 2010. Invasive insects impact forest carbon dynamics. Global Change Biology 16 (1), 88-101.

Collatz, G. J., J. T. Ball, C. Grivet, and J. A. Berry (1991), Physiological and environmental regulation of stomatal conductance, photosynthesis and transpiration: a model that includes a laminar boundary layer, *Agricultural and Forest Meteorology*, *54*(2–4), 107-136, doi: 10.1016/0168-1923(91)90002-8.

Finkelstein, P. L., and P. F. Sims (2001), Sampling error in eddy correlation flux measurements, *Journal of Geophysical Research: Atmospheres*, *106*(D4), 3503-3509, doi: 10.1029/2000JD900731.

Fitzmaurice, J., J. Wang, and R. L. Bras (2004), Sensible heat flux estimated from one-level air temperature near the land surface, *Geophysical Research Letters*, *31*(7), L07102, doi: 10.1029/2003GL018452.

Hollinger, D. Y., and A. D. Richardson (2005), Uncertainty in eddy covariance measurements and its application to physiological models, *Tree Physiology*, *25*(7), 873-885, doi: 10.1093/treephys/25.7.873.

Jenkins, J. P., A. D. Richardson, B. H. Braswell, S. V. Ollinger, D. Y. Hollinger, and M. L. Smith (2007), Refining light-use efficiency calculations for a deciduous forest canopy using simultaneous tower-based carbon flux and radiometric measurements, *Agricultural and Forest Meteorology*, *143*(1–2), 64-79, doi: 10.1016/j.agrformet.2006.11.008.

Le Quéré, C., et al. (2014), Global carbon budget 2013, *Earth Syst. Sci. Data*, *6*(1), 235-263, doi: 10.5194/essd-6-235-2014.

Liu, H., J. T. Randerson, J. Lindfors, and F. S. Chapin (2005), Changes in the surface energy budget after fire in boreal ecosystems of interior Alaska: An annual perspective, *Journal of Geophysical Research: Atmospheres*, *110*(D13), n/a-n/a, doi: 10.1029/2004JD005158.

Moghim, S., A. J. Bowen, S. Sarachi, and J. Wang (2014), Retrieval of hourly records of surface hydrometeorological variables using satellite remote sensing data, *Journal of Hydrometeorology*, *16*(1), 147–157, doi: 10.1175/JHM-D-13-0127.1.

Nieuwstadt, F. T. M. (1980), An analytic solution of the time-dependent, one-dimensional diffusion equation in the atmospheric boundary layer, *Atmospheric Environment (1967)*, *14*(12), 1361-1364, doi: 10.1016/0004-6981(80)90154-7.

Nieuwstadt, F. T. M., and B. J. de Haan (1981), An analytic solution of the one-dimensional diffusion equation in a non-stationary boundary layer with an application to inversion rise fumigation, *Atmospheric Environment (1967)*, *15*(5), 845-851, doi: 10.1016/0004-6981(81)90289-4.

Nieves, V., J. Wang, and J. Willis (2014), A conceptual model of ocean freshwater flux derived from sea surface salinity, *Geophysical Research Letters*, *41*(18), 6452-6458, doi: 10.1002/2014GL061365.

Oldham, K. B., and J. Spanier (2002), *The Fractional Calculus – Theory and Applications of Differentiation and Integration to Arbitrary Order*, Dover Publications, Inc., New York.

Parazoo, N. C., A. S. Denning, S. R. Kawa, S. Pawson, and R. Lokupitiya (2012), CO2 flux estimation errors associated with moist atmospheric processes, *Atmos. Chem. Phys.*, *12*(14), 6405-6416, doi: 10.5194/acp-12-6405-2012.

Peters, G. P., R. M. Andrew, T. Boden, J. G. Canadell, P. Ciais, C. Le Quere, G. Marland, M. R. Raupach, and C. Wilson (2013), The challenge to keep global warming below 2 [deg]C, *Nature Clim. Change*, *3*(1), 4-6, doi: doi:10.1038/nclimate1783.

Post, H., H. J. Hendricks Franssen, A. Graf, M. Schmidt, and H. Vereecken (2015), Uncertainty analysis of eddy covariance CO2 flux measurements for different EC tower distances using an extended two-tower approach, *Biogeosciences*, *12*(4), 1205-1221, doi: 10.5194/bg-12-1205-2015.

Saleska, S. R., et al. (2003), Carbon in Amazon Forests: unexpected seasonal fluxes and disturbance-induced losses, *Science*, *302*(5650), 1554-1557, doi: 10.1126/science.1091165.

Schimel, D. S. (1995), Terrestrial ecosystems and the carbon cycle, *Global Change Biology*, *1*(1), 77-91, doi: 10.1111/j.1365-2486.1995.tb00008.x.

Scott, R.L. 2010. Using watershed water balance to evaluate the accuracy of eddy covariance evaporation measurements for three semiarid ecosystems. Agricultural and Forest Meteorology, 150, 219-225. doi:10.1016/j.agrformet.2009.11.002

Scott, R. L., T. E. Huxman, D. G. Williams, and D. C. Goodrich (2006), Ecohydrological impacts of woody-plant encroachment: seasonal patterns of water and carbon dioxide exchange within a semiarid riparian environment, *Global Change Biology*, *12*(2), 311-324, doi: 10.1111/j.1365-2486.2005.01093.x.

Sellers, P. J., D. A. Randall, G. J. Collatz, J. A. Berry, C. B. Field, D. A. Dazlich, C. Zhang, G. D. Collelo, and L. Bounoua (1996), A revised land durface parameterization (SiB2) for atmospheric GCMs. Part I: model formulation, *Journal of Climate*, *9*(4), 676-705, doi: http://dx.doi.org/10.1175/1520-0442(1996)009<0676:ARLSPF>2.0.CO;2.

Sellers, P. J., et al. (1997), Modeling the Exchanges of Energy, Water, and Carbon Between Continents and the Atmosphere, *Science*, *275*(5299), 502-509, doi: 10.1126/science.275.5299.502.

Stephens, B. B., et al. (2007), Weak northern and strong tropical land carbon uptake from vertical profiles of atmospheric CO2, *Science*, *316*(5832), 1732-1735, doi: 10.1126/science.1137004.

Takahashi, T., et al. (2002), Global sea–air CO2 flux based on climatological surface ocean pCO2, and seasonal biological and temperature effects, *Deep Sea Research Part II: Topical Studies in Oceanography*, *49*(9–10), 1601-1622, doi: 10.1016/S0967-0645(02)00003-6.

Tans, P. P., I. Y. Fung, and T. Takahashi (1990), Observational contrains on the global atmospheric CO2 budget, *Science*, *247*(4949), 1431-1438, doi: 10.1126/science.247.4949.1431.

Vaughan, P. J., and D. L. Suarez (2002), Modeling above-canopy CO2 flux and evapotranspiration in wheat, *Environmental Pollution*, *116, Supplement 1*, S37-S44, doi: 10.1016/S0269-7491(01)00245-7.

Vickers, D., M. GÖCkede, and B. E. Law (2010), Uncertainty estimates for 1-h averaged turbulence fluxes of carbon dioxide, latent heat and sensible heat, *Tellus B*, *62*(2), 87-99, doi: 10.1111/j.1600-0889.2009.00449.x.

Wang, J., and R. L. Bras (1998), A new method for estimation of sensible heat flux from air temperature, *Water Resources Research*, *34*(9), 2281-2288, doi: 10.1029/98WR01698.

Wang, J., and R. L. Bras (1999), Ground heat flux estimated from surface soil temperature, *Journal of Hydrology*, *216*(3–4), 214-226, doi: 10.1016/S0022-1694(99)00008-6.

Wang, J., and R. L. Bras (2009), A model of surface heat fluxes based on the theory of maximum entropy production, *Water Resources Research*, *45*(11), W11422, doi: 10.1029/2009WR007900.

Wang, J., and R. L. Bras (2010), An extremum solution of the Monin–Obukhov similarity equations, *Journal of the Atmospheric Sciences*, *67*(2), 485-499, doi: 10.1175/2009JAS3117.1.

Wang, J., and R. L. Bras (2011), A model of evapotranspiration based on the theory of maximum entropy production, *Water Resources Research*, *47*(3), n/a-n/a, doi: 10.1029/2010WR009392.

Wanninkhof, R. (2007), The impact of different gas exchange formulations and wind speed products on global Air-Sea CO2 fluxes, in *Transport at the Air-Sea Interface*, edited by C. Garbe, R. Handler and B. Jähne, pp. 1-23, Springer Berlin Heidelberg, doi: 10.1007/978-3-540- 36906-6.

WRI, C. (2014), 2.0.(2014), Climate Analysis Indicators Tool: WRI's Climate Data Explorer, *World Resources Institute, Washington, DC*.

Yakir, D., and X.-F. Wang (1996), Fluxes of CO2 and water between terrestrial vegetation and the atmosphere estimated from isotope measurements, *Nature*, *380*(6574), 515-517, doi: 10.1038/380515a0.

Zhan, X., and W. P. Kustas (2001), A coupled model of land surface CO2 and energy fluxes using remote sensing data, *Agricultural and Forest Meteorology*, *107*(2), 131-152, doi: 10.1016/S0168-1923(00)00229-X.

Zhan, X., Y. Xue, and G. J. Collatz (2003), An analytical approach for estimating CO2 and heat fluxes over the Amazonian region, *Ecological Modelling*, *162*(1–2), 97-117, doi: 10.1016/S0269-7491(01)00245-7.